Gamma-ray evidence for cosmic-ray sources

Rogers, Martin John

Gamma-Ray Evidence for Cosmic-Ray Sources.

by

Martin John Rogers

A thesis submitted to the University of Durham
for the
Degree of Doctor of Philosophy
September 1988

Dedication.

This thesis is dedicated to my wife, Sue,
who put up with me and all of it,
with all my love.

Abstract.

The origin of cosmic-rays is one of the long-standing problems in astrophysics. In recent years, strong evidence has been found that certain classes of object contain and are able to accelerate particles to high energies. In this thesis the origin problem is addressed in two different ways.

Firstly, two different regions of the Galaxy are studied using γ-ray observations from the COSB satellite combined with atomic and molecular gas measurements. The Vela region contains a pulsar and a supernova remnant and is particularly valuable location for cosmic-ray studies because of its proximity, the association of the two objects, and the intensity of the γ-ray flux it produces. At greater longitudes, the region around the peculiar object η Carinae is also studied. It is rich in potential sources of cosmic rays including active stars and a spiral arm seen at a tangent at $l \sim 282°$.

Analysis of the Vela region reveals strong evidence for cosmic ray production at all energies observed by COSB. The supernova remnant seems the most likely candidate, but the possibility of the pulsar itself producing some of the particles cannot be ruled out. The excess γ-ray emission from around η Carinae does not appear correlated with the active stars but seems to be coming predominantly from the spiral arm. This is the first time evidence has been presented for cosmic-ray acceleration by the spiral shock in a particular, known spiral arm which is observed as a feature in the gas. The γ-rays are produced in the gas clouds associated with this arm.

The second approach to the cosmic-ray origin problem involves a model for cosmic-ray production in supernova remnants and is used in association with a Monte-Carlo simulation of their occurrence in the Galaxy. Unlike earlier models (Bhat *et al* 1987), the motion of the Sun is also taken into account and

the supernova explosions occur mainly in spiral arms. The results are in the form of a time sequence of energy density values and are compared in detail with ^{10}Be results. It is found that the model accounts for the long-term rise in the concentration of this radioisotope and does not predict large excursions from the mean energy density that beset older models. Thus the cosmic ray production by supernova remnants seems to be consistent with the radioisotope data.

Preface.

The work presented in this thesis was carried out between October 1985 and September 1988 whilst the author was a Research Student in the Physics Department of the University of Durham under the supervision of Professor A. W. Wolfendale,

Some of the research was carried out in collaboration with Professor Wolfendale and the members of his research group but the calculations and interpretations are solely those of the author.

Some parts of this thesis have been published as follows:

C. L. Bhat, C. J. Mayer, M. J. Rogers, A. W. Wolfendale and M. Zan. 1986 J. Phys. G: Nucl. Phys. **12** 1087

C. L. Bhat, C. J. Mayer, M. J. Rogers, A. W. Wolfendale. 1987 J. Phys. G: Nucl. Phys. **13** 257

C. J. Mayer, K. M. Richardson, M. J. Rogers, J. Szabelski and A. W. Wolfendale. 1987 A. & A. **180** 73

M. J. Rogers and A. W. Wolfendale. 1987 20th International Cosmic-Ray Conference (Moscow) **1** 81

J. Szabelski, C. J. Mayer, K. M. Richardson, M. J. Rogers and A. W. Wolfendale. 1987 20th International Cosmic-Ray Conference (Moscow) **1** 133

M. J. Rogers, M. Sadzinska, J. Szabelski, D. J. van der Walt, A. W. Wolfendale. 1988 J. Phys. G: Nucl. Phys. **14** 1147

Contents.

Chapter 1. Introduction.

1.1 Cosmic-Rays.

1.1.1 Observations.

The study of the properties of cosmic-rays (CR) has been a long and difficult one, stretching back to their discovery by Hess in 1912 (Hess 1912). Their origin is a major topic of research in astrophysics and it is this problem that is addressed in this thesis.

Early experiments by Elster, Geitel and Wilson (see Hillas 1972) revealed a 'dark current' in ionization chambers which was attributed to radiation from the Earth. Balloon-borne equipment revealed an increase in activity with altitude however, and further experiments were carried out during the 1920's by Millikan and others that proved beyond any doubt that the radiation was indeed 'cosmic'. It was pointed out by some experimenters that the Earth's magnetic field would affect the trajectories of the charged particles. Early experiments at various northern latitudes were inconclusive, but an expedition in 1932 around the Pacific showed a decrease in intensity (especially at high energies) towards the equator which followed the magnetic field lines. Using the theory of Størmer, Lemaître and Vallarta (1933) published the first mathematical analysis of the interaction of CR with the Earth's magnetic field. The experimentation continued, revealing the constituents of this radiation to be protons, electrons, γ-rays, and alpha particles and later more complex nuclei.

The Sun produces CR in flares which tend to have lower energies than their Galactic counterparts, but its major contribution is the modulation of this latter component which affects the spectrum below about 1–10 GeV where

the flux is high and is most easily measured.

Observations of the cosmic radiation have continued to the present day with balloon-flights and satellites which have made the composition of CR impinging on the Earth's atmosphere one of the most precise sets of astrophysical measurements. Other techniques are now employed to study this radiation especially at ultra-high energies (above 10^{18}eV) where there are extremely few events. For example, arrays of scintillators arranged over a large area detect the secondary radiation cascade produced by the primary particle the energy of which can be reconstructed by timing the events at the various detectors. Cerenkov radiation produced by the secondaries can also be analysed as a means of distinguishing CR from γ-rays at these highest energies.

This study is a necessary and integral part of determining processes and events that occur in interstellar and intergalactic space. The CR reveal such phenomena through measurements of the energy distribution, isotopic ratios and their isotropy: they span many orders of magnitude in energy, most elements in the periodic table are present (at least to Z=56) and their arrival directions are distributed isotropically. There is a vast number of isotopes, each with its own interactions so the potential analytical power in their study is immense. The spectra of sunlight and starlight and the study of the isotopic abundances of material in the solar system gives the abundances of each isotope which can then be compared to the CR abundances. This permits not only some information about the source of the CR to be determined, but also about which processes are involved as they pass through the interstellar medium. Knowledge of the nuclear processes that can occur is a necessary prerequisite for derivation of important quantities such as the escape time of the particles from the Galaxy, the grammage of the material traversed, as well as providing constraints on the possible acceleration mechanisms. This indirect route is the only one available because, being charged, the CR are deflected by the Galactic magnetic field and all directional information is lost. It is for this reason that the sources of CR are still not positively and unambiguously identified although work is now in progress to study the small flux of γ-rays in the primary radiation which come directly to the Earth undeflected and therefore will be able to examine CR source directly.

1.1.2 Sources of Cosmic-Rays.

It is the origin of the Galactic CR that has proved so enigmatic, but over the years, some very strong evidence has been accumulated for certain classes of objects being sources of CR. In an astrophysical setting, when a charged particle is accelerated in a magnetic field, synchrotron radiation is emitted which is detectable at the Earth provided the particle density and field strength are high enough. The small mass of the electron makes it the most susceptible to this form of acceleration, so measurements at radio wavelengths can reveal the presence of not only magnetic fields, but the electrons spiralling in them. 408 MHz is a typical frequency for observations of synchrotron radiation although the thermal component of the gas must first be removed. This is done by performing measurements at other frequencies and fitting a thermal curve to the intensities. The non-thermal remainder is attributed to electrons as other particles will not radiate at these frequencies because of their greater masses. It is for this reason that although protons are as plentiful in CR as electrons, it is the latter that have featured most prominently in CR studies.

Supernova remnants (SNR) are the extended gaseous remains of a massive, evolved star that underwent core collapse and shed its outer layers in an enormous explosion that liberated around 10^{51} ergs. Such an event does not happen often: it is estimated that a supernova (SN) occurs once every 30–100 years in the Galaxy, but they are the major cause of many of the objects observed in the sky as they are believed to initiate star-formation in gas clouds. Only the spiral structure of the Galaxy itself can be said to have as great an effect on the appearance and evolution of the interstellar medium. Despite this massive and sudden input of energy, the event itself is not the major candidate as a CR source. It is the shock wave that propagates outward into the surrounding gas and sweeps up this material into the shell that is a common feature of these objects. The large amount of energy involved ensures that there is plentiful ionized gas present which drags the magnetic field with it as the gas is swept up. The presence of both ionized gas and magnetic fields explains the observations of synchrotron radiation as the electrons are forced to spiral in the fields, and the elements are present for a CR source: particles,

fields and an energy source (the shock wave).

There are a number of phases through which the remnant passes as it expands. The first is the initial free expansion where the mass of swept-up material is negligible and the expansion is largely unimpeded by the interstellar gas. Gradually, the shock wave accumulates material and when the mass of swept-up gas is of the same order as the ejecta mass, then the remnant enters the adiabatic expansion or Sedov phase (Sedov 1959). This is the longest and probably most important phase for CR acceleration. Finally, the remnant cools radiatively, the expansion slows and the expansion velocity nears the average interstellar medium gas velocity so merging the remnant material with the ambient gas.

There are a number of other potential sources of high energy particles, although none as powerful as SNe. Active, massive stars such as early O-stars and Wolf-Rayets have strong stellar winds and high mass-loss rates which, when combined with the numbers of such objects in the Galaxy can add up to a significant input of energy into the interstellar medium (e.g. Cassé and Paul 1980, Völk and Forman 1982).

Strong magnetic fields are a necessary adjunct to any acceleration process for charged particles so any astrophysical location that contains such a field is also a good place to look for CR. The Galactic magnetic field is of the order of a few micro-Gauss and is not strong enough for this purpose unless compressed in some way and combined with other processes such as a shock. However, when a massive star collapses, as occurs during a SN, then the central object (a pulsar) can have a very strong field: of the order of 10^{10-12}G. In such an environment charged particles are continuously accelerated and cannot be anything other than relativistic, so the problem is to explain how they can escape from the pulsar. The trajectories of these particles have been estimated by numerous authors following the work of Gunn and Ostriker (1969).

Material flowing out from some object, be it stellar, interstellar or intergalactic, will collide with the surrounding material and the flow can, in some cases, terminate as a shock. Such a phenomenon is seen, for example, in the Solar System as the solar wind hits the magnetosphere of a planet and a shock forms. Particle acceleration has been observed to occur at such loca-

tions depending on the form and strength of the shock. At the other end of the scale, jets emitted from active galaxies and quasars encounter the intergalactic medium forming a shock and providing another environment for the acceleration of particles.

Clearly there is a wealth of potential sources for the cosmic radiation, but wherever they are formed, all directional information is lost via their interaction with the weak Galactic magnetic field. This introduces the subject of how these CR can interact in the interstellar medium and thus provide a way for their sources and their distribution to be uncovered. Before examining the γ-radiation produced by CR, the acceleration mechanism for these particles must be discussed.

1.1.3 Shock Acceleration of Cosmic-Rays.

A common theme in a number of the above CR source candidates is the presence of shocks. One of the most studied contenders for the acceleration mechanism of CR particles is known as diffusive shock acceleration and was developed almost simultaneously by a number of authors: Axford *et al* 1977, Krymsky (1977), Bell (1978), Blandford and Ostriker (1978). The idea was also implicit in a number of much earlier papers: Jokipii (1966,1968) and Fisk (1971). Parker (1958) and Hudson (1965, 1967) dealt with the first order Fermi process and Hoyle (1960) suggested that shocks could accelerate particles although he did not suggest an actual mechanism for this. A number of excellent reviews of this subject have been written (Axford 1980, 1981a,b, Drury 1983, Blandford and Eichler 1987, Ostriker and McKee 1988) which cover the subject from its simplest formulation to the more recent non-linear analysis.

The shock process is believed to occur in a number of astrophysical environments including SNR, active star stellar winds and the solar wind. The first of these is perhaps the most popular for the higher energy ($>$ 100 MeV/nucleon) particles as the amount of energy input by each SN is $\sim 10^{51}$ ergs which is easily sufficient for the CR energy budget.

The basis of the mechanism is first-order Fermi acceleration (Fermi 1949) in which particles receive energy by crossing a strong shock i.e. the velocity of the shock (v_s) is very much greater than the sound speed (c_s). Particles are accelerated by being passed by the shock and scattered off the turbulent gas downstream. Some are then convected further downstream whilst others pass back upstream where they are again scattered by the gas which isotropises the CR distribution. The shock then catches up with the particles and the acceleration cycle begins afresh. The CR are strongly scattered in the interstellar medium by hydromagnetic disturbances known as Alfvén waves. The process has a reasonably high efficiency: for example, averaging the Galactic CR power gives $\sim 3 \times 10^{40}$ergs s^{-1} (to a factor of three) and with a SN rate of 1 every 30 years, each SN must input $\sim 3 \times 10^{49}$ergs. This is approximately 3% of the total energy released by the explosion. Thus any serious alternative to the SNR origin of CR must provide either a greater efficiency or a much greater extent (such as spiral shocks (Duric 1984) and Chapter 3). CR must also be accelerated in the later stages of SNR expansion because as their mean energy is inversely proportional to the cube root of their number density, if they were accelerated in the first hundred years or so, their energy would be almost completely dissipated by the time the remnant was in the later Sedov phase. As a result it is the larger remnants that are believed to contain CR with greater energy. Loop I is a prime example of such a large remnant (Bhat *et al* 1985b).

That particle acceleration does occur by this process has been verified *in situ* by spacecraft passing through the Earth's bow shock where the solar wind collides with the magnetosphere. Similar bow shocks have also been observed around other planets, and similar processes occur in interstellar space, solar flares and stellar wind termination shocks. (See the review by Blandford and Eichler 1987). Although the Sun is a prolific source of extremely low energy CR, it is not these particles that are of primary interest but rather the generally higher energy Galactic CR that are responsible for γ-ray emission. The mathematical details of this process may be found in the reviews already cited and the references contained therein. What will also be found is the realisation that this shock acceleration process is a non-linear one as the accelerated particles can have a modifying effect on the shock structure and propagation. The

test particle model is not therefore accurate although it does act as a useful guide for the more advanced non-linear studies. There is a rough equipartition of energy between gas, magnetic fields and CR on a large scale in the Galaxy at least, which suggests that none of the three can be ignored and the problem must be solved in a fully self-consistent fashion. To date, this endeavour has met with limited success.

It is clear that shock acceleration is an excellent candidate for producing CR and the best sites to examine the evidence for this are SNR by virtue of the vast quantity of energy available and the high efficiencies that can be attained. Pulsars also have a means by which CR can be accelerated, namely their very intense magnetic fields, and this must be borne in mind as pulsars are believed to be the remains of the star that produced the SN explosion. The two are likely to be intimately connected.

1.1.4 Cosmic-Ray Variations.

The energy spectrum of solar CR is much steeper than that of the galactic CR, and it varies on a number of timescales. Produced in solar flares, these particles decay away in periods ranging from hours for GeV particles to days at lower energy. Their galactic counterparts are present continuously, bombarding the Earth from all directions with a high degree of isotropy until the very highest energies are reached. The intensity varies depending on the condition of the Sun (i.e. the amount of solar activity) and on the magnetic field strength of nearby planets. A phenomenon known as a Forbush decrease is perhaps the most important non-periodic variation of galactic CR over short timescales. It is due to interplanetary shock waves pushing CR ahead of them and thus causing a decrease in intensity behind.

Distinguishing solar modulation effects from genuine interstellar variations of the galactic CR is not an easy task, but a successful model has been formulated based on the fundamental equation of CR transport (Axford 1965, Parker 1965 and reviews by Jokipii 1971, Völk 1975, Fisk 1979). The CR are embedded in a highly turbulent and irregular drifting magnetic field so the

directions of motion of particles become random. This field is connected to the solar wind, so on top of the diffusion of the CR there is both a convection and an expansion energy loss as the wind moves away from the Sun. This model is able to explain in quite some detail many of the observed variations in CR intensity (Kota and Jokipii 1983). These variations occur over a variety of timescales from the eleven year sunspot cycle to tens of thousands of years and a number of radioisotopes have been used to uncover them.

The most common CR-produced radionuclide is ^{14}C which is the result of proton bombardment of nitrogen in the atmosphere. This reaction has an energy threshold of 34 MeV (Laumer *et al* 1973), and the average energy of the protons involved in this reaction is about 1 GeV based on data from Read and Viola (1984). At solar minimum, when the modulation of the galactic CR intensity is lowest and the intensity of CR is highest, the concentration of this radioisotope in the atmosphere has been measured to increase. This occurs over in a timescale of years. Over much longer periods (to 10^4 years), there is a roughly sinusoidal variation (Suess 1980, Neftel *et al* 1981, Sonnett 1985) of the concentration. For longer periods, longer half-life isotopes are required meaning that alternative sources of radioisotopes must be used instead of the organic reservoirs of the ^{14}C. Lunar rocks and meteorites with known exposure histories and geometries (perhaps taken from debris associated with a cometary orbit), can be analysed for radioisotopes with half-lives from 10^5 to 10^7 years and can be used to determine the CR flux over similar periods. Listed in increasing half-life, these radioactive elements include: ^{81}Kr (2.1×10^5 years), ^{36}Cl (3.0×10^5), ^{26}Al (7.2×10^5), ^{10}Be (1.5×10^6) and ^{53}Mn (3.7×10^6). To 10^9 years, there are only two radioisotopes ^{129}I (1.6×10^7 years), and ^{40}K (3.7×10^9) that have been studied (Voshage 1962, 1978, Nishizumii *et al* 1983, 1985) although a new technique involving the stable ^{129}Xe nucleus has been developed (Marti 1985).

Studies of this sort have a direct relevance to questions about the possibility of a local SN within the last 10^5 years near the Sun (Clayton 1984, Clayton *et al* 1986). The argument is unresolved as ^{26}Al and ^{81}Kr seem to give conflicting results.

In its motion around the Galaxy, the Sun will encounter not only SNR,

but giant molecular clouds and the spiral arms in which shocks are believed to be embedded and which contain higher concentrations of gas and dust. Such 'close encounters' are expected to have considerable influence on the motion of the Sun (Delhaye 1965) and studies of the velocity dispersions of stars near the Sun are a major topic of research (Olano 1982, Goulet 1984, Lacey 1984, Wielen 1974,1977, Bash 1986, Higdon and Bash 1981, Mayor 1982, Palouš 1983 and many others.) Also, as the Sun passes through or by these objects, it is predicted that the CR intensity will increase. If a SN has occurred nearby ($\leq$ 100 pc), for example, then the increase is expected to show up in a number of the various radioisotopes with the appropriate half-life (of the order of 10^5 years.) SNR are prime candidates for CR acceleration but their distribution in the Galaxy is not expected to be uniform as their explosion sites will be near the star forming region in which the massive, short-lived parent star was formed. This is generally believed to occur in or near the giant molecular clouds which are found predominantly in the spiral arms and are associated with the spiral shocks such arms contain.

Geological mass extinctions, the Oörť comet cloud, crater ages and the search for a solar companion are all related to this field of CR variations (e.g. Shoemaker and Wolfe 1986 and an extensive review by Wilkinson 1987) in that they are also dependent on phenomena such as spiral arm passage by the solar system.

It is a large task to assemble all the pieces of information required to model the passage of the Sun through the Galaxy. Integration of the motion in either direction — past or future — is liable to errors due to a close encounter with a massive gas cloud which can alter the velocity of the Sun sufficiently to make subsequent prediction impossible. Nevertheless, some attempts have been made (e.g. Bash 1986). The motion of the Sun, its relative position with respect to the spiral arms, the frequency and evolution of CR sources are all relevant pieces of information required and each has its uncertainties. The predicted variation of the CR intensity is the object of the study and so an interesting problem can be addressed: Assuming a certain CR production model, does the radioisotope data now available preclude that model on the basis of variations in the CR record over the past 10^6 years?

Little more can be asked without much improved data both from stellar observations and radioisotope measurements, but the answer to this question can put a useful constraint on the model for CR used. Chapter 4 addresses this topic by the use of a Monte-Carlo simulation

1.2 The COSB Mission.

The COSB γ-ray telescope was launched in 1975 by ESA under the control of a group of universities in Europe known as the Caravane Collaboration. The experiment was a multi-layered spark chamber with an anti-coincidence CR dome to discriminate against charged particles and a means to determine the energy and angle of incidence to the telescope pointing direction of the incoming γ-ray photon (Fig. 1.1) The most likely interaction of an incoming γ-ray is pair production in the electromagnetic field of a nucleus. The cross-section is proportional to Z^2 so tungsten ($Z = 74$) sheets were interleaved between the 16 1.5cm grid gaps in the spark chamber. The grids themselves consisted of orthogonal wires with a 3mm separation. The gap nearest the anti-coincidence dome and the three nearest the scintillation counters had no tungsten immediately above them. When no pulse was detected in the dome, the detection of descending electrons in the triggering mechanism (B1,B2,C) caused a high voltage to be applied across each of the gaps. The resulting discharges occurred along the electron tracks and their position was recorded to reconstruct the event. This allowed the arrival directions of the initiating photon to be determined. The energy of the event was measured in the scintillation crystal (E) with a further scintillator (D) to provide a high energy event correction.

A high polar orbit was chosen to maximise useful observing time by removing the shielding of the Earth's magnetic field, but unfortunately this led to a high background count rate via interactions of the CR with the telescope itself producing γ-rays. The estimation of this background was the subject of intense study by the COSB group and the importance of this quantity cannot be overstated. A long-term trend in both background and sensitivity was detected (Fig. 1.2) part of which could be attributed to changes in the

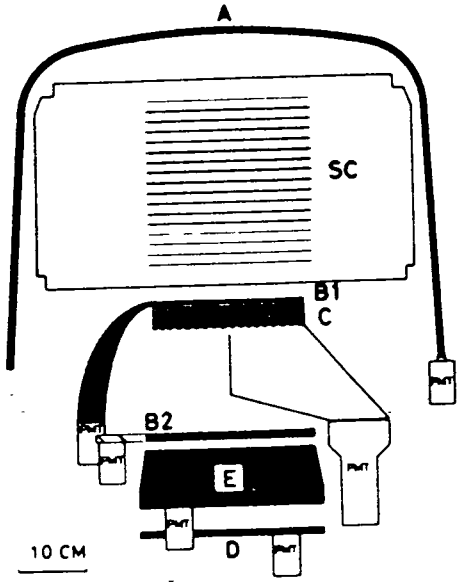

Figure 1.1.
The COSB telescope, showing the major components. A: Anticoincidence dome. SC: Spark chamber. B1,B2: Scintillation counters. C: Directional Cerenkov counter. D: Scintillator to provide additional information on high energy events for which absorption in the calorimeter is incomplete. E: Caesium Iodide scintillator used as energy calorimeter.

solar-modulated CR flux. The background is also dependent on the inclination angle from the telescope axis. Both of these effects are corrected for in the program construct intensity maps supplied with the datasets.

Observations were made for seven years until 1982 when the gas used to recharge the spark chamber was exhausted. In this time 209,537 γ-rays were observed, the majority from the Galactic plane, but with some high latitude observation periods. Pre-flight calibration of the instrument was checked in flight by observing a point source (Vela) which confirmed the earlier ground-based tests. The point spread function (PSF) was found to be energy dependent becoming narrower with increasing energy. In the spark chamber electron/positron pairs produced by the incoming γ-ray gave the information required to reconstruct the energy and direction of the photon. The PSF also

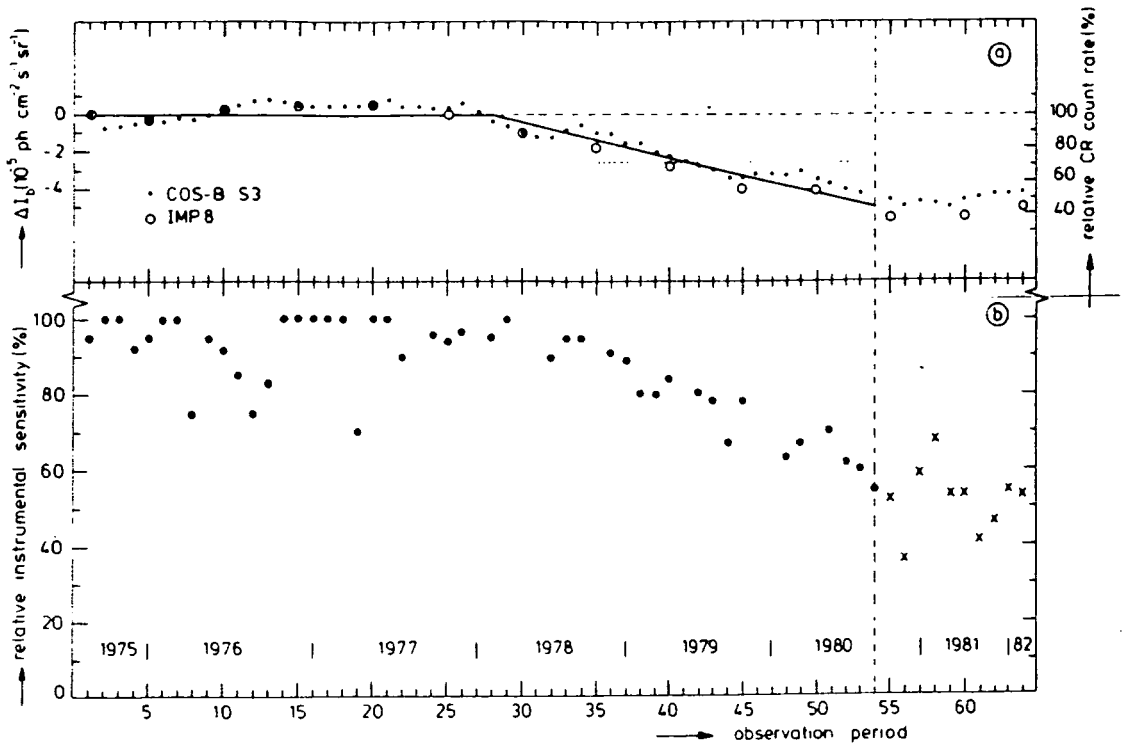

Figure 1.2.

a. Variations of the instrumental background at 70–5000 MeV (left-hand scale) and the relative variations of the CR particle count-rate (right-hand scale) as measured by COSB S3 scaler. The thick curve indicates the smoothed low-latitude instrumental background.

b. Relative sensitivities of the 65 observation periods of COSB. See Bloemen 1985 for details.

depends on the pair opening angle used in the selection of acceptable events. For each observation period, which lasted from 10 minutes to 10 hours, the exposure was calculated along with corrections for various instrumental effects. In total there were 65 pointing directions over the seven years covering all of the galactic plane.

All these data are contained in the final COSB database available on magnetic tape as a suite of programs with the data sets themselves. The γ-ray data are in the form of records containing all the information available about each photon and maps of γ-ray intensity can be constructed with a variety of parameters. The energy interval, pair opening angle, background spectral index and other selection criteria to do with the observing conditions can all be specified. The COSB manual provides guidelines as to the preferred or

recommended values of these parameters.

The smallest bin of the data is a 0°.5 × 0°.5 pixel. The γ-ray intensity over larger regions can be calculated using the following expression:

$$I_\gamma = \frac{\sum N_i - \sum \Delta N_i - I_b \cdot \sum E_{b,i}}{\sum E_i} \qquad 1.1$$

with an error for large N of:

$$e_\gamma = \frac{\sqrt{\sum N_i - \sum \Delta N_i}}{\sum E_i} \qquad 1.2$$

Here, N_i is the number of γ-ray photons in the i-th bin, ΔN_i is a correction for each bin based on the observing conditions, E_i and $E_{b,i}$ are the exposures for the source and background respectively. I_b is the background intensity for the particular energy band, given in the COSB manual.

This construction means that in order to correctly calculate I_γ there must be bin by bin summing of N_γ and the exposures over the bins involved. The value of I_γ for a region cannot be just the average of the intensities for all the bins, although if the number of γ-rays is large, then the difference between these two methods is not significant and in some cases, the easier method of averaging intensities may be used provided a less accurate result is acceptable.

The improvement in resolution with increasing energy is an important property of the COSB telescope enabling finer detail to be distinguished provided the region of interest is uncluttered. The unfortunate effect of using higher energy bands is that the number of γ-rays decreases and the statistics become much poorer. Often there is a trade off between these two features, usually in favour of better counting statistics. The main cause of the poorer resolution at lower energies is the multiple scattering of electrons in the tungsten sheets in the spark chamber.

The PSF has been published in the COSB manual for the three standard energy bands of 70–150, 150–300, and 300–5000 MeV for various pair opening angles as shown in Figure 1.3; this figure gives the normalised profile for the three standard energy bands. It takes the form of a sum of six Gaussians with

variable amplitudes and is considered reliable for only the given parameters and energy intervals. An earlier form of the PSF does exist in the form of an exponential (see Chapter 2) published by Hermsen (1980) which can be used for any energy interval by interpolation of the curve parameters from the figures in his thesis. This is adequate for non-standard energy bands, but the resulting PSF is not believed to be as good a representation of the actual form of the beam.

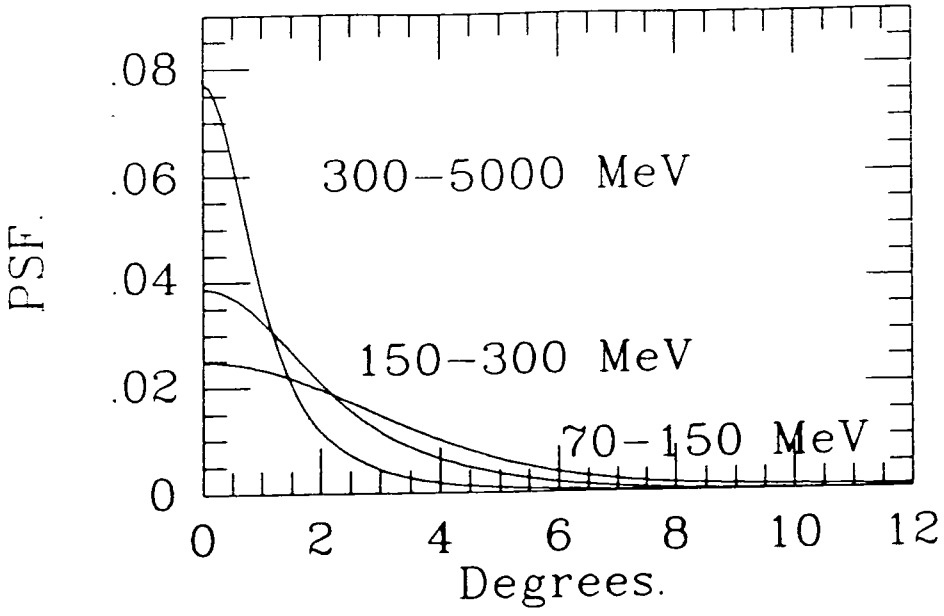

Figure 1.3.
Point spread function for the three standard COSB energy bands giving the probability per unit solid angle to measure a photon at an angle θ degrees from the incidence direction. The curves are normalised to unit area.

The telescope has a half width at half maximum at the lowest energy band of 3°.5 which drops to 1°.1 for the highest. The resolution is very poor compared to that available at other wavelengths, but γ-ray astronomy is still in its infancy, and these are a significant improvement on earlier balloon-borne experiments, and better than the earlier satellites such as SAS II.

A knowledge of the PSF is crucial for work with observations at other wavelengths which are usually at much higher resolution.

1.3 γ-rays.

1.3.1 γ-ray Sources.

The ratio of intensities between γ-rays and CR at energies of a few GeV is $\sim 10^{-6}$ which would seem to indicate that γ-rays are not a significant part of the radiation detectable at the Earth compared to the bulk of that detected. The overriding factor is that γ-rays are undeflected in their traversal of the Galaxy unlike the charged CR so despite the poor statistics, a great deal of valuable information may be obtained. At the γ-ray energies detectable by COSB, propagation losses by pair production and inverse Compton scattering are negligible.

Of the total detected radiation, some is due to γ-ray sources such as the Crab and Vela pulsar. Hermsen (1980) lists those sources detected by COSB along with suggestions for their identification. Some are unambiguous: those associated with pulsars and the high latitude source attributed to 3C273. Some are probably the result of enhancements in the gas (e.g. the Carina and Cygnus regions) which may or may not contain genuine sources as well, and one (Geminga) has not yet been definitely identified at other wavelengths. There is also a diffuse component arising from general CR-gas interactions as distinct from 'sources' due to higher density gas, and a possible unresolved source contribution, currently estimated at 10–20% of the flux (Protheroe *et al* 1979, Houston and Wolfendale 1983,1984, Fichtel and Kniffen 1984). However, in the outer Galaxy, and at high latitudes all the sources should be resolved.

Given the existence of these γ-ray sources, it must be asked whether these are also CR sources with interactions with the gas surrounding the source responsible for the γ-ray emission. To ask this requires some understanding of the CR-gas interactions that can occur both near the sources and also in the

interstellar medium.

1.3.2 γ-ray Production Mechanisms.

The interaction of electrons with the magnetic field has already been mentioned, although the production of γ-rays by the synchrotron process is reserved for very high energy particles and/or very intense fields. The intensity of γ-rays from bremsstrahlung near gas atoms falls off with energy as a power-law and dominates photon production methods for γ-ray energies below about 100 MeV. The Inverse Compton process occurs when a low-energy photon scatters off a CR particle and the photon ends up with a higher energy. The source of the photons that are elevated to γ-rays can be starlight or even the 2.7K background if the energy of the particle is high enough. For nuclei, the main source is via proton-proton collisions with the gas in the interstellar medium: a proton-hydrogen nucleus collision will produce π_0 mesons amongst the reaction products. The required threshold energy, T, is easily calculated for this reaction as:

$$T \equiv E - m_p = 2m_\pi + \frac{(m_\pi)^2}{2m_p} \qquad 1.3$$

inserting the appropriate values yields $T = 296$ MeV. The neutral pion decays isotropically in its rest frame into (usually) two photons giving a peak in the γ-ray spectrum at $m_{\pi_0}c^2/2 = 67$ MeV. There are other reaction products: Σ_0 hyperons and secondary π_0 from the decay of kaons contribute a small part of the total γ-radiation.

γ-ray emission from the radioactive decay of certain nuclei (such as ^{26}Al) has also been observed. Such measurements serve to place constraints on nucleosynthesis in stars and/or SN which then has a bearing on questions about the early history of the Solar System. The electron and positron annihilation line at 0.511 MeV has also been observed showing that positrons do occur in the Galaxy formed as the result of spallation reactions by CR on gas nuclei and by pair production by photons in the vicinity of one of these nuclei.

Generalising, the higher energy (> 300 MeV) photons are produced mainly from protons whilst the < 100 MeV photons come from electrons.

A definite signal from nuclei (mainly protons) has yet to be discovered. However, there are reasonable indications that CR nuclei are present in particular sources such as some SNR. The evidence for electrons is far easier to observe: for example, the Crab pulsar and remnant have synchrotron, X-ray and γ-ray measurements all consistent with electrons being present in the remnant, which when combined with the observation that the pulsar powers the remnant, indicates that it must have CR electrons as part of the energy budget along with magnetic fields and the thermal and bulk motion of the gas.

1.4 Gas.

1.4.1 Observations.

Where there is no gas, the only source of γ-rays is the interaction of a radiation field with CR via inverse Compton scattering provided there is sufficient energy. Where the radiation field required for this process does not have sufficient numbers of photons to make the intensity of resultant γ-rays significant (i.e. observable), no gas means no emission. This occurs for volumes of space such as the Outer Galaxy where the starlight photon field (for instance) is much less than the inner regions. As a consequence, the amount of target material is of great importance when estimating the CR flux along a particular line of sight. The bulk of the gas in the interstellar medium is hydrogen both in atomic and molecular forms. It is the column density of this gas that is needed for comparison with the γ-ray intensity along the same line of sight.

Observations of atomic hydrogen can have a very high resolution especially interferometric measurements which can reach down to the milliarcsecond level. For the large scale surveys of the Galaxy much poorer resolution is sufficient and is indeed necessary to enable the observations to be

performed without excessive observation and data processing times. The HI 21cm data used in this thesis is a composite low resolution survey of the whole sky made up from surveys by Heiles and Cleary (1979) for latitudes above 10° and Weaver and Williams (1973) and the Durham–Parkes survey of Strong *et al* (1982) $|b| < 10°$. A spin temperature of 135 K was assumed in correcting for saturation effects which although a rather simplistic approach, should not produce unacceptable errors (Strong *et al* 1982). The data above 10° were assumed to be optically thin. The average resolution was 72.6 arcminutes.

Molecular hydrogen does not have any convenient emission lines and so cannot be observed directly unless the gas is hot when it can be seen at micron wavelengths. Such conditions occur deep inside molecular clouds in active star-forming regions and constitute a tiny fraction of the total, mostly cold, gas. For this reason, an indirect method is used. ^{12}CO radiates at 2.6 mm via its $J = 1 \rightarrow 0$ rotational transition which is thought to be excited by collisions with molecular hydrogen. The conversion between ^{12}CO and H_2 is the subject of much controversy and is discussed in the next section. There are two surveys of the sky in ^{12}CO, the first by the Massachusetts Stony Brook group using the Five College Radio Astronomy Observatory at the University of Massachusetts in the greater detail and covering only approximately the first quadrant within a degree of the Galactic plane at a resolution of 50 arcseconds (FWHM). The second by the Columbia group (Dame *et al* 1987) covers the whole longitude range extending to ±5° in latitude and sometimes higher. The resolution is poorer (0°.5 at worst) and the sky is undersampled diluting the signal at large distances. This gives rise to the allegation that the Columbia group missed the cold clouds which are fairly uniformly distributed in the Galaxy according to Solomon, Sanders and Rivolo (1985) and that they see only the warmer clouds which tend to congregate more in the spiral arms. It would of course be best to use the fully-sampled dataset for this work with γ-rays as the quantity of gas is vital to the search for CR and their sources. However, in the regions of interest in this thesis, the Columbia survey is the only one available and has therefore been used exclusively.

Ionised hydrogen is also present in the interstellar medium appearing mainly as HII regions where recombination occurs. These protons also form targets for CR, but the column densities involved are much lower than the

atomic and molecular components so with the large bins used in this thesis (at least $0°.5 \times 0°.5$), the ionised gas can be ignored.

The binning of both the atomic and molecular gas received on magnetic tape is $0°.5$ and both must be convolved to the PSF of the γ-ray telescope before any analysis can be made. This is done by deconvolving the gas data using the original telescope beam (or an approximation to it based on the sampling of the data), to give a map of the sky as seen with an infinite resolution beam. This is then convolved using the COSB profile to give the gas data as seen by a telescope with the same resolution as COSB. As this changes with the parameters selected, the convolution must be performed for each parameter set. The higher energy bands give a noticeable improvement in resolution of the data and result in quite different numbers for each bin especially where the gas column density is low. It is therefore crucial that the appropriate resolution gas data are used with the corresponding resolution γ-ray data.

1.4.2 CO to H_2 conversion.

The conversion of ^{12}CO to molecular hydrogen is achieved by multiplying the antenna temperature of CO in K kms^{-1} by a constant to give a column density af molecular hydrogen in atoms cm^{-2} thus:

$$N(H_2) = \alpha_{20} \times 10^{20} \int T(v)dv \qquad 1.4$$

The constant used here known as α_{20}, is not to be confused with the X of some authors which gives the number of *molecules* of hydrogen: α_{20} is simply twice X. Such an equation is not theoretically correct for the usually optically thick ^{12}CO but empirically it follows the much less abundant and usually optically thin ^{13}CO. Equation 1.4 is therefore correct for the range of values normally found in molecular clouds.

The value of α_{20} is the subject of some debate as various methods have given widely differing results over the past decade or so. Fortunately, there seems at last to be a convergence of estimates from these methods. Values tended to be higher in the past with the early ^{12}CO measurements of Solomon

and Sanders (1980), and Solomon, Sanders and Scoville (1979a,b) using the Stony Brook telescope and employing local thermodynamic equilibrium arguments. Visual extinction data from star counts and infra-red measurements have also been used (Sanders 1981, Solomon, Sanders and Scoville 1984). More recently, techniques for estimating the masses of clouds in the inner Galaxy using the virial theorem have been developed.

γ-rays have also entered the debate as a useful tool for this kind of work (Strong *et al* 1987, Bloemen 1986, Richardson 1988). Assuming interactions of CR with the interstellar medium and including an inverse Compton component allows an estimate of the total column density of gas to be made, given certain assumptions about the CR flux. Further, if CR are not excluded from clouds and the ionized gas component is small (as is expected), then α_{20} can be determined as the atomic hydrogen density is known from 21cm measurements. Methods of estimating α_{20} can be found in a number of wavelength bands and they are not restricted to just the gas data themselves. Bhat *et al* (1986c) using a variety of techniques including γ-ray, X-ray, infra-red and virial methods, find $\alpha_{20} = 3 \pm 1$ with a decrease towards the Galactic Centre. Unfortunately, the CO emissivities themselves are significantly different between the two telescopes. This further source of disagreement has a number of causes (Bronfman *et al* 1987) including different statistical analyses and instrumental calibration.

The recently published Columbia CO survey (Dame *et al* 1987) is now self-consistent unlike the earlier work from this group because the azimuthally averaged emissivities can be used to reproduce the intensities integrated over velocity and latitude. (See Bhat *et al* 1986c).

The most recent estimates of α_{20} have an average of about 4.5 ± 2 with the trend converging on about 4. In the absence of any better estimates, and to be mostly consistent with the γ-ray analysis of the COSB and Durham groups, it is this value that has been adopted throughout this thesis.

1.4.3 γ-ray Emissivity.

Having obtained the molecular hydrogen from the CO observations, the total gas column density for each bin can be calculated by adding the atomic and molecular components. It is this gas that forms the target material for CR and from these interactions γ-rays are produced. For a given CR flux, increasing numbers of γ-rays are produced for increasing gas density and this is reflected in the quantity known as emissivity per atom denoted by $q/4\pi$. In principle, this quantity should be theoretically calculable according to the equation:

$$\frac{q}{4\pi} = n \int I(E_p)\sigma(E_\gamma|E_p)dE_p \qquad 1.5$$

where n is the volume density of the target nuclei, $I(E_p)$ is the intensity of CR nuclei (i.e. mainly protons) of energy E_p and $\sigma(E_\gamma|E_p)$ is the cross-section for the production of γ-rays with energy E_γ from the CR protons. This cross-section is given by Stecker (1971) as an integral over the energies of the pion created in the collision. It is not well known especially at high energies but at low energies a reasonable fit to the experimental data is a reaction that proceeds via a nuclear isobar at 1.238 GeV. This model unfortunately requires an additional integration over the available isobaric energies (Dermer 1986).

The emissivity due to the bremsstrahlung process is given by Stecker (1975) as:

$$q(E_\gamma) = 4.3 \times 10^{-25} n \frac{I(>E_\gamma)}{E_\gamma} \text{atom}^{-1}\text{s}^{-1}\text{MeV}^{-1} \qquad 1.6$$

Again, this is uncertain and is dependent on the intensity of electrons which is not well determined.

The emissivity has been calculated by Bhat *et al* (1986b) using the π_0 decay emissivity spectrum given by Stephens and Badwhar (1981) and a bremsstrahlung estimate determined according to Equation 1.5. The spectra were both normalised by fitting to the observed emission and Figure 1.4 shows the result. Additionally, the fraction of γ-ray flux that can be attributed to nuclei at a particular energy range was determined and Figure 1.5 shows that

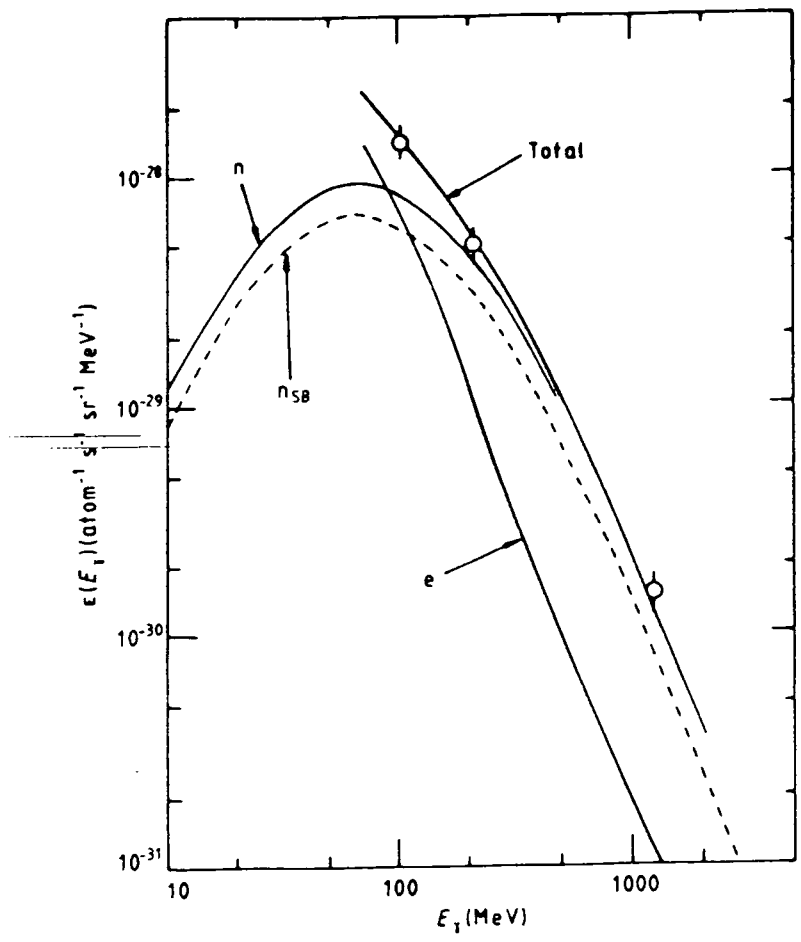

Figure 1.4.
γ-ray emissivity spectrum $\epsilon(E_\gamma)$ showing the nuclear and electronic components. Also shown is the Stephens and Badwhar (1981) estimates, denoted n_{SB}. The circles are from Strong (1985) showing 67% confidence limits and are plotted assuming the spectrum to have an E_γ^2 shape. Figure is taken from Bhat *et al* 1986.

the proton component dominates at the two higher energy bands of the COSB telescope. The significance of this is that solar modulation which affects the proton spectrum below about 1 GeV should not affect the determination of $q/4\pi$. Greater confidence can be placed in the γ-ray techniques as a result.

The local emissivity, representing the local CR flux, can be used as a guide for what may be expected elsewhere in the Galaxy. Naturally, the emissivity depends on the galactic location and the availability (or not) of CR acceleration sites. Dividing the observed emission by the total gas density along the line of sight gives the emissivity and where this is high, the CR intensity over that line of sight can be said to be high also. Some other information — such as the distribution of gas in the area — can, in some cases, be used to predict the location of the bulk of the emission and the

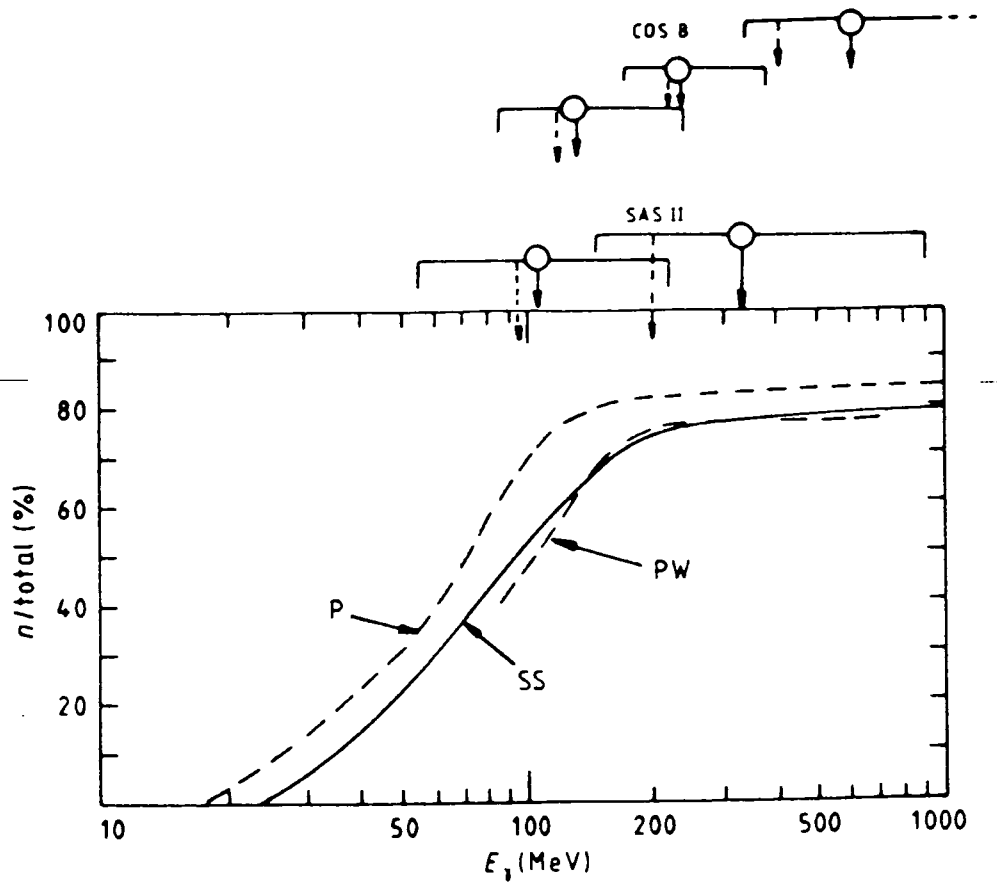

Figure 1.5.
Fraction of γ-rays due to the interaction of CR nuclei as a function of γ-ray energy. The median energies of the energy bands for the two telescopes are shown. Refs. P: Poon (1983) local spectrum. PW: Bhat *et al* 1986. SS: Sacher and Schonfelder (1984) anti-centre spectrum. Figure is taken from Bhat *et al* 1986.

enhancement in the CR intensity. Genuine γ-ray sources such as the Crab, Vela and Geminga must, of course, be removed from the γ-ray intensities first before calculating the emissivity. Removal of these γ-ray sources is not always an easy task, as it requires a model for the object in question to determine the expected number of photons produced. If the source is expected to be point-like, then there are methods of estimating the flux from the source by using 'correlated counts' (See Appendix A).

1.5 Summary.

The question of the origin of CR is important and far-reaching in its

implications for contemporary astrophysics. The answer will provide powerful insights into many realms of research, ranging from the origin of the universe, the creation of the solar system and conditions favourable for life, to the processes of star formation and Galaxy evolution. Without good models for the many ways of imparting energy to nuclei and electrons, much of the information contained in the CR raining down on the Earth's atmosphere is lost and to neglect them is to ignore a full third of the energy budget of the Galaxy. For example, it is perfectly acceptable to model the turbulent motions of gas in magnetic fields, uncovering the processes of star formation and the production of radiation during the lifetime of the bulk of a galaxy's mass, but it is absurd not to incorporate CR which contain such a large quantity of energy, have a profound effect on interstellar processes and contain a 'potted history' of the Galaxy.

This chapter has introduced the various components for the study of Galactic CR involving γ-rays and gas as well as the sources of the particles themselves in the shock acceleration process. Some of the limitations of the observations and the models have been noted and some of these will return to frustrate the analysis in the following chapters.

This study makes a two-pronged attack on the problem. Firstly, by considering the indirect evidence for CR and their action in the interstellar medium, namely that of producing γ-rays. Secondly, an alternative approach that considers their action local to the Solar System as a result of assuming a certain model for their production and time evolution.

The γ-ray observations that have been described in earlier sections have been employed in pursuing evidence for CR acceleration in two particular regions of the Galaxy: around the Vela pulsar (Chapter 2), and surrounding η Carinae (Chapter 3). Both these objects are listed as γ-ray sources, but they have very different properties reflecting two very different potential CR acceleration sites. This is significant as it reflects the Galaxy-wide nature of these particles and their effects in different astrophysical situations.

The second prong to the study is by considering the direct effect of CR on the energy density of the interstellar medium near the Solar System over very long timescales (Chapter 4). This work has relevance in non-astrophysical

fields such as geophysics, and provides a link between the Galactic scale and local phenomena. In some senses, this work is more directly connected to the CR as they produce tangible evidence on the Earth's surface, in the atmosphere or in interplanetary space in the form of radionuclides. Unfortunately, the measurement and interpretation of this evidence is still a young science and further work is still in progress to strengthen the conclusions already obtained. This work provides useful guidelines and is a powerful incentive for further measurements. Such study may provide answers to important geological and geophysical questions involving the mass extinctions of flora and fauna and the past history of the Solar System.

Finally, the conclusions are summarised in Chapter 5 with an examination of the prospects for future work.

Chapter 2. The Vela Region.

2.1 Introduction.

The Vela pulsar dominates the γ-ray sky in the anti-centre region of the Galaxy. It is the relatively small distance of this object from the Sun (about 0.5 kpc) that makes it so prominent as it is actually four times less luminous than the second highest flux source in Hermsen's (1980) γ-ray source catalogue, the Crab. With a flux above 100 MeV of 13.2×10^{-6}ph cm^{-2}s^{-1}, Vela has a flux $2\frac{1}{2}$ times greater than the Crab.

The proximity of Vela allows detailed studies of its properties at these high photon energies which complement observations at optical, radio and X-ray wavelengths.

The γ-ray signal is pulsed at the pulsar radio period which makes the source unambiguously identified with the neutron star. Comparison with the Crab enables constraints to be placed on the production mechanisms for these high energy photons, as well as highlighting some differences between the two sources. For example, the ratio of pulsed luminosities ($L_{\rm Crab}/L_{\rm Vela}$) is $\sim$8 for γ-ray energies above 100 MeV from SAS II (Thompson *et al* 1975, Ögelman *et al* 1976), $\sim$ 80 for 1 keV X-rays (Harnden and Gorenstein 1973), whereas for X-rays with energies between 1.5–10 keV, the ratio is $\sim$ 1000 (Rappaport *et al* 1974) and is $\sim$ 5000 at visible wavelengths (Kristian 1970, Lasker, Braker and Saá 1972). This implies that the various photon production mechanisms of the two pulsars in the above respective energy bands may be distinct. Alternatively, the differences may simply arise because the Crab is a much younger pulsar than Vela. The point to note is that conclusions about the Crab, which is possibly the most studied extra-solar object, cannot necessarily be applied

to Vela. The Crab pulsar is the remnant of the supernova (SN) explosion that was recorded by the Chinese in 1054 AD (Clark and Stevenson 1977) and thus its age is very well determined. Vela, on the other hand, has age estimates ranging from (1–10) $\times$ 10^4 years (Reichly, Down and Morris 1970, Radhadkrishnan *et al* 1969) although suggestions have been made recently that this range could be too high by a factor of two (Stothers 1980) and a figure between (5–8) $\times$ 10^3 years might be more accurate. Whatever the value, Vela is considerably older than the Crab and this is reflected in the major difference between the two: the prominence of the associated supernova remnant (SNR). The Crab Nebula is the first object in Messier's catalogue which reflects its importance in astrophysics: a whole IAU Symposium has been dedicated to its study. In contrast, Vela has a much fainter remnant, insignificant when compared to the Crab in the optical waveband, but with a radio flux that is greater in magnitude and extends over an area $\sim$50 times that of the Crab SNR. The morphology of the two objects is considerably different as the Crab SNR is a plerion or 'filled-centre' remnant, whilst the Vela remnant is a large shell seen in both radio and X-rays (Milne 1980, Kahn *et al* 1985, Harnden *et al* 1985). There is some confusion about whether there is more than one remnant in the region. The whole complex is denoted Vela XYZ, referring to the three radio regions of which some observers believe to be a single object. Vela X has sometimes been classified as a separate plerionic remnant (see the review by Weiler and Panagia 1980). Milne and Manchester (1986) find three good reasons why Vela X is not a plerion but simply an enhanced section of the whole remnant. They base their arguments on observations in X-rays, on measurements of the pulsar position (which is not coincident with Vela X) and on improved fluxes at various radio wavelengths that give new estimates of the spectral index.

Vela X is half the size of the whole complex which measures some 5° in diameter. It seems likely that there is but one remnant in the region with Vela X being powered less directly by the Vela pulsar than the Crab Nebula is powered by its pulsar. The Crab appears to be expanding with an input energy equal to the energy loss of the pulsar as measured by its spin-down rate.

The estimated ages of the Vela pulsar and remnant have been used as

evidence that the two are associated and are the result of the same SN explosion. Stothers (1980) argues that because the true pulsar age is usually less than the characteristic age (given by $\tau = P/2\dot{P}$) then the pulsar should be 5000–8000 years old. The Vela remnant is usually quoted as having an age $\sim 10^4$ years based on assumptions about its initial energy, its pre-supernova gas density, and whether or not the remnant is currently in the Sedov phase.

Recent observations of the pulsar (supposedly Lasker's (1976) M star) have shown that it has a very small proper motion. This has lead to claims (Bignami and Caraveo 1988) that the association of the remnant with the pulsar is doubtful since it could not have moved from the geometrical centre of the remnant in the time available. Larger ages are proposed to preserve the association, but must be rejected in the light of evidence from the SNR itself (Stothers 1980). The measurement of the proper motion is a useful observation but cannot alter the similar dispersion measure and distance estimates of the two objects. The biconical model of Manchester (1987) predicts a small proper motion and is capable of of explaining not only the Vela remnant's complex morphology, but also the numerous exceptions to the standard model of a spherical remnant expanding into a homogeneous medium.

There are still many problems, however, and considerable improvements can be made both in the observations and the theory of the Vela region. This chapter makes a contribution from the γ-ray region of the spectrum. The brief review above of some properties of the Vela pulsar and a comparison with the Crab pulsar is necessary as the pulsar itself is not the main subject of this chapter. The Vela pulsar is a prime candidate for the production of cosmic-ray particles (as well as γ-rays directly) and these should manifest themselves by interacting with the gas around the neutron star and producing an extended emission region or 'halo' of γ-rays around it. It is these γ-rays, produced by CR solely from the pulsar and not part of the the general Galactic flux, that are being sought in this chapter. To remove all the other γ-rays requires a knowledge not only of the atomic and molecular gas and the pulsed fraction of γ-rays, but also the point spread function (PSF) of the telescope. The latter must be well understood because a knowledge of the photon distribution around the object is critical in order to remove the pulsed γ-ray component. The 'background' contribution to the γ-ray intensity is defined here as that

produced by ambient CR interacting with the gas. To remove this component it is necessary to assume values for the conversion ratio from CO to H_2 (α_{20} with units of 10^{20}atoms $cm^{-2}K^{-1}kms$) as well as the γ-ray emissivity so that the amount of molecular hydrogen can be obtained and then the expected γ-ray intensity produced by it can be calculated. Thus:

$$I_\gamma = q/4\pi(N_{\rm HI} + \alpha_{20} W_{\rm CO})$$

where $W_{\rm CO}$ is the velocity-integrated CO antenna temperature in K km s^{-1}. If there is any signal remaining after these various subtractions, and if no other explanation can be found, then the possibility that the signal is genuinely the result of CR diffusing from the pulsar or the SNR and not due to the general ambient CR flux must be seriously examined. The details of the acceleration mechanism are not relevant here, but the aim of the analysis is to see whether there are both electrons and nuclei being accelerated by the pulsar and/or remnant. It is possible (though unlikely) that the SNR is solely responsible for the acceleration of these particles and some attempt must be made to see how this idea fits in with earlier work done using γ-rays from SNR (e.g. Bhat *et al* 1986a,b, Bhat *et al* 1987). Theoretical predictions of the fraction of the initial energy of the SN (E_0) that is in the form of CR at a given time are based on the work of Blandford and Cowie (1982). These authors show that by the time a SN reaches the end of the Sedov phase of its expansion, as much as 50% of E_0 could be carried by CR. According to this theory, the larger, older remnants should be the ones that are prime CR accelerators. In this respect, Vela is a better candidate for this analysis than the Crab. Other remnants have been studied for evidence of CR production. Loop III has been analysed by this author (§2.3.2) (Rogers and Wolfendale 1987) and Bhat *et al* (1985b) examined Loop I, using both γ-rays and radio data.

Continuing the study of remnants in this fashion requires that the various components of the emission from the Vela region be examined. This study breaks new ground by virtue of the presence of the pulsar.

2.2 γ-rays.

2.2.1 The Point Spread Function.

The general form of the COSB telescope PSF has been published by Hermsen (1980) as an exponential thus:

$$f(\theta_x, \theta_y) = exp(-(\theta_x^2/a^2 + \theta_y^2/b^2)^c) \qquad 2.1$$

where the θ_i are the distances in degrees from the beam centre in two orthogonal directions, and a, b are constants for a given latitude or declination. Near the Galactic plane or near the celestial equator, the function is circularly symmetrical and $a = b$. Nearer the poles, a and b can be adjusted to give the appropriately shaped PSF. c is a constant dependent on energy and pair opening angle. When $c = 1$, this gives a Gaussian function, whilst $c = 0.5$ gives a genuine exponential. The function f gives the angular distribution of photons around a point source. This earlier version is not the most accurate description, as there is an extended 'tail' at large angles from the beam centre. A later, more accurate version takes the form of a sum of six Gaussian distributions each with different widths and amplitudes. The PSF is dependent both on photon energy and the pair opening angle of the electron/positron pair in the detector, as well as on other parameters. The manual to the final COSB database (Mayer-Hasselwander 1985) gives the dependence of the PSF on these parameters for three standard energy bands and quotes the fitted amplitudes of six Gaussians for fixed widths of 16,8,4,2,1 and 0.5 degrees which are summed to give f. It is useful to determine the PSF for non-standard energy bands, not only as a check on the behaviour of the COSB telescope at these energies, but also to enable the improved resolution at higher energies to be used to investigate the γ-ray sky in greater detail. Knowing the PSF for non-standard energy bands (i.e. not 70–150, 150–300 or 300–5000 MeV) permits the gas data to be convolved to these non-standard bands. This is necessary if emissivities are to be calculated as accurately as possible. The data given in the COSB manual come with a recommendation not to interpo-

late the amplitudes of the fitted functions to other energies and pair opening angles, as this will not result in appropriate PSF's for those parameters.

One way of finding the PSF for the non-standard energies or other non-standard parameters is to examine a bright point source and to fit a profile to the observed emission. The problem is to distinguish between those γ-rays that come from the source and those which form part of the general 'background' (i.e. non-source) and tend to blur the distribution. A pulsar is ideal for this purpose as the timing can be used to select only pulsed γ-rays which are known to come from the point source. Inevitably, there may be some background contribution when this phase selection is performed since the pulsed phase bins cannot be made too narrow as the signal-to-noise ratio becomes very poor.

Using the COSB database, photon numbers in annuli around the source with phases corresponding only to source pulses were counted. Figure 2.1 shows the distribution with distance from the source of pulsed γ-ray numbers (N_P^*) for the three standard energy bands, along with the 'Gaussian' PSF taken from the COSB manual estimated with the same parameters as those employed to construct the map of γ-ray intensities used for the flux analysis. The PSF is normalised to unity at 0°.5. The correspondence between the pulsed signal and the published PSF is reasonable in all three bands, even with the relatively broad annuli used here. The non-pulsed component is defined as:

$$N_{NP}^* = N_T - N_P^* \qquad 2.2$$

where N_T is the total number of γ-rays observed in the annulus. N_T is also plotted in Fig. 2.1 and gives a first indication of the background from the gas around Vela (i.e. the non-source emission) as it is broader than the pulsed component. Indeed, this is what would be expected if most of the non-pulsed component were coming from the gas around the pulsar rather than appearing as an unpulsed ('DC') signal direct from the source. However, the non-pulsed fraction (N_P^*) contains significant contamination from the pulsed emission because the pulses have non-zero temporal width. In addition the pulsar, in common with others of its kind, exhibits an 'interpulse' that is part of the genuine pulsed signal (the 'AC' part); if the pulsed beam were somehow switched off,

the interpulse would disappear along with the pulse spikes.

To estimate the true pulsed γ-rays requires a knowledge of the non-pulsed emission which, for the purposes of this thesis, is taken to mean everything coming from the Vela region that is not associated *directly* with the pulsar i.e. does not have an angular distribution of photons that is consistent with a point source. Figure 2.2 shows a stylized pulsar phase histogram that defines the eight regions used here. N_P^* corresponds to N_{BDFH} since the phase selection can only divide the histogram vertically. N_{AE} is the non-source background detectable by phase selection and is used to estimate the number of background γ-rays in the other bins i.e. N_{BCD}. With such a division using the phase selections indicated in the figure, the genuine pulsed component N_{FGH} corresponds to $N_T - 2N_{AE}$ whilst the non-pulsed photon numbers is just $2N_{AE}$. This is because the phase division used here gives half the total phase to N_{AE}, so N_{BCD} is expected on average to equal N_{AE}, assuming this non-source background is flat with phase which should be the case if no pulsed γ-rays contaminate it. This process of dividing the phase histogram can only give a good estimate of the number of pulsed and interpulsed photons if N_T (and hence usually N_{AE}) is large and the averaging is therefore reliable. The advantages of this method of estimating the number of pulsed photons instead of just N_P^* are that not only are a larger number of γ-rays involved in estimating the PSF, but also the non-pulsed component should be free of any direct pulsed emission from the neutron star thus making the identification of the γ-rays produced by the CR from the pulsar more certain.

Using 800–5000 MeV γ-rays from Vela, the pulsed phase selection can be performed according to Fig. 2.2 and the number of photons per unit solid angle can be plotted against distance from the source. The background N_{AE} can be obtained from the database and the genuine pulsed signal estimated. Figure 2.3 shows the resulting normalised distribution of photons as a function of distance from the source compared to that measured at 300–5000 MeV. Also shown is the distribution expected for this lower energy band from the COSB manual. As expected, the width at half maximum is narrower, suggesting an improvement in resolution with increasing energy. The half-width at half maximum is 0°.8 at 800–5000 MeV compared to 1° at 300–5000 MeV which is itself slightly lower than the value of 1°.1 quoted by COSB for the 300–5000

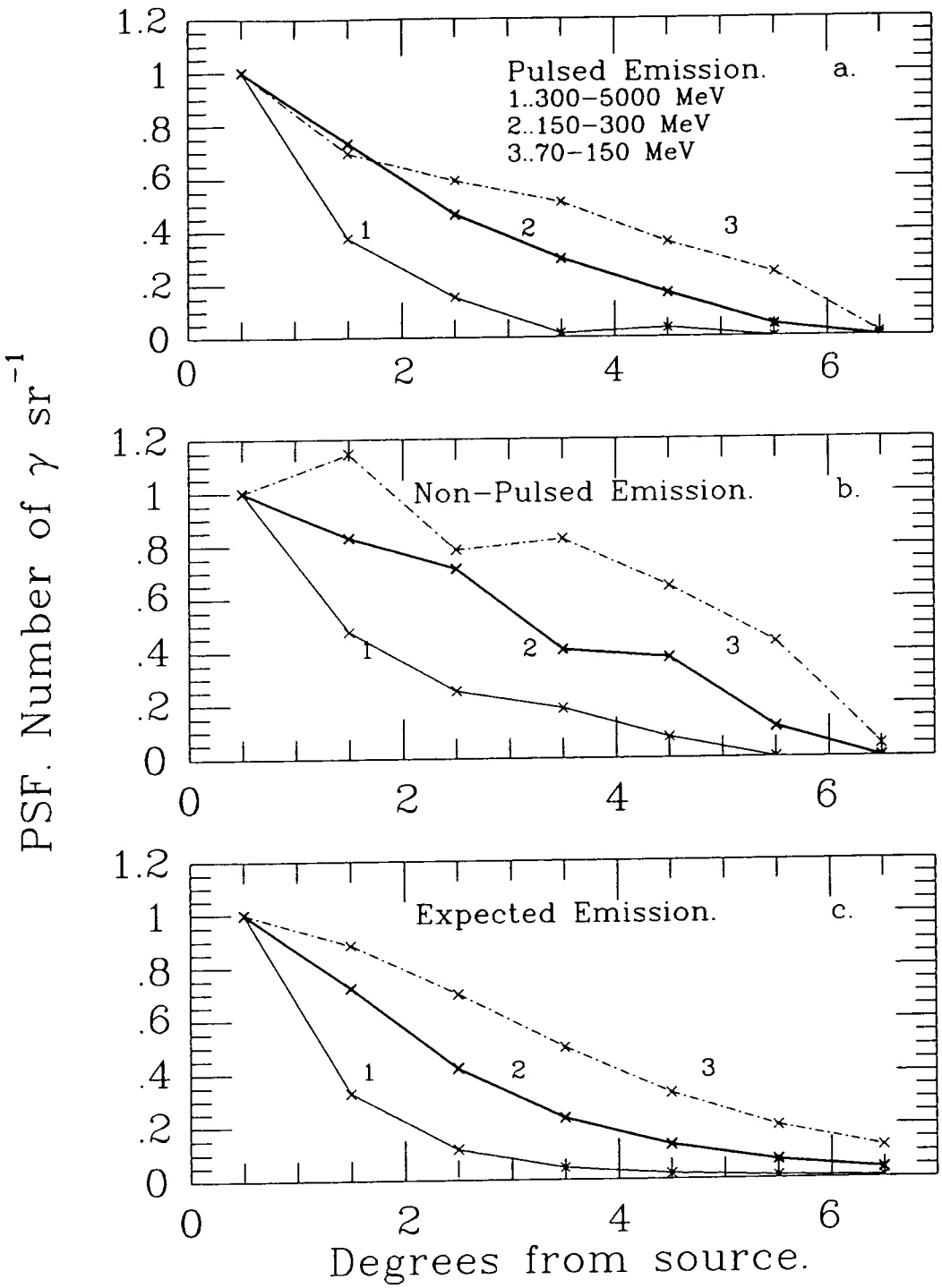

Figure 2.1

Distribution of number of: *a.* pulsed (N_P^*). *b.* non-pulsed (N_{NP}^*) γ-rays for the three standard COSB energy bands normalised at 0°.5. *c.* The PSF as determined by the summation of six Gaussians.

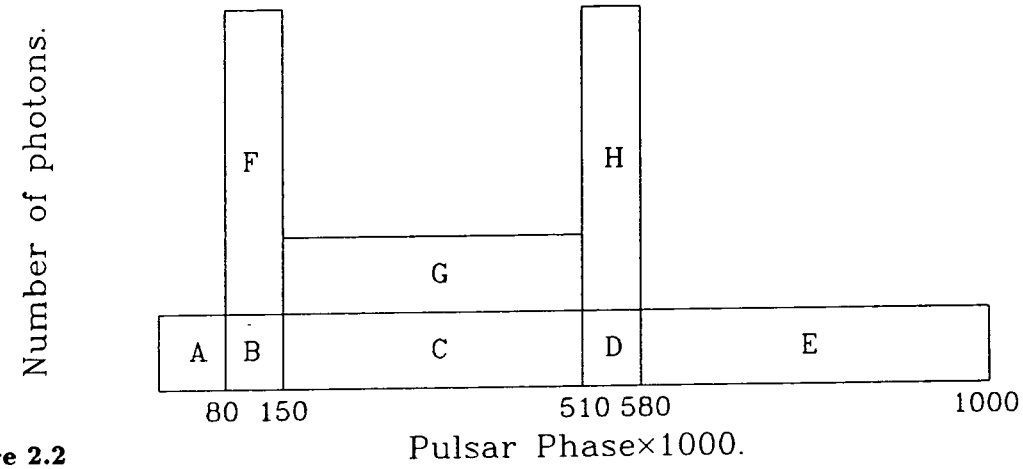

Figure 2.2

Stylised pulsar phase histogram showing actual phase divisions. See text for meaning of each block.

MeV band.

The 300–5000 MeV photon number distribution (Fig. 2.1a) does not match the expected curve (Fig. 2.1c) at all points and this can be attributed to three causes. Firstly, errors in the estimate of the background from N_{AE}. Secondly, statistical fluctuations in the numbers of γ-rays overall. Thirdly, the exposure of the telescope varies slowly across the whole region so the number of photons observed should be weighted accordingly i.e. by using intensities, which take into account the exposure in each bin. However, when phase selection is required, this weighting is not possible because the photons are gathered not only over a number of bins, but also from several observing periods each of which have different exposure histories. Thus each γ-ray would need to be treated on an individual basis. Such a process would yield little reward for the effort involved as the statistical fluctuations would still be present and dominate this third source of error. Bloemen (1985) does not consider the variation of exposure across the Vela region to be a significant source of error. He bases his conclusion on seven observation periods all having different telescope aspect angles to the pulsar and different exposures. This conclusion has been confirmed using all the data and the variation of exposure across the region

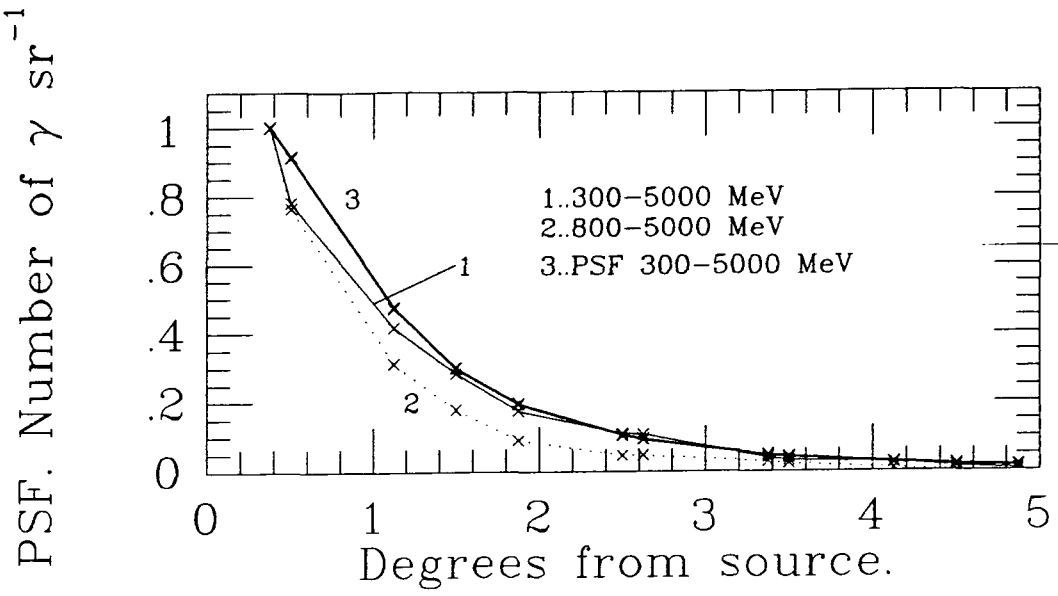

Figure 2.3

Distribution of the number of γ-rays per unit solid angle against distance from the source for two energy bands normalised to unity at 0°.375. The higher energy band is markedly narrower than the lower band. Also shown is the published COSB PSF.

in each 0°.5 × 0°.5 ($l \times b$) bin is less than 30%. The exposure variation is reduced considerably when annular bins around the source are used or the data are averaged in longitude and/or latitude. Fluctuations of exposure between annular bins are less than 1%.

The 800–5000 MeV photon number distribution behaves in the expected fashion; it has a long tail and is close to the 300–5000 MeV curve for small angles (Fig. 2.3) and the the values of the curve can be used to solve for the amplitudes of six Gaussians having the same widths as used in the COSB manual. It is not expected that these amplitudes will be similar to the published values, partly because of the warning given in the manual about interpolation, but also because the fit will be highly sensitive to any fluctuations in the data (see, for example, the range 2°.5–2°.7 in the 800–5000 MeV curve). Table 2.1 contains the results of fitting the Gaussian functions to both the 800–5000 and 300–5000 MeV data. They are normalised to give a value of 1.0 at $\theta = 0°.375$

Degrees from source	PSF 300–5000 MeV	PSF 800–5000 MeV
0.0	1.139	
0.375	1.0	1.0
1.125	0.4689	0.3238
1.875	0.1900	0.1086
2.625	0.0887	0.0490
3.375	0.0427	0.0286
4.125	0.0221	0.0078

Table 2.1

to facilitate comparison with the measured values. The photon number distribution (PSF) at 800–5000 MeV is also plotted in Figure 2.3 and the fit can be seen to be good over the whole range of angles used. This PSF could be used as an alternative to the earlier form given by Hermsen (1980) and does not require estimates of the parameters a, b and c from his figures of their variation with energy and pair opening angle.

2.2.2 DC Component.

The total γ-ray emission from Vela can be divided into its constituent components, thus:

$$N_T = N_P + N_{DC} + N_{CR} + N_{BGR} \qquad 2.3$$

where T = total, P = pulsed, CR refers to the γ-rays from CR that have diffused from Vela, whilst BGR refers to γ-rays produced by CR interacting with gas in the line of sight through Vela and are unconnected with it. N_{DC} is the number of γ-rays that come directly from the pulsar and are non-pulsed but follow the form of the PSF along with the pulsed γ-rays. Before any estimate of N_{CR} can be made (which is the goal of this study), this 'DC' component must be investigated. Grenier, Hermsen and Clear (1987) indicate that the non-pulsed emission is likely to be only a few percent at most, so this steady

component will probably be very small (if indeed it is present at all) and hence undetectable by the COSB experiment. To confirm or deny this proposition, the pulsed component must be subtracted from the total emission to reveal the non-pulsed component which will be made up of the last three terms of Eqn. 2.3 above. The analysis by Kanbach *et al* (1980) concludes that this DC component is less than a few percent of the total emission for all energies and is consistent with zero.

The γ-ray data in the 300–5000 MeV energy band have been summed in latitude from $-5°.25$ to $0°.25$ for each $0°.5$ interval in the longitude range $l = 255°$ to $l = 275°$ thereby ensuring that all of the Vela emission is included. Reducing the problem to one dimension facilitates the calculations and enables the distribution to be clearly visualised. A two dimensional analysis would decrease the number of γ-rays per bin; an accurate estimate of the non-pulsed contribution would not then be possible because of the larger statistical errors. The longitude range $258°.75$ to $268°.25$ was used to provide numbers of total and background (N_{AE}) γ-rays. The true non-pulsed number of γ-rays, N_{NP}, was set to twice N_{AE} since it is derived from precisely half the pulsar phase. The exceptions were when $2N_{AE} > N_T$, in which case N_{NP} was set to equal N_T, and beyond about 6° from Vela where N_P was assumed to be zero. The difference between total and non-pulsed numbers of photons gave the estimate for the pulsed contribution. If it is present, the DC component should have a similar angular distribution to the pulsed component.

The cross correlation method of Hermsen (1980) (see Appendix A) can be used to see if a non-pulsed signal with a spatial distribution similar to that of the PSF is present in the data. Performing this analysis with 20 bins and nearly 490 γ-rays gave a value of $C = -0.054$ and a significance $C/\sigma = 0.19$ indicating that the DC component is likely to be zero and thus can be ignored in Eqn. 2.3.

Increasing the low energy limit to 800 MeV and using similar binning to the 300–5000 MeV band gave a slightly more significant result: $C = 0.211$ with $C/\sigma = 1.47$ with 12.4 correlated counts with a significance of 1.38. These correlation coefficients are still small numbers and are well within the errors of both the data and the binning scheme. At the higher energy, the DC level

is also likely to be zero, although future studies need to check whether this steady component is energy dependent.

The analyses by Kanbach *et al* (1980) and Grenier, Hermsen and Clear (1987) divide the phase histogram more finely and include a 'trailer' to the second pulse in phase bins 0.58–0.77. In the present case, this phase interval is in bin 'E' i.e. in the background part of the phase. If the trailer were part of the DC level it might have been expected to be seen in this analysis, but no suggestion of a trailer has been seen at this higher energy band possibly because photon numbers are low. Grenier, Hermsen and Clear use 50–5000 MeV i.e. the whole energy range of the database and consequently have many more γ-rays in their phase histogram. The fact that a trailer was seen by these authors cannot be used as evidence for a possible energy dependence of any trailer because the phase intervals used in the present analysis are too broad.

It is perhaps not surprising that the DC level is low or zero considering the relatively low number of γ-rays. Its value is crucial however for estimating N_{CR} because, if it is significant, then many of the photons attributed to CR from the source would be assigned to the DC component. It is thus necessary to analyse the data in a different fashion using the angular distribution of photons rather than taking just a straight average through the source.

Constructing annular bins around the source gives a distribution of γ-rays that matches the PSF of the COSB telescope (§2.2.1). These data give one upper limit for the percentage contribution of the total flux that goes into the steady component. Estimating the pulsed component (N_{FGH}) from the phase histogram and dividing the non-pulsed by the pulsed number of γ-rays gives the maximum percentage of the pulsed photons that the DC component can have. This maximum implies that all the non-pulsed γ-rays in the central annulus are DC i.e. there is no contribution from CR interacting with the gas in the line of sight. This situation is obviously incorrect, but serves to place a upper limit on N_{DC}. For an acceptance angle of 1°, the DC component contributes a maximum of 13% of N_P. Restricting the angle to 0°.75 gives the same result. Above 800 MeV, the maximum DC contribution falls to 10%.

An improved upper limit for the DC component can be made by calculating the flux in each annulus around the source and varying the DC percentage

used. By assuming a certain uniform value for both the emissivity and α_{20} the γ-ray flux expected from the interstellar medium along the line of sight can be computed and subtracted from the non-pulsed part of the emission. The remainder consists of the contribution from any DC component and γ-rays produced by CR from Vela itself. Figure 2.4 shows the flux at an angle θ from the source for $q/4\pi = 0.61 \times 10^{-26}$ph atom^{-1}s^{-1}sr^{-1}, $\alpha_{20} = 4.0$ and various DC levels. (Henceforth, emissivity values will be stated in units of 10^{-26}ph atom^{-1}s^{-1}sr^{-1}). Clearly a DC contribution of 10% is too high and an upper limit of 8% is more acceptable, giving zero flux in the 2° bin. A closer inspection of these fluxes using narrower bins reduces this figure further to below 5%, but the errors on the points become too large for any definite conclusion.

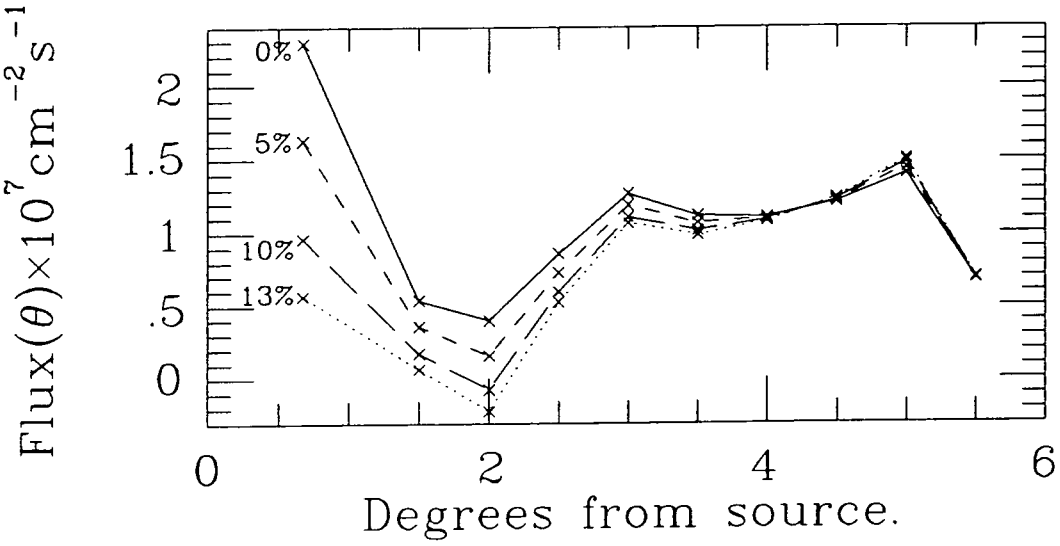

Figure 2.4

Variation of flux with angle from the source for the 300–5000 MeV energy band and various DC levels. The annular bin width is 0°.5

In summary, the upper limits for the steady component are consistent with those derived by Kanbach *et al* (1980) using different energy intervals and phase bins. The simplest 'best-estimate' is that the DC value is zero for all energy bands, although the possibility that it is non-zero has been considered in the following analysis.

2.2.3 Gas.

In order to estimate the contribution to the observed γ-ray flux from CR accelerated by Vela only, the gas distribution and the ambient CR flux must be known so that the γ-ray intensity expected from the gas in the source direction can be subtracted. The molecular gas distribution used here is derived from preliminary CO maps of the region supplied by Dame (1986) in advance of publication. When the final Columbia CO survey (Dame *et al* 1987) became available a year later (after the present work was complete) it was found that the earlier digitised contour map differed from the published survey by less than 3%. Any small differences disappeared when the gas data was convolved to the COSB resolution.

Throughout this analysis a value for α_{20} of 4.0 atoms $cm^{-2}K^{-1}km^{-1}s$ was assumed, which is representative of the many estimates of this quantity for the Galactic anti-centre direction (See Chapter 1 for references.) The total column density of neutral hydrogen was obtained by multiplying the integrated CO antenna temperature by α_{20} and adding the HI column density derived from 21cm measurements. Multiplying by the assumed γ-ray emissivity gave the expected γ-ray intensity from CR-gas interactions towards the source, which was then subtracted from the observed non-pulsed γ-ray emission. Any significant excess of γ-rays in the remainder would indicate another source of CR in the region, with the Vela pulsar (and/or SNR if the two are physically connected) being the most compelling candidate. CR sources apart from Vela, or additional changes in emissivity with longitude for example, might also account for some of the excess. These possibilities are thought to be less likely because the majority of the gas lies at an average distance of 1.3 kpc from the Sun, this being estimated from the velocity information contained in the CO

data. This is much further away from the Solar System than the Vela pulsar. The pulsar has a latitude of $-2°$ and so lies well below most of the molecular gas which is concentrated in the Galactic plane. The pulsar is therefore well away from peaks in the gas which would confuse the issue by introducing uncertainties about processes occurring within such molecular clouds such as star formation. Wolf-Rayet stars might also be expected to contribute to the excess CR budget if only by their high mass loss rates ($\sim 3 \times 10^{-5} M_{\odot} yr^{-1}$ Smith 1982) but examining catalogues of such objects reveals only one within 1 kpc of Vela. Fortunately it lies well below the plane and is over 5° away from the source thus placing it outside the latitude range of both this analysis and the CO data. Thus WR stars, which have been postulated as strong sources of CR (e.g. Montmerle 1979), are not likely to be the cause of any effects noted here. Figure 2.5 shows the case for the 300–5000 MeV energy band. The pulsar manifests itself clearly at 263°.75, but well away from this position the total, background and expected intensities are very similar and can be taken to be identical within the errorbars. Off source, the distribution of intensities expected from the gas about the total intensities shows that the assumed emissivity is correct. Nearer the source, as the total intensity increases, the background (non-source) values remain close to the expected points. The match between background and expected is fair, but there are a number of bins that have background values higher than expected from the gas. Averaging background intensities over the source region reveals a slight enhancement over the γ-ray intensity expected from the gas. The enhancement or excess is not correlated with the total intensity and cannot be attributed to a fraction of the pulsed signal that has spilled over and is appearing in the non-pulsed background.

An alternative method of describing the same situation is to divide the observed background intensities by the gas column densities in each bin to obtain the emissivity required for the observed intensity to equal the expected intensity. Such values can be compared to the assumed value of 0.61 (for 300–5000 MeV). Figure 2.6 clearly shows the excesses above this value. It is significant to note that, although the errors are quite large, both shortward and longward of the source where the CO column density increases, the emissivity values drop to the assumed value, or even below it. This indicates that the

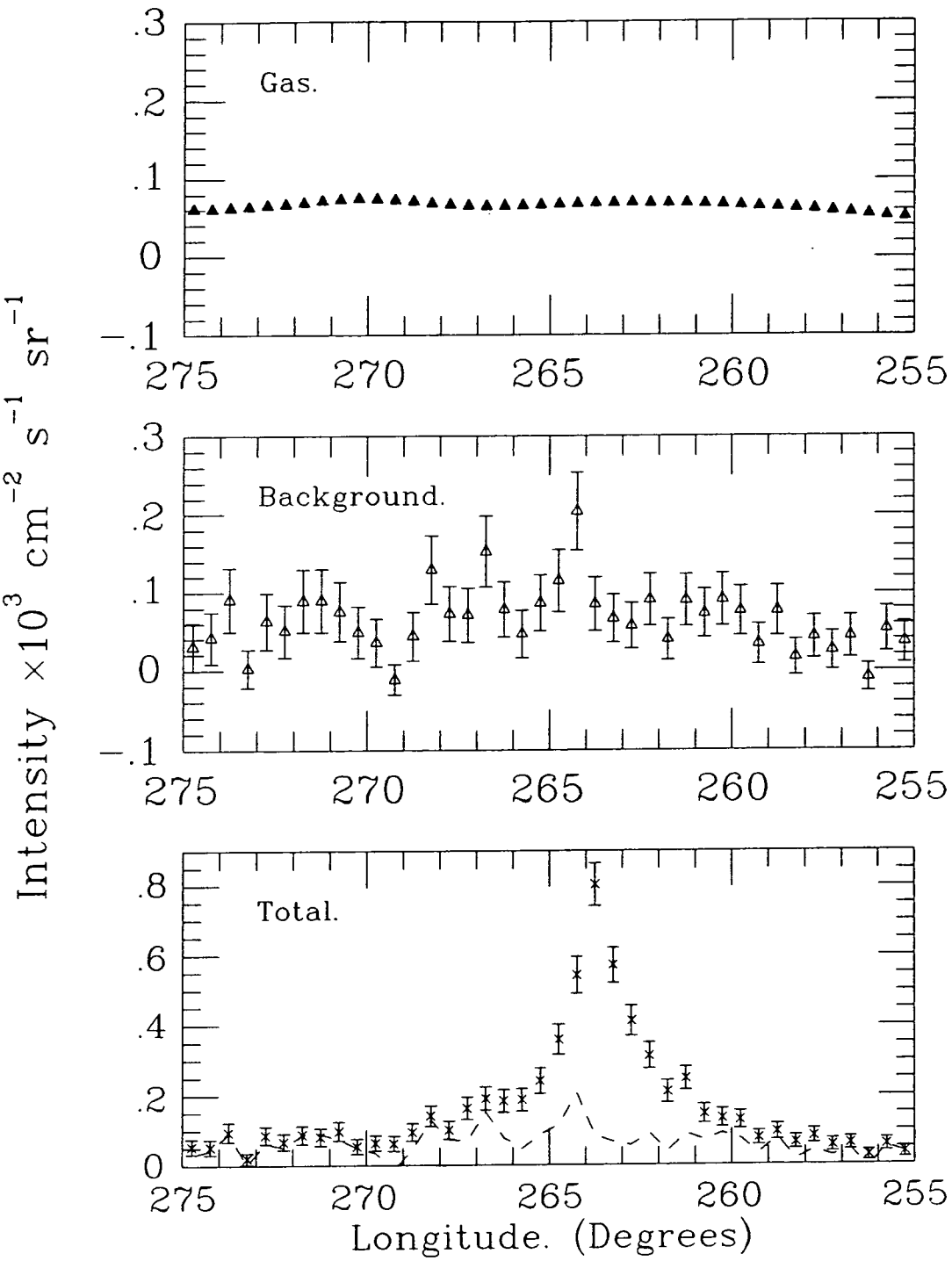

Figure 2.5

Plots of intensities from a longitude profile through the source. The latitude range is −5°.25–0°.75. *a*. Intensity of emission expected from the gas. *b*. Background emission (i.e. $2N_{AE}$). *c*. Total emission. The background is also shown (dashed line). All graphs refer to 300–5000 MeV energy band.

excess is not correlated with the more distant molecular gas, or any sources that they might contain, but that it is local to the pulsar.

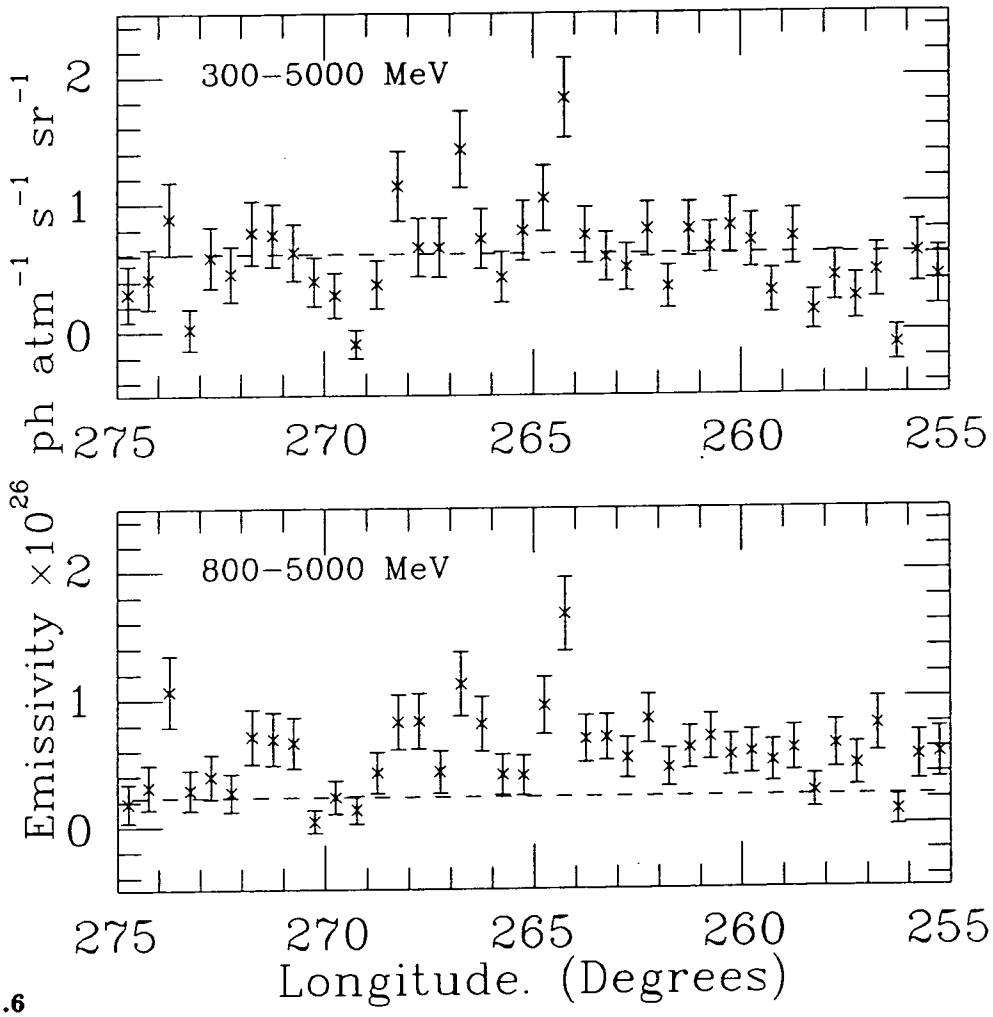

Figure 2.6

Plots of emissivities in units of photons atom^{-1}s^{-1}sr^{-1} from a longitude profile through the source. The latitude range is the same as Fig. 2.5.

The identification of a γ-ray excess associated with the Vela pulsar has consequences for the proposition that the Vela remnant is not associated with the pulsar but is a chance superposition. It could be plausibly argued that the SNR is associated with the molecular gas and therefore lies well beyond

the pulsar. In this case, the excess γ-ray emission would not therefore be attributable (in the first instance) to the remnant because of the factor of about six reduction in intensity due to the greater distance of this object from the Sun. It is worthy of note here that spectral measurements made by Jenkins, Silk and Wallerstein (1976) of stars with distances from the Sun less than 1 kpc contain many spectral lines some of which could only have been produced in conditions typical of a SNR. Similarly, if the pulsar and SNR are coeval, the γ-ray excess must be treated as coming from both objects although one of them may be the dominant source. No techniques are available to distinguish between the γ-rays from CR generated by the pulsar and those produced by the SNR so some model must be applied to predict the expected γ-ray contributions from CR produced by both remnant and neutron star. This does not seem to be a profitable line of inquiry at the present time as the further division of the already low intensities involved would produce large errors on the respective flux estimates and make definite conclusions difficult. Such analysis must await the next generation of γ-ray telescopes. A better approach here would be to take either extremum case and attribute all the emission to either the pulsar or the remnant.

2.2.4 Flux Estimates.

The cross-correlation method employed by Hermsen (1980) and other workers in the Caravane Collaboration to investigate point sources provides an excellent tool for estimating the flux and significance of sources provided that the spatial profile is known beforehand. For point sources, the observed profile is, of course, the PSF of the telescope, whilst for extended sources, the problem is not so simple since the source profile required to match against the observed distribution of γ-rays is unknown. As a consequence the region over which the flux is estimated must be defined. For the Vela region, the CR diffusing from the pulsar, or those produced in the SNR should be present around the pulsar position. If the SNR is $\sim 10^4$ years old (e.g. Weiler and Panagia 1980, Kahn *et al* 1985), then the CR will still be largely confined within the remnant which will have an angular diameter of about 1°. However, they will not be easily seen in γ-rays considering the binning of the γ-ray data and the subtractions

that have already taken place. The pulsar, however, has presumably been producing CR throughout its lifetime and using the same age as the remnant, these CR could have diffused to fill a sphere of radius $\sim$ 10°. The energy density of these CR will need to be sufficiently high to be distinguishable above the ambient flux. One requirement for CR production by a SNR is that the CR remain close to the shock since they gain energy by repeatedly crossing and recrossing it. If they do diffuse downstream to infinity, they will not gain any more energy from this process. Drury (1983) predicts that the probability of diffusing downstream is not high. He estimates it to be $4U/v$ where U is the bulk downstream gas velocity, and v is the mean particle speed relative to the bulk motion. By assumption for the shock process to operate, $U/v << 1$, so very few particles escape. Also, models of CR production by SNR (e.g. Blandford and Cowie 1982) predict that the amount of energy going into CR increases with remnant age, so a young remnant is not expected to be as prolific a CR source as one that is larger and older. The pulsar produced CR however, are accelerated at the source in the intense magnetic fields and gain all their energy there before escaping. There is no incremental energy gain like that of the repeated shock crossing.

Estimates of the observed flux have been made by taking concentric circles around the source position, summing the total intensity within each circle and then multiplying by the solid angle that the circle subtends at the detector. The radii of the circles (θ_r) are increased in increments of $\sim$ 1° out to an arbitrary limit where there are no pulsed γ-rays and all the observed emission arises from CR–gas interactions (and possibly from any DC component). Although the PSF has a long tail, the numbers of γ-rays observed at large angles from the source is low, so the radial extent of the pulsed emission is taken to be 5°.25. All the emission beyond this value (i.e. the total intensity) is equated to the non-pulsed contribution. The γ-ray emission contributed by the gas is subtracted from the non-pulsed intensity assuming a uniform emissivity over the region of 0.61 for 300–5000 MeV and 0.23 for 800–5000 MeV. This gives a map of γ-rays intensities produced solely by CR from the pulsar and/or SNR within a circle of 5°.25 centred on the pulsar bin at $(l, b) = (263°.75, -2°.25)$. From this map any DC component can be subtracted by multiplying the pulsed emission by an appropriate factor and performing the subtraction bin by bin.

For each $0°.5 \times 0°.5$ bin around the source position the angle between it and the source bin was calculated. For bins lying within a certain radius, denoted θ_r, the intensities were summed enabling a flux to be derived. Unfortunately, the distribution of emissivity values (Fig. 2.6) through the source is fairly flat, so it is not obvious to which radius the bins should be summed to estimate the flux. The approximate width of the pulsed signal is no guide for this radius as there is no reason to expect the γ-ray intensity produced by CR from the source to be coextensive with it. On average however, the emissivities do return to the assumed value of $q/4\pi$ about 5° away from the source giving a diameter of 10°, consistent with the estimate of the extent of CR diffusion, so this diameter has been used as a guide for the upper limit for radii of the circles around the source. For any CR signal to be interpreted as coming directly from the source, the γ-ray flux must drop with radial distance from the source as the CR are not expected to diffuse great distances during the estimated source lifetime. For this reason, the actual upper limit used was 7° to enable the behaviour of the flux as a function of radius to be investigated. The number of bins within the 5° circle is quite large (349) which ensures that the summation of intensities gives a correct value for the total intensity within the errors of the data. (See Chapter 1 for a brief discussion on the summation of intensities.)

In order to perform an error analysis on the intensities, the accuracy of the HI and CO values that are used to construct the final map must be known. As this information is not available bin by bin, such an analysis cannot be done. However, the main source of error in the molecular hydrogen column densities comes from the conversion factor, α_{20}, as the errors on the CO map especially are much smaller than the γ-ray intensity errors. The Vela region is slightly away from the Galactic plane, so the molecular gas is much less abundant than at $b = 0°$, and so the error on the emissivity has a greater bearing on the final map than the uncertainty in α_{20}. The emissivity is better defined than the CO–H_2 conversion ratio and has been estimated by many authors for many different regions of the Galaxy. For simplicity, one error is used to encompass the errors from all three quantities giving a value of the emissivity of 0.61 ± 0.21 above 300 MeV. This brackets the values obtained by most methods of calculating $q/4\pi$.

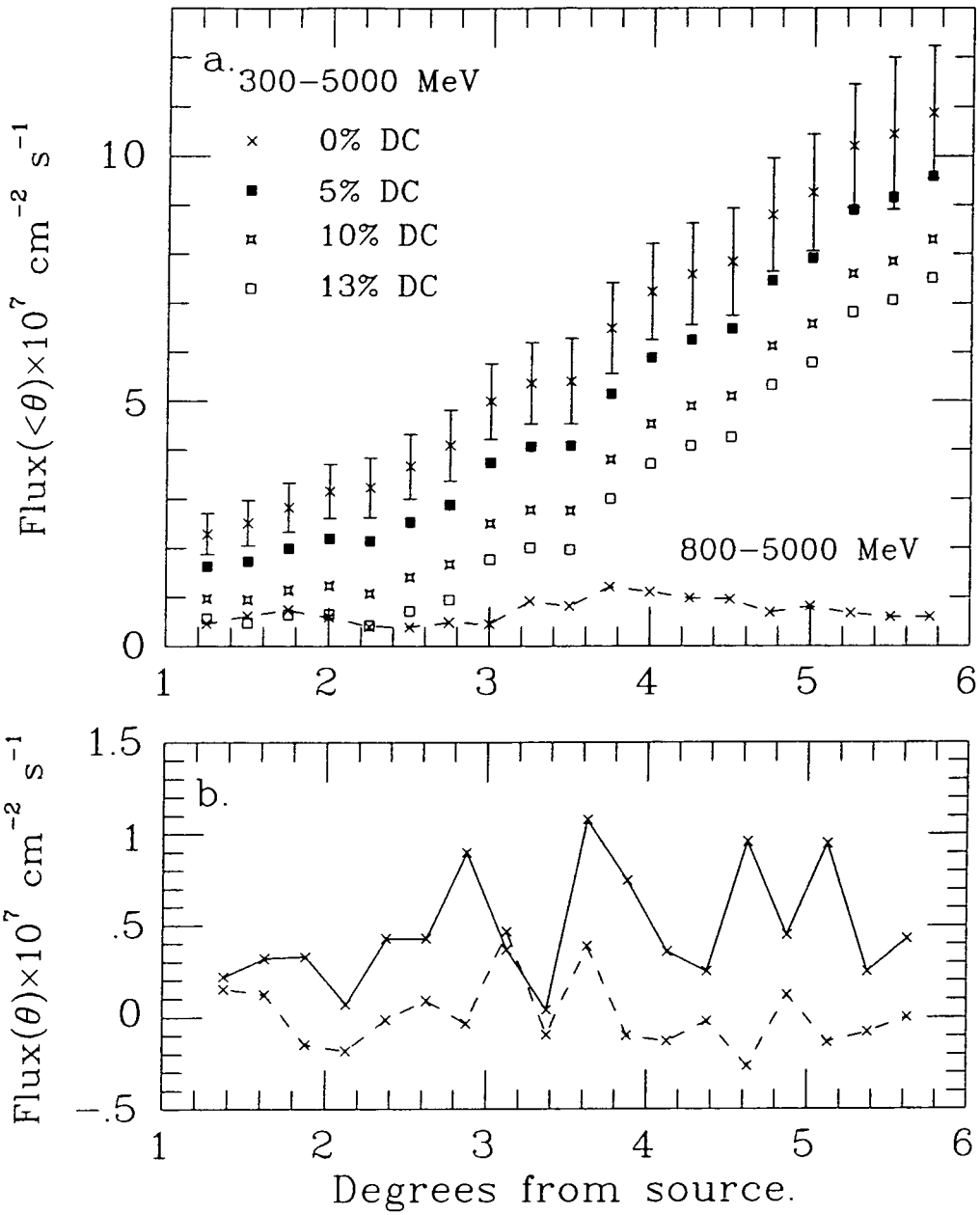

Figure 2.7

a. Fluxes within θ_r degrees from the source. 300–5000 MeV for various DC levels and 800–5000 MeV for 0% DC. *b.* Fluxes at θ_r degrees from the source. 0% DC only for the two energy bands. Some errorbars on the figures are omitted for clarity.

The γ-ray flux produced by source CR only for both above 300 and above 800 MeV as a function of radius for various DC levels are plotted in Figure 2.7. Varying the emissivity by $\pm 30\%$ gives Figure 2.8 which shows clearly that for a DC level of 0%, high values of emissivity are required to reduce the flux within the radius (θ_r) to zero. For $\theta_r = 1°.25$, $\frac{q}{4\pi}|_{DC=0} = 1.8$ whereas for $\theta_r = 5°.0$, $\frac{q}{4\pi}|_{DC=0} = 1.0$. With higher DC values these figures decrease of course, but not to zero: e.g. they become 0.9 and 0.86 respectively for the (unrealistic) upper limit of DC=13%. As has already been discussed, the DC component is probably zero and for reasonable values of the emissivity, significant fluxes of γ-rays from pulsar-produced CR are seen.

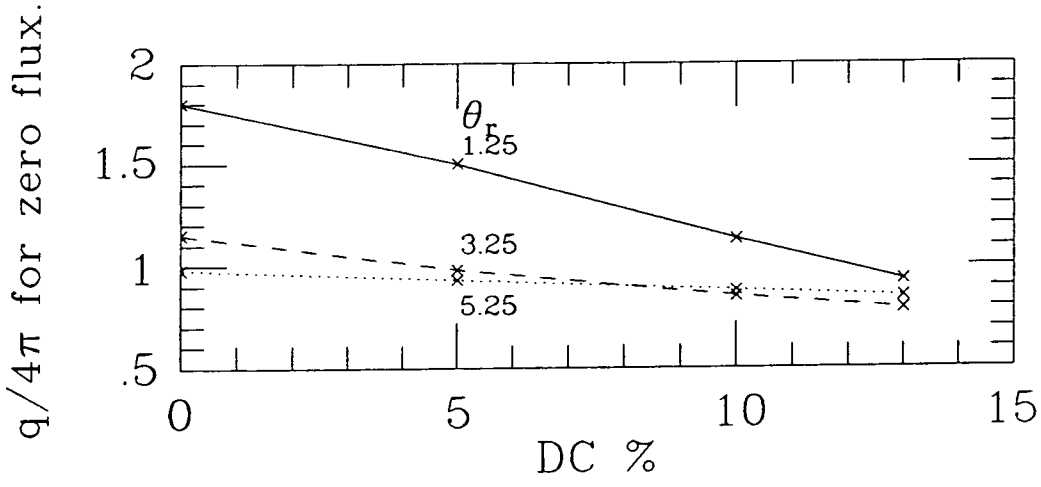

Figure 2.8

Values of emissivity for zero 300–5000 MeV flux within certain θ_r for against DC level.

Above 800 MeV there are fewer γ-rays, making the errors larger and any excess γ-ray emission from pulsar-produced CR less certain. Adopting the same method as for > 300 MeV, the emissivity was again varied by about 30%. For 0% DC, the value of $q/4\pi$ for zero flux within a given radius increases with decreasing maximum radius. For $\theta_r = 5°.0$, $\frac{q}{4\pi}|_{DC=0} = 0.26$, whilst for $\theta_r = 3°.25$ this rises to 0.32. (Fig. 2.8 and 2.9.) It is clear then that there is

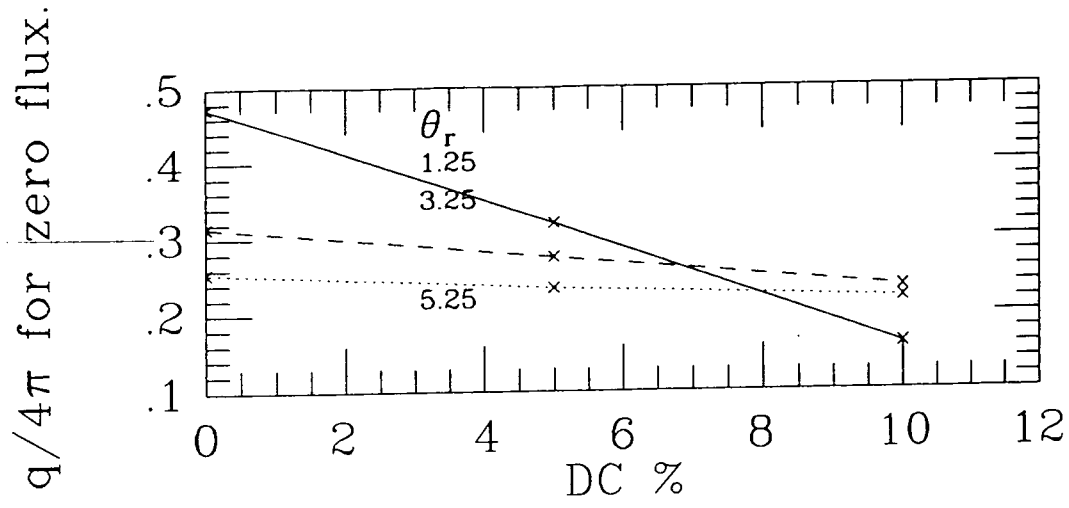

Figure 2.9

Values of emissivity for zero 800–5000 MeV flux within certain θ_r for against DC level.

very little signal left at this high energy — a not unexpected result in view of the lower number of photons.

Going to lower energies, namely 70–150 MeV where the γ-rays are expected to be produced mainly by electrons, the γ-ray flux within a given annulus is also non-zero (Fig. 2.10). If the emissivity depends on energy as a power-law with index 2.0, then this flux would be zero (within the errors) for θ_r to 5° away from the source. Here, a lower index of 1.85 has been used to obtain a value of $\frac{q}{4\pi}|_{70-150} = 1.1$. The reason is as follows: A steep energy dependence would imply that no electrons are being accelerated by the pulsar and/or remnant in contrast to the nuclei (protons) that produce the γ-rays at higher energies. This would be a surprising result in view of the synchrotron emission detected from the pulsar. The more acceptable value of the power-law index used here means that both electrons and protons produce γ-rays in the source region. Thus a constraint can be placed on the γ-ray spectral index, namely that it should be less than 2 because if protons are capable of being accelerated by the pulsar, then electrons also must be accelerated. Such a constraint is not new and is no more stringent than other estimates of the power-law index, but it serves a useful purpose in highlighting some of the

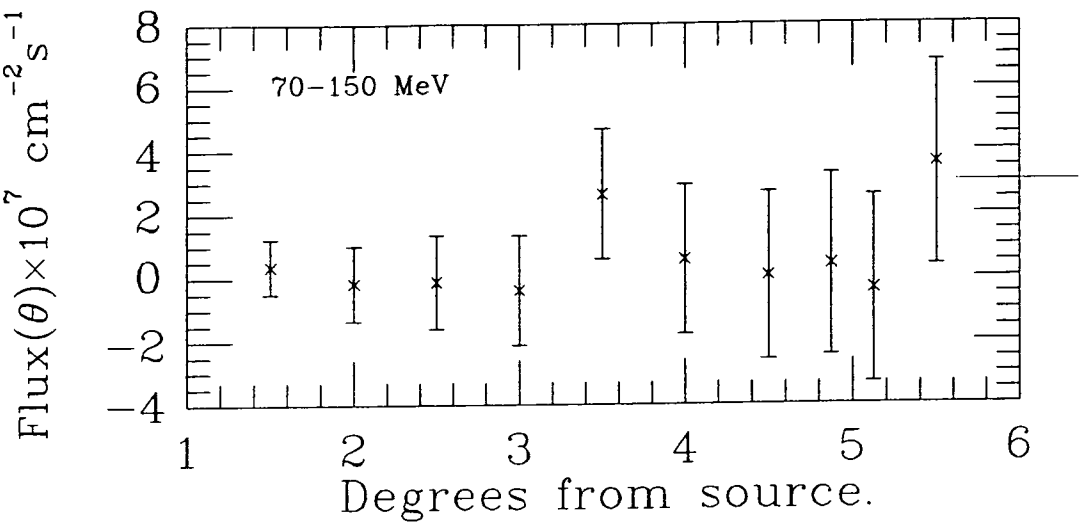

Figure 2.10

The 70–150 MeV γ-ray flux attributed to CR from the source in annuli around the source.

underlying assumptions of the analysis.

The fluxes of γ-rays produced by the source CR were used to investigate the spectral behaviour of the pulsar and source CR-produced γ-rays. Plotting flux($> E_\gamma$) against energy, E_γ, for four energy bands showed that the total emission could be represented rather crudely by a power law of slope -1 for the integral spectrum, with some evidence for a softening with increasing energy. For the emission produced by CR from the source, even with only four points, it is clear that the spectrum cannot be represented by a single power law as there is a distinct steepening at higher energies. This suggests that most of the flux emerges in the medium energy region i.e. that there is an excess of lower energy protons and/or a deficit of electrons. The errors on the flux estimates are large making a fit to the differential flux spectrum difficult. The integral curve provides a better picture as there is no additional loss of significance due to the division of the energy bands.

2.3 Discussion.

2.3.1 Vela.

§2.2.4 described the methods used for estimating the γ-ray flux from the Vela region arising from CR accelerated in the region. Having removed the contribution to the emission from ambient CR–gas interactions, what remains is hopefully a significant signal corresponding to these 'local' (to the source) CR. The value of the emissivity used has a critical effect on the fluxes obtained, and the conclusions drawn here must be seen in that light. If γ-ray emissivities were found in future work to be higher than assumed here by more than 40% then the signal found in each energy band would disappear, and all the emission could be attributed to ambient CR interactions. However, if the γ-ray emission from regions away from the source is examined using the assumed value of the emissivity, then the average signal is zero. This means that any increase in emissivity required to account for the excess signal around the source would leave the 'off–source' regions with negative intensities on average since too many γ-rays originating in the interstellar gas are being subtracted. This situation is not acceptable because where there are no sources, all the γ-ray emission should be attributable to the gas. Indeed, at low energy (70–150 MeV) even a 20% increase in $q/4\pi$ would produce such negative intensity values thereby posing problems for modelling electron production in the region; a negative flux indicates either there is excess emission from the gas, or that the pulsar is under-abundant in electrons. The origin of the electrons in both scenarios is a problem as is the reason why the pulsar might have fewer than expected, but such ideas must await future observations in γ-rays with much improved statistics.

The fluxes derived here for the three energy bands show that for reasonable values of the emissivity, some of the total emission can be attributed to CR produced by the Vela pulsar and/or SNR interacting with the gas local to the source(s).

For 70–150 MeV, the signal is exceedingly weak and within the errors

is consistent with zero indicating that particles capable of producing γ-rays in this energy interval (usually thought to be electrons) are not abundant. The value of $q/4\pi$ used here (1.10) may perhaps be too high, and a value 10% lower might be more appropriate near the plane as the emissivity falls with decreasing latitude. Even with a lower emissivity, the errorbars do not permit any firm conclusions, even though the γ-ray fluxes will then be positive in all annuli around the source. Within 5° from the source, the source CR-produced γ-ray flux is 3.13×10^{-7}ph cm^{-2}s^{-1} which is about 6% of the total emission from Vela in the same solid angle. The flux within each annular bin is consistent with zero, but shows a slight rise with radial distance. When a normalised intensity in each annulus is calculated by dividing the flux by the annular area (normalised to unity for the 1°.25–1°.75 annulus), the result is a rather erratic curve (Fig. 2.11). On average, this normalised intensity is positive, but again, the errors preclude any definitive statement about the origin of these γ-rays in this 70–150 MeV energy interval.

At 300–5000 MeV, the γ-rays produced by CR associated with the source originate mainly from CR nuclei colliding with interstellar hydrogen to produce π_0 mesons which then decay to give two γ-rays. This production mechanism is expected to dominate other process (e.g. electron bremsstrahlung) above 300 MeV so the 800–5000 MeV interval would be a more discriminating sample of the behaviour of protons than that above 300 MeV as the resolution improves with increasing energy. Unfortunately, there are fewer photons above 800 MeV which outweighs the advantage of a clearer distinction between electrons and protons.

Photon counting statistics are sufficiently good at 800–5000 MeV to allow a meaningful analysis. The flux from an annulus rises slowly with distance of the annulus from the source. Compensating for the effect of increasing annular area gives (Fig. 2.11) a roughly flat curve. Again, if the γ-ray emissivity were to rise even by about 20%, nearly all the emission could be accounted for by the gas in the line of sight, but such an increase at 800–5000 MeV has implications at lower energy, namely $\frac{q}{4\pi}|_{70-150} \sim 1.4$ suggesting a deficit in CR electrons in the source region unless the γ-ray spectral index is less than 1.85. This does not seem to be an acceptable solution, so the 300–5000 MeV signal can be attributed to nuclei (protons) being associated with, and presumably

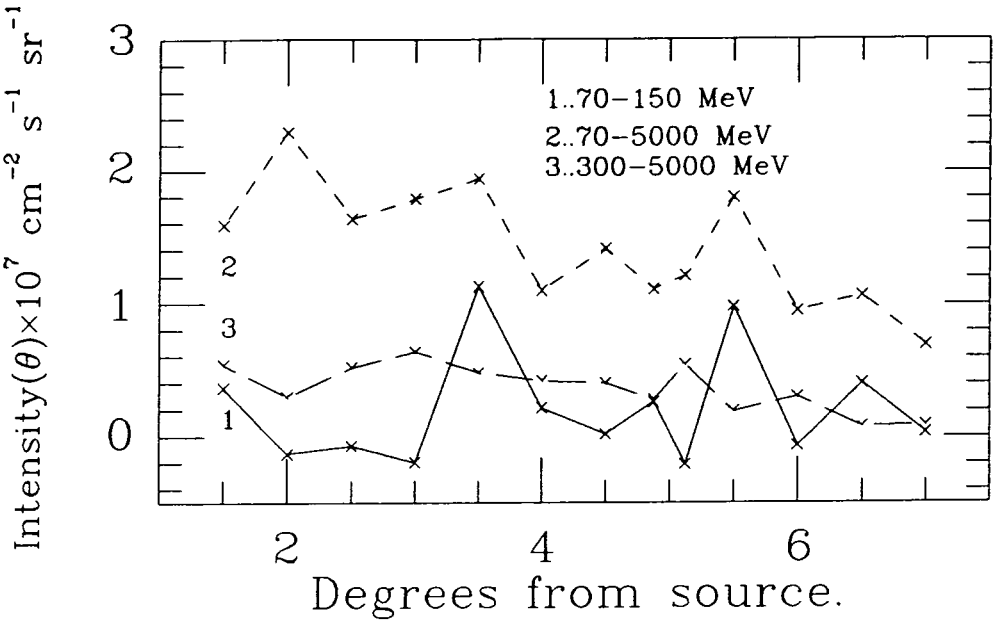

Figure 2.11

Flux divided by area of annulus. The area of the 1°.25–1.°.75 annulus is taken as unity.

accelerated by, the source.

The maximum DC level above 300 MeV is 8% of the pulsed signal for $q/4\pi = 0.61$, whilst $q/4\pi = 0.4$ allows a DC level up to 13% for all annular bins less than 5° away from the source. The favoured values are $q/4\pi = 0.61$ and DC level =0% which give a flux for the γ-rays produced by CR associated with the source of $(1.02 \pm 0.13) \times 10^{-6}$ph cm^{-2}s^{-1} which is 17 ± 2% of the total flux from the same region. Of course, this fraction varies with θ_r, having a minimum of 11% and an average of 13.9%. The higher contribution to the γ-ray emissivity from CR accelerated in the source for larger radii arises from the much lower fraction of pulsed γ-ray emission at large distances from the source.

At 800–5000 MeV, the residual γ-ray fluxes suffer from large errors because of the poor photon statistics, but the general trends are still apparent and confirm the results from the 300–5000 MeV band in which there are greater numbers of photons. The flux within 5° of the source becomes negative for all values of DC if $q/4\pi$ is greater than 0.26. This emissivity 'threshold' increases

with decreasing radial distance from the source reaching 0.48 for DC=0% at $\theta_R < 1°.25$. A reasonable upper limit for the DC level at 800–5000 MeV is 5% of the pulsed flux which produces zero integrated flux at 2°.5 from the source, but it is difficult to determine the best value for either the DC component or $q/4\pi$ because of the fluctuations in the data and photon counting statistics. As $q/4\pi = 0.23$ is favoured from analyses elsewhere in the Galaxy, DC values above 5% of the pulsed signal are clearly too high. For a DC level of 0%, which is the most likely (and simplest) case, the flux within 5° of the source is 8×10^{-8}ph cm^{-2}s^{-1} or 6% of the total flux. The normalised flux shows the same flat distribution versus θ_r with no indication of any dependency on the narrower PSF of the telescope at this higher energy thereby giving support for the contention that the emission is extended and not point-like. An additional check on this hypothesis is to consider how the integrated pulsed flux varies with θ_r since the pulsed component must originate from a point source. In this case, the integrated pulsed flux in each annulus decreases with θ_r giving a curve that flattens with increasing distance from the source. This behaviour is in contrast to the background and non-pulsed fluxes that rise linearly with distance from the source.

2.3.2 Loop III

Following the successful identification of an excess γ-ray intensity towards Loop I, attributable to CR being accelerated by this old remnant (Bhat *et al.* 1985b), the search for further evidence of particle acceleration was made towards Loop III. This radio loop is older than Loop I, lies at a greater distance and is less prominent at 408 MHz. Such observations can account for the lower γ-ray emission.

The excess emission ΔI_γ was calculated for the three standard COSB energy bands and 100–5000 MeV, by subtracting the γ-ray emission expected from neutral hydrogen in the line of sight from the observed emission in the Loop. The longitude range 80°–170° at latitudes between 10°–30°was assumed here to lie inside the Loop region. Studies of SNR at high latitude are facilitated by negligible amount of molecular gas out of the Galactic plane and the

absence of nearby sources.

The γ-ray emissivity used to estimate the emission expected from neutral hydrogen (in this case, all HI) was derived by two methods to give an idea of the sensitivity of the results to the assumed emissivity value. Firstly, the Galactic average emissivity ($I_\gamma/N_{\rm HI}$) taken over all longitudes at the same latitude as the Loop was calculated and secondly, the Loop III region was excluded from the longitude range. In both cases, ΔI_γ was positive, with a lower significance for the higher latitude band (20°–30°) than the lower (10°–20°). However, the overall significance of this result is not high because of the significant errors in the data resulting from poor counting statistics at these high latitudes. The resulting emissivities for the two cases were: $\frac{q}{4\pi}|_{\rm inside} = 0.91 \pm 0.07$ and $= 1.38 \pm 0.3$ whilst $\frac{q}{4\pi}|_{\rm outside} = 0.64 \pm 0.1$ and $= 0.55 \pm 0.85$ for the (10°–20°) and the (20°–30°) latitude bins respectively. The outside values are consistent with the expected value of the emissivity ($\sim$ 0.63), whilst the higher values inside indicate that CR could be being accelerated in the remnant.

Finally, a brief comparison with Loop I showed that the emissivity inside Loop I was 50% higher than in Loop III, whilst outside the two Loops, the values were the same within the errors. This is consistent with the ages, distances and sizes of the two remnants because Loop I is the larger and closer of the two.

This analysis of Loop III has provided a useful backup to the results from Loop I and gives further weight to the argument that SNR are sources of both electrons and protons. The photon statistics at such high latitudes are not satisfactory for this kind of comparative work but the results are an incentive for a closer examination of individual large SNR in the Galaxy. This is likely to be a highly rewarding field of study when improved photon numbers are obtained at higher latitudes.

2.3.3 A Source Model.

The source of CR producing the γ-rays seen near the pulsar is uncertain. The pulsar might seem to be the obvious choice, but there is also a SNR in the

region which is capable of shock accelerating CR. Of course, it is most likely that both are sources of CR, but as has already been noted, the chances of distinguishing the two objects with the present data are low, unless reliable models of both objects become available.

Jenkins, Silk and Wallerstein (1976) use IUE data to show that the Vela SNR is expanding into a highly inhomogeneous medium where the density enhancements exceed the average by a factor of 10. Comparison of the cooling times of the newly shocked gas with the estimated age of the remnant gives the density of gas ahead of the shock as 1–10 atoms cm^{-3} with a blast-wave velocity of 470 ± 80 km s^{-1}. A velocity of this magnitude suggests an initial explosive energy of 5×10^{50} ergs, similar to that normally expected from a SN.

Serious doubts have been raised (Bignami and Caraveo 1988) about the association of the Vela remnant and the pulsar. A common scenario for SNe is that they are the end product of short-lived massive stars which do not drift far from their birth places because of their short lifetimes. They are believed to form in giant gas complexes such as the Orion molecular clouds, and often clusters of these type of OB stars occur in association with SNR and gas complexes. Montmerle (1979) has studied these 'SNOBs', finding numerous examples in the Galaxy. However, the molecular gas in the Vela region where a SNR might be expected lies much further away from the Sun than the pulsar, so it is worth speculating that the pulsar and Vela XYZ are not causally connected and that another (unidentified) remnant is associated with the pulsar. This would be plausible if such a hypothetical remnant had the same age as the pulsar and the gas density in the region was low, or if it was a 'radio-quiet' type of remnant (Blandford and Cowie 1982). This hypothetical remnant would have a angular radius about 5° corresponding to a radius of 45 pc at a distance of 500 pc.

In line with evidence from giant radio Loops I and III, the Vela SNR (observed or hypothetical) can be fitted to the theoretical curve of energy input into CR versus radius of the remnant. Calculations by a number of authors (Axford 1981, Drury and Völk 1981, Blandford and Cowie 1982) predict that the energy input into CR (E_{CR}) increases with radius whilst the shock acceleration mechanism operates.

With the fluxes obtained here, estimates can be made of the energy input into CR assuming a particular SNR shock acceleration model. Above 300 MeV, the γ-ray flux within 5°.25 of the source (i.e. within a radius of 45 pc) generated by CR from the source is $\sim 1 \times 10^{-6}$ph cm^{-2}s^{-1}. The expected flux from Blandford and Cowie's model is $2.2 \times 10^{-5} B^{-1.33}$cm^{-2}s^{-1} where B is the magnetic flux in μG. This implies a magnetic field of $10\mu G$ which is within a factor of two of the expected value of about $5\mu G$. These figures correspond to a total proton energy of 5×10^{48} ergs to be compared to $\sim 6 \times 10^{48}$ ergs from the model with $B = 5\mu G$ and a proton to electron density ratio of 6. However, in reality, the remnant has a radius of approximately 20 pc from radio measurements of Vela XYZ so the model predicts a flux of 1.1×10^{-6}ph cm^{-2}s^{-1} for a magnetic field of $5\mu G$. This corresponds to a proton energy of 8×10^{48} ergs. For comparison, the observed flux within 20 pc is 3.3×10^{-7}ph cm^{-2}s^{-1} i.e. about a factor of 3 lower than the model predicts.

The agreement between these estimates is surprisingly good in view of the uncertainties involved. It is the model that is perhaps the most tentative, as many of the problems of the shock acceleration mechanism have yet to be resolved. Also, the proton/electron ratio is not well known and is little more than a guess. The filling factor of the pre-shock medium is also relevant and can alter the model predictions by an order of magnitude or more depending upon whether the medium into which the shock passes is of the McKee and Ostriker (1977) type or is a dense molecular cloud.

At lower energies, where electrons dominate, the value of the magnetic field predicted by the model using the observed flux within 5° of the source is higher again by a factor of 2.5, and the energy input into electrons is $\sim 6 \times 10^{47}$ ergs. This is a factor 1.7 times lower than the model predicts, but represents reasonable agreement considering the errors.

As the observed γ-ray flux decreases, the magnetic field required to sustain this flux increases. Thus the very low flux observed above 800 MeV would require on average a high field, which is contrary to expectations. It is more probable that either the model is not working well at these higher energies or the data are too poor in quality, or perhaps that the shock is not accelerating particles as efficiently regardless of the value of the magnetic field. The

most likely of these possibilities is that the poor quality of the data causes the discrepancy, but unfortunately little can be done about the problem until new observations are made. However, it is clear that the SNR model can explain the γ-ray emission observed around Vela. At very high energies, where the errors are largest, the model and observations are not in good agreement. However, this is not necessarily an indication that the model is wrong, but simply a reflection of the difficulty in obtaining significant results when the statistics are poor. The SNR model and the observations complement each other and when new results are forthcoming at high energy, the validity of the model for the acceleration of protons can be further tested.

Unfortunately, the energy distribution of electrons and protons cannot yet be predicted individually. For the present, the broad division of 70–150 MeV γ-rays being produced mainly by electrons and those above 300 MeV being produced by nuclei must be retained. This division highlights the need for a better understanding of the nature of the shock acceleration process. Despite the problems, it is clear that the SNR model is an excellent candidate for the production of γ-rays as the energies required by observations agree with the model to within an order of magnitude.

The age and size of the Vela SNR has still to be resolved and the contribution from the pulsar needs to be assessed. The angular size used here for the flux estimation ($\theta_r \sim 5°$) is approximately the angular extent of the excess γ-ray flux surrounding the pulsar position and would correspond to a remnant of radius $\sim$ 45 pc at a distance of 500 pc with an age $\sim 10^4$years (Sedov phase), if the medium into which it expands has a density of $\sim 0.08\text{cm}^{-3}$. This age is the same as that of the pulsar, but the remnant observed at radio wavelengths has a radius of only about 2°.5. This means that the estimates of the energy input into CR using a 45 pc radius are too high by a factor of about five. Initially, this could be seen as support for the conjecture that the pulsar is contributing a significant fraction of the CR in the region by accelerating particles to great distances (Thielheim 1987). However, the model works very well for a smaller radius (20 pc) and can account for the whole of the flux using the expected value of the magnetic field. This suggests that there is another cause for the larger angular extent of the emission. The PSF of the COSB telescope which spreads the point source pulsed emission over

a few degrees will also spread the extended emission in a similar fashion. A simple model is to consider the γ-ray excess flux as a 'top-hat' function set equal to zero beyond a radius of 20 pc where the CR from the SNR and/or pulsar have not yet reached. This is then convolved with the COSB beam to produce the observed profile that extends beyond 20 pc, and decreases slowly with increasing distance from the source.

An alternative model is that the pulsar itself is responsible for the CR that produce the excess γ-rays. The CR would be accelerated by the pulsar and then diffuse away forming a 'bubble' of radius X in time T where:

$$X = \sqrt{2DT} \qquad 2.4$$

D is a diffusion constant and the factor 2 is strictly relevant only for one-dimensional diffusion. With $D = 5 \times 10^{28}\text{cm}^2\text{s}^{-1}$, and $T = 10^4$ years, $X = 58$ pc or 6°.5 which is close to the observed angular diameter of the excess γ-ray emission. This distance is increased by a factor $\sqrt{3}$ if $6D$ is used in Eqn. 2.4 in the case of three dimensional diffusion. Obviously a model of the energy density of CR produced in this manner is required, along with some estimates of the emissivity so the expected γ-ray flux can be calculated. Using $6D$ in Eqn. 2.4, a value of X of 45 pc, gives a diffusion constant of $1.0 \times 10^{28}\text{cm}^2\text{s}^{-1}$ which is towards the low end of the acceptable range, but may be appropriate for the Galactic plane. Alternatively, the age of the pulsar may be lower than 10^4 years as Stothers (1980) suggests, in which case $D = 2.0 \times 10^{28}\text{cm}^2\text{s}^{-1}$

2.4 Conclusion.

This chapter has presented results from an analysis of γ-rays from the Vela pulsar and the surrounding areas. Estimating the various components of the total γ-ray emission has revealed a small but significant excess, which is probably caused by CR from a local region around Vela rather than ambient CR from the rest of the Galaxy. Table 2.2 summarises these results for above 70 and above 300 MeV in terms of the percentage of the total flux within a given radius of the pulsar position for a given energy interval.

Degrees from source	Percentage of total flux.		
	70–5000 MeV	300–5000 MeV	800–5000 MeV
5.25	16.8	17.5	3.8
4.75	16.1	16.1	4.1
4.25	15.2	15.3	6.4
3.75	15.2	14.4	8.5
3.25	14.0	13.3	7.1
2.75	13.4	11.7	4.2
2.25	13.0	10.9	4.0
1.75	12.9	12.7	8.7
1.25	14.2	13.5	6.7

Table 2.2

The figures presented in Table 2.2 are the main results of the analysis and show that CR electrons and protons are present around the source. The errors are large, but the fluxes are still significant. Further work with improved counting statistics are required especially at the highest γ-ray energies ($>$ 800 MeV).

The next step has been to attempt to identify the source of the excess CR. There are two possible models: firstly, a SNR could have accelerated the CR by diffusive shock acceleration to energies required to produce the observed γ-rays. Secondly, there is the pulsar itself. The first of these models could be fulfilled by the Vela XYZ complex. Theory predicts that the energy input into CR increases as the remnant expands, so if Vela X alone is the accelerating SNR, there is a problem because using the observed γ-ray flux predicts a larger radius for Vela X than is observed. This supports the view of Milne and Manchester (1986) that Vela X is part of the whole complex.

Although the association between the remnant and pulsar has been questioned (Bignami and Caraveo 1988), there are published models (Manchester 1987) that not only explain the anomalous appearance of SNR in general, but when applied to Vela also predict the very low pulsar proper motion. The distances to the Vela remnant and pulsar are the same within the errors, and

apart from the lower age estimates of Stothers (1980), their ages are also in reasonable agreement.

It is reasonable then to assume that the pulsar and SNR were produced by the same SN explosion and that both are now potential sources of CR. The extent of the emission ($\sim$ 5° in radius) is larger than the remnant, and so the energy in CR is larger than that expected on the basis of the models by Blandford and Cowie (1982) and others with the same radius. The observed Vela XYZ complex has a radius of $\sim$ 20 pc giving fluxes in good agreement with the model predictions. A large part of the spread in this emission has been attributed to the PSF of the COSB telescope which tends to smear the true signal. This effect cannot be removed because deconvolution of the γ-ray data with a bin size of 0°.5 will produce erroneous results. The beam has a FWHM of $\sim$ 1°.2 above 300 MeV, so the true emission region will have an angular size much closer to 20 pc. It is not clear whether all the emission can be explained in terms of a SNR acceleration model. What is now required is some theoretical understanding of the rôle pulsars play in CR acceleration on a Galaxy-wide scale. This will complement the SNR models and hopefully will also shed light on their interaction and evolution as sources of the bulk of Galactic CR.

The SNR model can produce the observed γ-ray fluxes with reasonable values of the magnetic field, indicating that this is a valid description of particle acceleration in the Vela region. Obviously, improved measurements at all γ-ray energies and a better understanding of the relationships of SNR and pulsars are required to resolve the source ambiguity. SNR are excellent candidates for the acceleration of both electrons and protons because the mechanism is able to explain the γ-ray emission from such regions. Three remnants have now been identified in γ-rays, of which Vela has provided direct evidence for CR acceleration by the source.

Chapter 3. The Carina Region.

3.1 Introduction.

It has long been appreciated that the Carina region of the Milky Way is a fascinating part of the sky for study at all wavelengths. The η Carinae Nebula with its associated HII regions is the most prominent optical object and a spectral analysis of stars in the vicinity reveals an unusually high proportion of Wolf Rayet (WR) stars and OB associations. HI maps show a marked increase in column density at longitudes around 282° and, recently, CO surveys show in some detail the extent of the molecular gas component in and near the Galactic plane in Carina.

It is generally true that the more interesting the region of sky, the more difficult it is to elucidate the details of its structure and the processes occurring there. Bok has been one of the champions of Carina, producing numerous papers addressing the problems of spiral structure in this region as well as attempting to fit other observations of, for example, giant stars, HII, and Cepheids to the gas structure (Bok 1937,1959, Bok *et al* 1970). Over the years as observational data have accumulated, it has become apparent that the line of sight becomes a tangent to a spiral arm at around l = 280°–282°. The wealth of information now available over a very wide range of wavelengths including measurements of radio HII regions (Georgelin and Georgelin 1976, Georgelin *et al* 1979), Cepheids (Tammann 1970), young Galactic star clusters (Becker and Fenkart 1970), and HI kinematical distances, all points to the existence of spiral structure extending from the Solar neighbourhood out to much greater helio- and galacto-centric distances. The recently published Columbia 'all-sky' CO survey (Dame *et al* 1987) delineates this spiral structure particularly well. However, when attempts are made to fit this feature to other Galactic spiral

arm tracers, difficulties are encountered which are reflected by the confusion in the literature. Where does the Carina arm go inward of the tangent point? Does it stretch to the Sun, or does it connect somehow to the Sagittarius arm (also seen in CO, for example, with a tangent at $l = 312°$.) What then of the local material commonly called the Orion arm or Local Spur? Yuan (1970), for example, finds no evidence that the Carina arm connects to either the Orion or Sagittarius arms, whereas Courtès *et al* (1970) and Garzoli (1970) join Carina to Sagittarius considering them a 'structural and kinematic continuity'. For a useful comparison of the interpretations of the data, see Bok (1971). There is considerable room for improvement in all observations of this region, and therefore the latest (and last) part of the electromagnetic spectrum to be utilized in astronomy can be examined to see if any weight can be lent to any particular model.

The most successful theory of spiral structure proposed thus far is that of density waves. It was first put forward in a series of papers by B. Lindblad starting in 1941, but did not receive general acceptance at the time because of the large numbers of assumptions and approximations he used. The idea was developed further by P. O. Lindblad (1960) and B. Lindblad (1963), but the credit for the initial development of the currently accepted version belongs to F. H. Shu. Further extensive work was done by Lin, Shu and Yuan and others in the late 1960's. The early studies found linear solutions to the equations governing the spiral pattern and the gas response (e.g. Lin *et al* 1969). The work was taken further with the slightly non-linear solutions of, for example, Vandervoort (1971) and the highly non-linear regime (Roberts 1969). Much of this work deals with a 'grand design' spiral pattern that extends from an inner resonance (the Lindblad resonance) outward in the form of (usually) a two- or four-armed spiral. These are often approximated by a logarithmic spiral of the form: $R = R_l e^{\phi \tan i}$ where ϕ is the azimuthal angle, R_l is the arm scale factor, and R is the galactocentric radius. i is the arm inclination defined as the angle between the tangent to the arm at a given point and a circle around the Galactic centre through that point. Lin, Yuan and others use $i = 6°.2$ and $R_l = 8.26$ kpc (e.g. Yuan 1970). Woltjer (1965) finds $i = 6°$. Unfortunately, the Carina arm does not fit easily into these low i models of the global (i.e. whole Galactic) pattern. Using the Columbia CO data, the present author

has derived here values for these two parameters: $i = 9°.04$ and $R_l = 9.17$ kpc. Similarly, the Local Spur does not fit into the pattern, having values of i quoted in the literature much higher than 6° with typical values in the range 20°–30°. Yuan declares that it does not seem possible to model the primary spiral pattern of the Galaxy with values of i as high as this.

Many authors have attempted to account for the observations of young objects such as OB stars and HII regions. Lin (1970) puts forward a number of ideas, suggesting that these objects have migrated out from the Sagittarius arm or that they are part of a local pattern moving at 15 km s^{-1} kpc^{-1} or a trailing pattern travelling faster than the local circular speed. A trailing pattern is one in which the spiral arms rotate such that the inner parts of the arm lead the outer parts and the impression is that the arms should wind up on themselves.

A feature of density wave theory is that in addition to the primary mode spiral arms, additional modes could be present. Usually only the short wavelength modes are considered as these are expected to be most prominent, but these other modes could account for some of the features with larger inclination that are observed. It must be said that an *ad hoc* introduction of these modes just to fit the data is not satisfactory from a theoretical standpoint. Another possibility that can be derived from the non-linear version of the theory which does not require this *ad hoc* treatment is the appearance of resonances. The epicyclic frequency is the frequency with which an object travelling around the Galaxy in a circular orbit performs an epicycle in that orbit when subject to a small perturbation. At the Lindblad radius, the epicyclic frequency at that radius equals the rotation speed of the spiral pattern (Ω_p) and a resonance occurs through which the spiral arm cannot usually propagate. The observation of large amounts of molecular gas around 4 kpc from the Galactic centre has been attributed to this resonance. The other terminal resonance occurs where the speed of the spiral pattern equals the circular gas velocity (i.e. they are in corotation) which, for a pattern speed of $\sim$ 13.5 km s^{-1} kpc^{-1} and a flat rotation curve beyond the solar circle, occurs at $\sim$ 18.5 kpc. The production of resonances is an important feature of the theory with a number of consequences. One of these is the prediction of 'ultra-harmonic' resonances of which more will be said in §3.2.3.

The evidence for CR sources is considered here both from the nature of the objects in the Carina region and from the γ-ray intensities. Alternative models for the sources are discussed with reference to the data, with the aim of putting the region in the context of the rest of the Galaxy.

3.2 The Carina Region.

3.2.1 COSB Sources.

The motivation for the study of this region stems from the work of the COSB collaboration which aimed at discovering the γ-ray source population of the Galaxy. Initially, many more sources were thought to exist, but the generally accepted view now is that most of the γ radiation detected by the satellite is diffuse emission and not dominated by large numbers of unresolved point sources. It is this diffuse emission that is of prime concern in this chapter. This emission is produced by π_0-decay and electron bremsstrahlung caused by CR propagating through the interstellar medium, rather than being produced at and seen directly from a point source such as Vela (Chapter 2.)

Hermsen (1980) lists the 2CG catalogue of γ-ray sources with estimates of their positions, fluxes and significances. Some have unambiguous identifications, such as the Crab and Vela by virtue of their pulsed emission, and others by their positional coincidence — 3C273 and the molecular cloud ρ-Oph. for example. Apart from the enigmatic Geminga (2CG195+05), there are two strong sources associated with large gas complexes, which are both annotated as 'could be an extended feature'. One of these is the Carina region in which Hermsen finds two sources (2CG284+00 and 2CG288+00) using his cross-correlation analysis. That there are γ-rays from this region has been well documented by the COSB collaboration in their analyses of the Galaxy. Figure 3.1 shows a γ-ray map of the Carina region at 70-5000 MeV, and clearly demonstrates why this region is included in the list of γ-ray sources.

These sources may be indeed be extended but this does not answer the

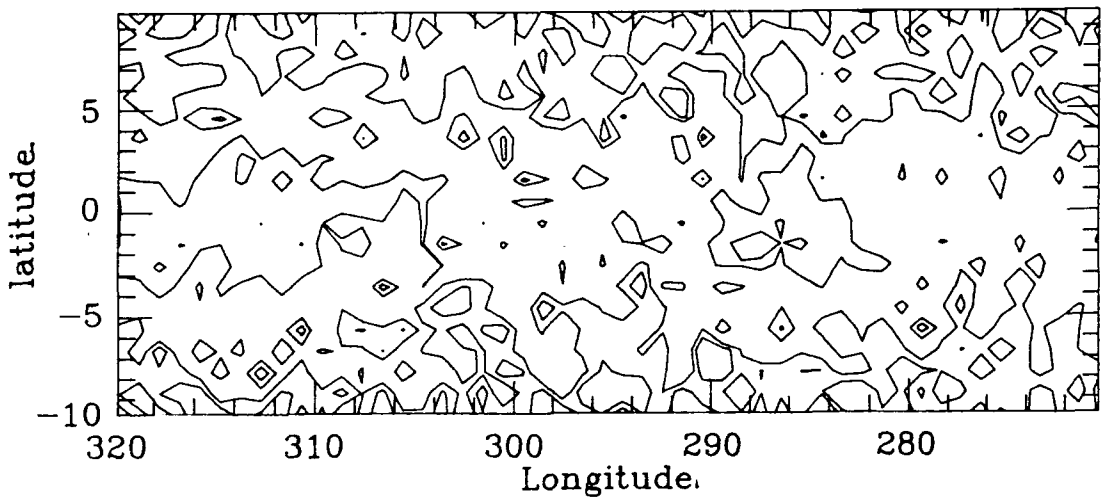

Figure 3.1
70–5000 MeV γ-ray map of the Carina region. Contours at: $(1, 2, 5, 10) \times 10^{-4}$ ph cm^{-2}s^{-1}sr^{-1}

question of the origin of the radiation. Pollock *et al* (1987) state that the evidence for an excess above that expected from the gas alone is 'weak' and suggest that a likely explanation is the irradiation of gas clumps by a 'normal' flux of CR. With the recently available CO data, and better estimates of the conversion ratio of CO to H_2 (α_{20}), the evidence for an excess is much better than simply 'weak', especially for 2CG284+00 (see §3.3).

3.2.2 The Nature of η Carinae and Its Nebula.

Most of the studies of this fascinating southern sky object in the optical, infra-red and X-ray wavebands have concentrated on η Carinae itself as this is

thought to be the prime cause of most of the effects observed in the nebula. It was not until Walborn (1975) took interference filter photographs of the nebula and in the following year made spectrograms of various parts (Walborn and Liller 1977), that the association of η Carinae itself with the nebula was finally established. Some regions of the nebula were found to be reflecting the central object's peculiar spectrum. Thus very early and massive O stars that produce much of the emission nebulosity are also associated with η Carinae. This lends support to the idea that this object is also very massive.

Two models of the region (Davidson and Ostriker 1972) have subsequently been tested mainly by X-ray observations. The first model considered the central region to be a massive, slowly expanding supernova remnant (SNR). Energy was supplied to the remnant by a central pulsar that produced non-thermal radiation in the infra-red and in X-rays. The second model postulated a very massive star that ejected a significant fraction of a solar mass of material in an outburst observed in 1843. The ejecta then became visually opaque as dust grains formed and re-radiated the absorbed stellar radiation in the infra-red. Either model required a shock in the form of an expanding shell heating the gas.

This outburst was thought to be possibly a SN, but X-ray observations made by Seward *et al* (1979) using the *Einstein* observatory show that the event had an energy of $\sim 10^{46}$ergs with an initial gas density of ~ 20 cm^{-3}, with a current mass of emitting gas of $\sim 0.01 M_{\odot}$. These values do not support the SNR hypothesis, but do support the idea that the gas is heated by a shock, especially when the symmetrical appearance of the nebula about the central object is considered. The X-ray observations (e.g. Seward *et al* 1979) predict a temperature of $\sim 10^8$ K, which is an order of magnitude higher than that derived from the expansion velocities of the outer condensations of gas which travel at between 750 and 1000 km s^{-1} (Walborn 1976). However, the higher temperatures probably come from only a small part of the emitting region, so there is no real contradiction. The X-ray observations therefore argue against the SNR model since the expected non-thermal luminosity would then be $> 10^{38}$erg s^{-1}. Energies of this order would lead to a flatter spectrum at higher energies than is actually observed. This argument uses the remnant shell diameter obtained from the X-ray observations which agree with those

at optical wavelengths.

The outburst of 1843 which was followed by observers at the time, yielded a light-curve that is reproduced in Walborn and Liller (1977). A fourth magnitude object brightened to about the zeroth magnitude and remained there for approximately twenty years before it declined to about the sixth magnitude at which it has subsequently remained. Davidson (1971) proposed a scenario for this outburst in which he argued that the object was more probably a very massive evolved star well beyond the main sequence rather than a very young star approaching it. The pulsationally unstable star ejected material forming an expanding shell which increased the visual radiation to the zeroth magnitude although the total luminosity remained roughly constant. Dust grains gradually formed making the object more opaque in the visible and brightening it in the infra-red. At the present time, η Carinae is the brightest infra-red object at 20μm outside the Solar System, having a bolometric luminosity of $\sim 2 \times 10^6 L_\odot$ (Westphal and Neugebauer 1969). This infra-red continuum emission is thermal in origin.

The nebula itself, NGC 3372, is much larger (2°) than the central 'homunculus' ($10'' \times 15''$) and is comprised mainly of a large HII region containing many powerful early stars. In fact, the HII region includes three O3 stars which have not been observed to occur in such numbers anywhere else in the Galaxy. Some parts close to η Carinae are reflection nebulosity and there is a general expansion in the central region of around 600 km s^{-1}.

This review of some of the properties and observations of NGC 3372 makes it clear that there is considerable activity and considerable amounts of energy being liberated. The velocities of some parts of the nebula and the fairly high densities involved make it almost certain that shocks are present. Strictly, the whole Carina Nebula should be considered as an agglomeration of CR source candidates as there are so many possible sources. In dealing with γ-rays as a potential tracer of the CR in this whole region, it must be remembered that the point spread function (PSF) of the telescope is such that it will not be possible to identify any individual source and reference to η Carinae as a possible CR source must be taken to mean the whole Nebula and not just the central object or homunculus.

3.2.3 Spiral Structure and Shocks.

The presence of shocks in the spiral arms of galaxies has been demonstrated conclusively by Matthewson *et al* (1972) in studies of M51 which have revealed an enhancement in synchrotron radiation in association with optical and HI arms. This enhancement has been ascribed to electrons being accelerated at the shock. In this Galaxy, the circular gas velocity is greater than the pattern speed at the same radius over a wide range of galactocentric radii, so that shocks can form near the minima of the pattern. The gas flows into the shock, is compressed and emerges outside the arm where it expands. Such compression is expected to trigger gas cloud collapse and hence initiate star formation giving rise to bright OB stars and their associated HII regions which then delineate the arm optically. It is therefore expected that when an arm is observed at radio wavelengths, say in HI or CO, the young objects should appear at larger longitudes than the gas peak in quadrants I and II, and smaller longitudes than the peak in quadrants III and IV. Even a casual inspection of the situation in the Carina region in quadrant IV shows that the tangent to the arm is very well marked in CO, especially when the velocities are taken into account (Fig. 3.2), but that the OB and WR stars appear longward of the tangent point. If the model of gas compression and star formation is correct, then this observation can only be accommodated by the geometry of the arm. Both the CO and HI have maxima at $l = 282°$ a longitude which is commonly believed to be the actual tangent to the arm. Assuming this longitude indicates the region of maximum compression, it should also approximately mark the shock front and, for that part of the arm that lies on the side of the tangent point nearer to the Sun, the young stars and HII regions should lie at lower longitudes (i.e. towards $l = 270°$). The arm is, of course, curved and at higher longitudes the line of sight should pass through many young stellar objects, the peak in the gas density, and the shock (in that order), on the near side of the tangent point. The η Carinae nebula, if associated with the shock, should lie in front of the shock and be a product of it. Also, the WR stars should have a spatially distribution consistent with being formed behind (downstream of) the shock.

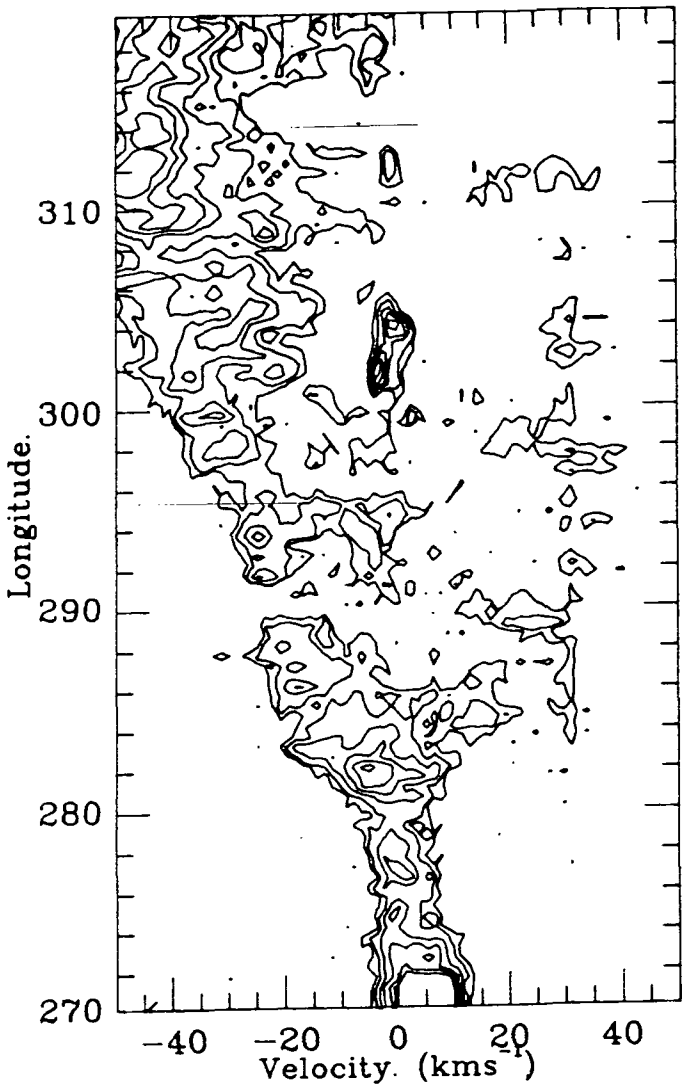

Figure 3.2
CO longitude-velocity contour map from Columbia CO survey. Contours at: 0.5,1,2,3,4,5 K

The CO data obtained by the Columbia group have been recently analysed by Grabelsky *et al* (1987) and Cohen *et al* (1987) for the Carina region. Cohen *et al* have compiled a list of molecular clouds from $l = 270°$ to $l = 320°$ which corresponds to increasing galactocentric distance along the Carina arm. They identified many of the nearer clouds with known optical and radio objects. Using the longitudes and distances of these objects, a least-squares fit to an equation of the form $R = R_l \exp^{\tan i\phi}$ has been performed to estimate the inclination i and scale factor R_l of this arm. These are found to be: $i = 9°.04$ and $R_l = 9.17$ kpc. Figure 3.3 shows a plan view of the Carina arm with the positions of the molecular clouds of Cohen *et al*, along with HII regions (Humphreys 1972), WR stars from catalogues in the literature (e.g. Smith 1968a,b,c, Stenholm 1975) and η Carinae. The least-squares estimate of the position of the arm is also drawn. This figure shows clearly that most of the

HII regions and WR stars lie *outside* (i.e. downstream of) the arm in agreement with the model described above. There are, by definition, approximately half of the molecular clouds either side of the least-squares line, so the shock is expected to lie somewhat interior to this line i.e. at smaller R_l with an inclination similar to the least-squares estimate. These molecular clouds are thought to be the direct product of the spiral shock (Elmegreen 1979, Elmegreen and Elmegreen 1979). The estimates of R_l and i give a tangent at $l = 284°.7$ which can be compared with the observed CO peak at $l = 282°$, where there is an abrupt increase in the numbers of young stellar objects. These two values of tangent longitude are not necessarily inconsistent because of the finite spatial extent of the clouds and the greater prominence of nearby clouds which might, by chance, lie outside the mean position. If this is the case, then the apparent tangent will occur at a higher longitude than the actual tangent.

The HI has a maximum at the same position as the CO and the argument about the finite spatial extent of the clouds also applies, but it is less important because of the lower density contrast between arm and interarm.

Roberts (1969) investigated shock formation in spiral galaxies using density wave theory and applied the results to star formation. His figure 6 (Fig. 3.4) shows the gas density along a typical streamtube for his model two-armed galaxy. The region of high density is quite narrow, lying on the inner side of the HI arm, but outside the shock. Initially, it would be expected that lines of sight through the lowest density regions just before the shock would appear as minima in the gas distribution, but as the arm curves, these lines of sight cut the highest density regions in two places (the near and far points) leading to a higher column density of gas apparently *inside* the shock. This effect is not likely to be as obvious in HI as in CO, again because of the lower density contrast.

Various CR source candidates such as OB and WR stars, all fit reasonably well into the picture of a spiral arm having a high gas density near the shock with various products of star formation occurring downstream. SNR should also be present as the end product of massive star evolution, and all these objects may contribute to the CR population over long periods of time ($\sim 10^5$ years). The shocks and ionised gas that are predicted and/or observed

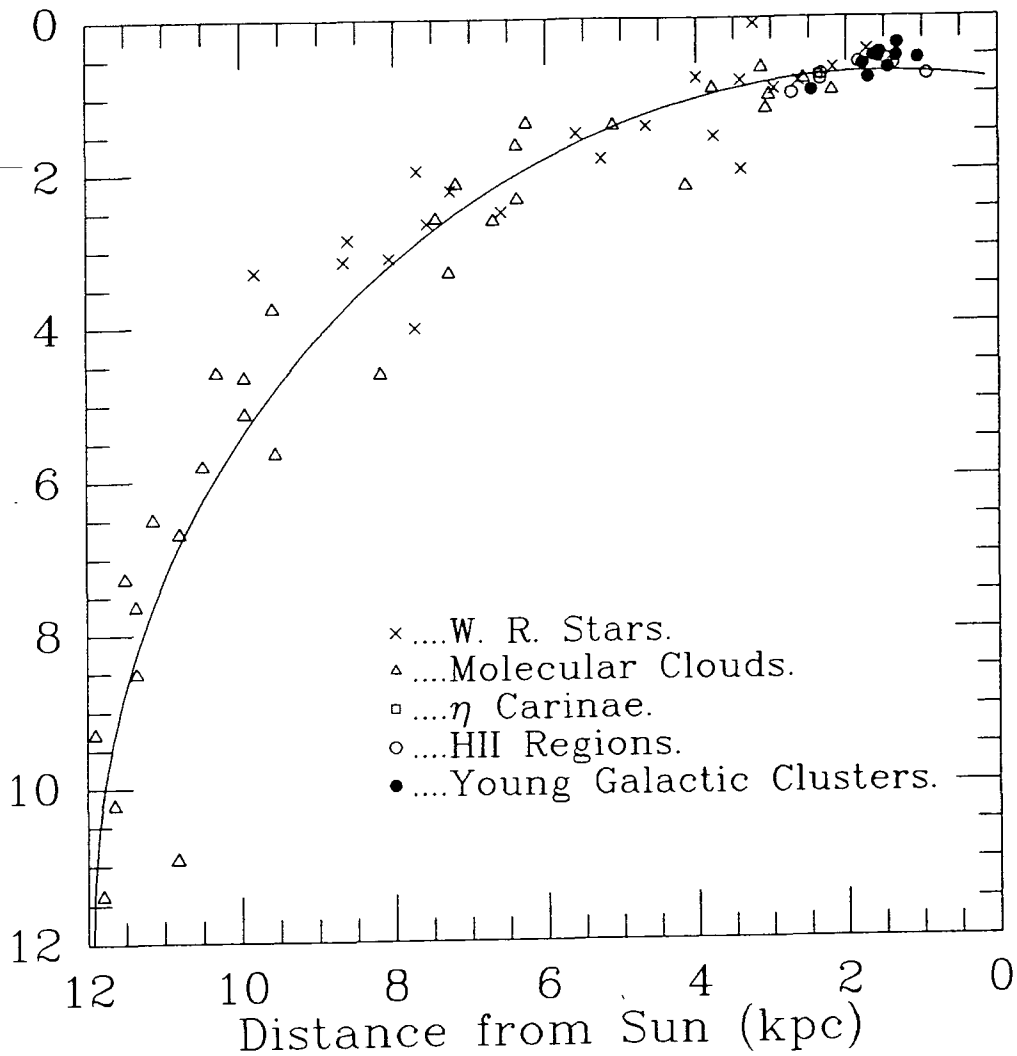

Figure 3.3
Plan view of the Carina spiral arm showing the positions of molecular clouds (Cohen *et al* 1987) and Wolf-Rayet stars. The least-squares fit through the clouds is also shown.

in the region should be visible at X-ray energies. The X-ray evidence against the η Carinae outburst being a SN has already been mentioned (§3.2.1). The *Einstein* observatory also detected X-rays from a number of specific sources

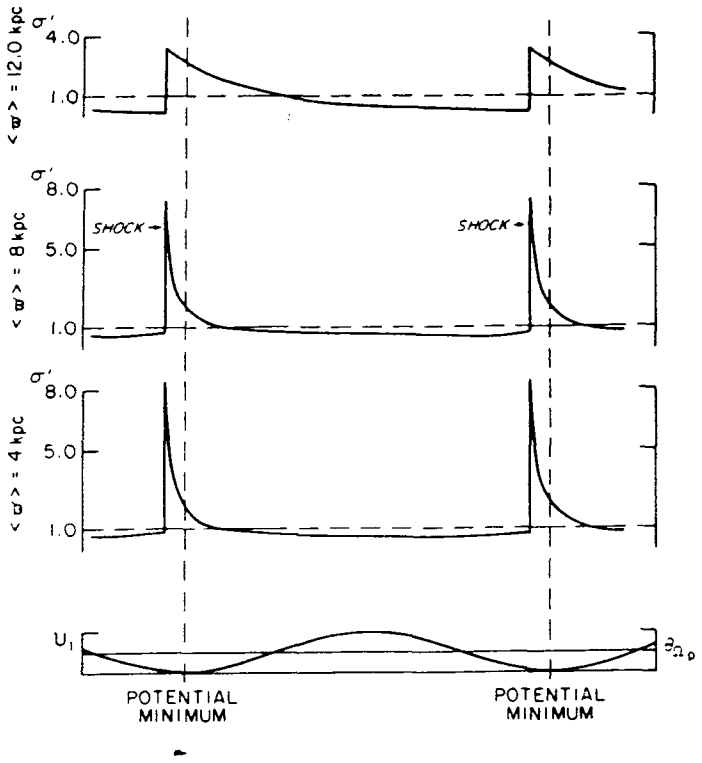

Figure 3.4
Figure 6 of Roberts (1970) showing the response of the gas to the passage of a spiral shock.

including η Carinae, a WR star and six O stars (Seward *et al* 1979) with a total energy output of 1.5×10^{34}erg s^{-1}. The Carinae Nebula emits diffuse X-ray emission produced by hot gas that has a cooling lifetime long enough for the emission not to be inconsistent with a SN origin (with the event occurring 10^6—10^7 years ago). Alternatively, the emission could be associated with a single massive star at the centre. The SN model has additional backing as the SN rate is expected to be higher than the Galactic average in view of the large numbers of O stars in the area. However, the SNR would have to have a morphology that is unique in the Galaxy and since stellar winds are also consistent with the diffuse emission, the SN model may be discarded. The complicated morphology of the Nebula makes source identification difficult, but is not an obstacle to the stellar wind hypothesis.

The final question that can be addressed is how the Carina spiral arm fits into the global pattern i.e. whether it connects with other spiral features. The observations produce conflicting points of view and no clear pattern can be inferred, especially on the near side of the tangent. The position of the Carina arm is not obvious from the data for galactocentric radii lower than the radius of the tangent, and thus spiral arms seen in quadrant I cannot be joined to the Carina arm unambiguously. Simonsen (1976) models the Galaxy using density wave kinematics to fit the observed gas features and he finds that the Carina arm is not part of the main pattern but originates near the Sun. He argues that the lack of gas around $l = 290°$ indicates that the arm terminates and does not cross $l = 0°$. Density wave theory in its basic form caters for major spiral arms which extend from the inner Lindblad radius out to corotation and typical models have two or four arms with various (usually low) pitch angles. Carina does not fit easily into these models, but a proposal by Shu, Milione and Roberts (1972) in a discussion about galactic shocks seems to explain the presence of arms between the major ones in a 'natural' fashion in the context of the theory. For certain values of the wave frequency, 'ultra-harmonic' resonances can occur which produce a secondary compression of the interstellar gas and generate secondary spiral features downstream of the major arm shock. In their model, the main ultra-harmonic resonance is found at $R = 10.6$ kpc and extends to 11.6 kpc — values which are not too far from the actual position of the arm as determined here from the CO observations. Such resonances are also proposed as explanations for the high inclination spurs and 'feathers' that are observed between major arms in external galaxies; the Orion Spur may be an example of such a spur in this Galaxy. Therefore, from density wave theory at least, a substantial 'secondary' shock is to be expected in the Carina arm. It is emphasised that these features are secondary only in the sense that they do not extend to the inner Lindblad radius, and do not appear throughout the Galactic disk.

It has been demonstrated above that the observed gas distribution behaves roughly as expected for a shock compression profile similar to that of Roberts (1969). Likewise, the positions of young stellar objects are consistent with the Roberts model. The shock lies just interior to the gas maximum and should be visible in γ-rays just longward of $l = 284°.7$. The γ-ray evidence

must now be examined to see whether it is compatible with this model and whether these observed γ-ray features can be attributed to any of the above phenomena.

3.3 The γ-ray Evidence.

3.3.1 Emissivity.

Contour maps of γ-ray intensities at three standard energy bands and at 800–5000 MeV are presented in figure 3.5. It is evident that there is an excess in intensity (I_γ) beginning at around $l = 280°$ and extending to greater longitudes. What is of interest here, however, is not just where I_γ increases but where the emissivity (denoted $q/4\pi$ — see Chapter 1) increases. To find this quantity for each bin, the total intensity was divided by the total gas column density in that bin. Any excess in $q/4\pi$ above the expected value suggests that there is an excess of CR in that region above that which is expected purely on the grounds of ambient (i.e. general Galactic) CR-gas interactions. Here, the latitude range is restricted to $|b| < 5°$, as the objects of interest here are well within this range and the CO emission drops away fairly rapidly at greater latitude. Three energy bands are of particular interest: 70–150 MeV γ-rays are produced mainly by electrons, whilst those at energies above 300 MeV come from nuclei, i.e. mainly protons. The γ-rays with $E_\gamma > 800$ MeV are also examined since at these energies instrumental resolution is much improved. Figure 3.6 shows the longitude profiles of emissivity in 1° longitude bins for each of these three energy bands. The picture is least clear for the 70–150 MeV band, probably due again to the poor resolution. At $l = 275°$ the very low emissivity does not appear to correlate with any star or gas cloud. The low emissivity value at this longitude is due to a low I_γ rather than an enhancement in the gas, so it is probably statistical in nature although it must be noted that it occurs over two bins. The main peak in emissivity occurs at $l = 285°.5$ with fairly large fluctuations on either side. These fluctuations continue at larger longitudes up to about $l = 305°$ where the variations become less frequent.

Apart from the aforementioned deficit, there are no obvious 'holes' in this emissivity. $q/4\pi|_{70-150}$ remains roughly constant beyond the peak although at a marginally higher value ($q/4\pi = 1.31 \pm 0.05$) than that shortward of it ($q/4\pi = 1.25 \pm 0.07$). These values of the emissivity and those that follow are in units of 10^{-26}ph atm^{-1}s^{-1}sr^{-1}.

Turning now to 300–5000 MeV, there is more structure in the fluctuations. Between $l = 270°$ and $l = 282°.5$, the value of $q/4\pi = 0.64 \pm 0.02$. It is roughly constant and within the errors is the same as the canonical (i.e. whole Galactic average) value of 0.63. From $l = 283°.5$ and continuing to about $l = 294°.5$, the emissivity increases to a peak of 1.25 at $l = 285°.5$ and remains enhanced at 0.92 ± 0.06 until it returns to the pre-tangent values of 0.63 ± 0.04 between $l = 295°.5$ and $l = 305°.5$. From $l = 306°.5$ to the end of the profile, $q/4\pi$ again is high on average (0.72 ± 0.03).

Finally, at 800–5000 MeV, further detail is revealed: there are three broad peaks and a pronounced trough. There is the peak at $l = 285°.5$—$295°.5$ with $q/4\pi = 0.52 \pm 0.08$, but this is now separate from more enhanced emission lying between $l = 290°.5$—$297°.5$. A trough occurs between $l = 299°.5$ and $l = 303°.5$ with $q/4\pi = 0.065 \pm 0.02$ whereas for $l = 304°.5$—$319°.5$ $q/4\pi = 0.22 \pm 0.02$, similar to the 'expected' value of 0.23.

To summarize these results: there is clear evidence for enhanced γ-ray emission around $l = 285°$ extending over a couple of degrees in longitude. Additionally, this enhancement extends longward to about $l = 295°.5$ with a gap around $l = 288°$ in the 800–5000 MeV energy band. At higher longitudes, there is evidence for a slight enhancement around $l = 312°$.

3.3.2 Spectral Features.

Rogers *et al* (1988) analysed the COSB database for γ-rays above 300 MeV and above 800 MeV, finding the spectral index to be flatter in the local arm than in the interarm regions. They found some support for this contention from radio synchrotron radiation that showed a similar but much less marked tendency for spectral flattening in the local arm. The difference in spectral

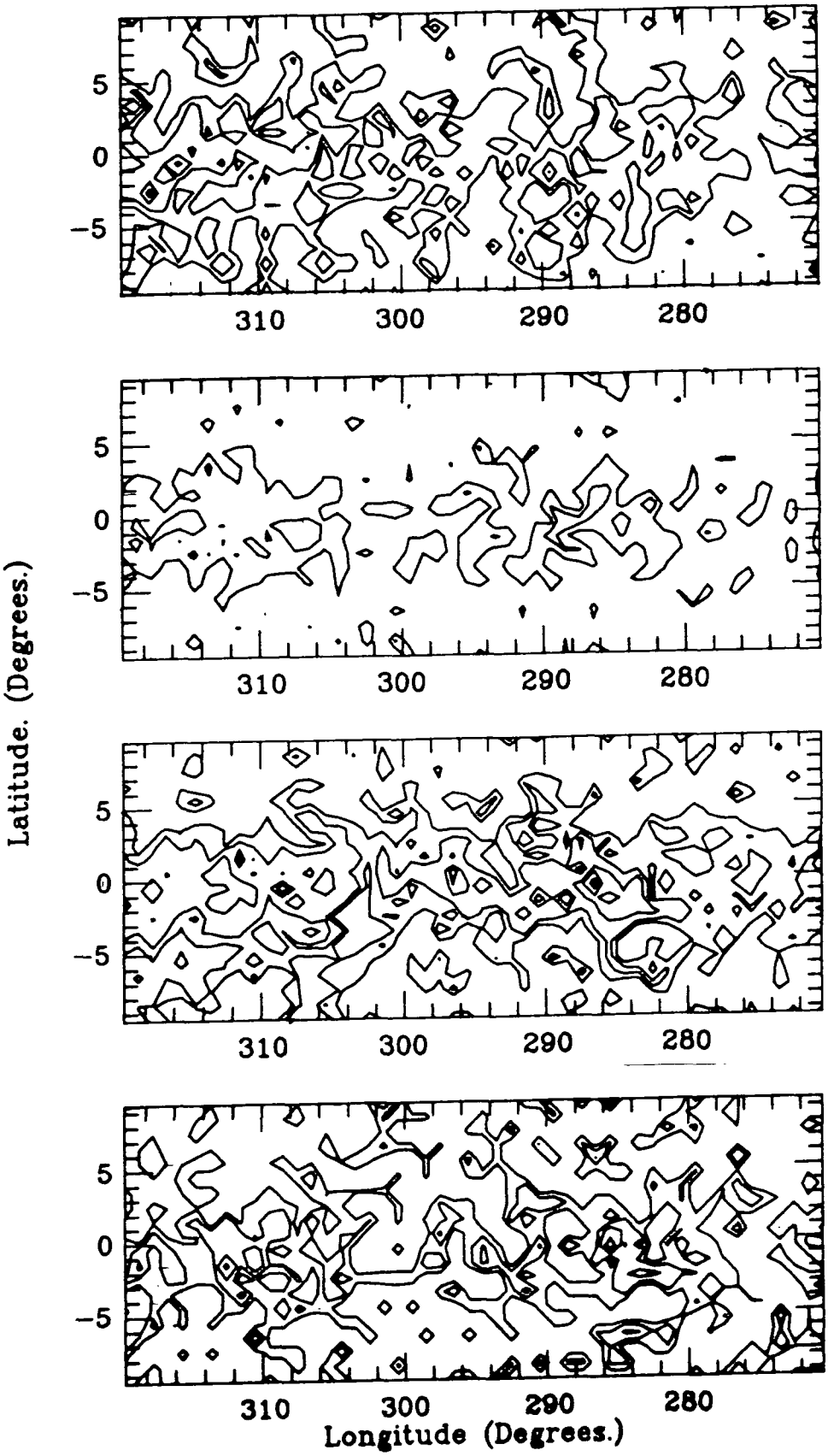

Figure 3.5

Contour maps of γ-ray intensity from the Carina region. *a.* 70–150 MeV. Contours at $(1, 2, 5, 10) \times 10^{-4}$ph cm^{-2}s^{-1}sr^{-1} *b.* 150–300 MeV. Contours at $(1, 2, 5, 10) \times 10^{-4}$ph cm^{-2}s^{-1}sr^{-1} *c.* 300–5000 MeV. Contours at $(0.5, 1, 2, 5) \times 10^{-4}$ph cm^{-2}s^{-1}sr^{-1} *d.* 800–5000 MeV Contours at $(0.2, 0.5, 1, 2) \times 10^{-4}$ph cm^{-2}s^{-1}sr^{-1}

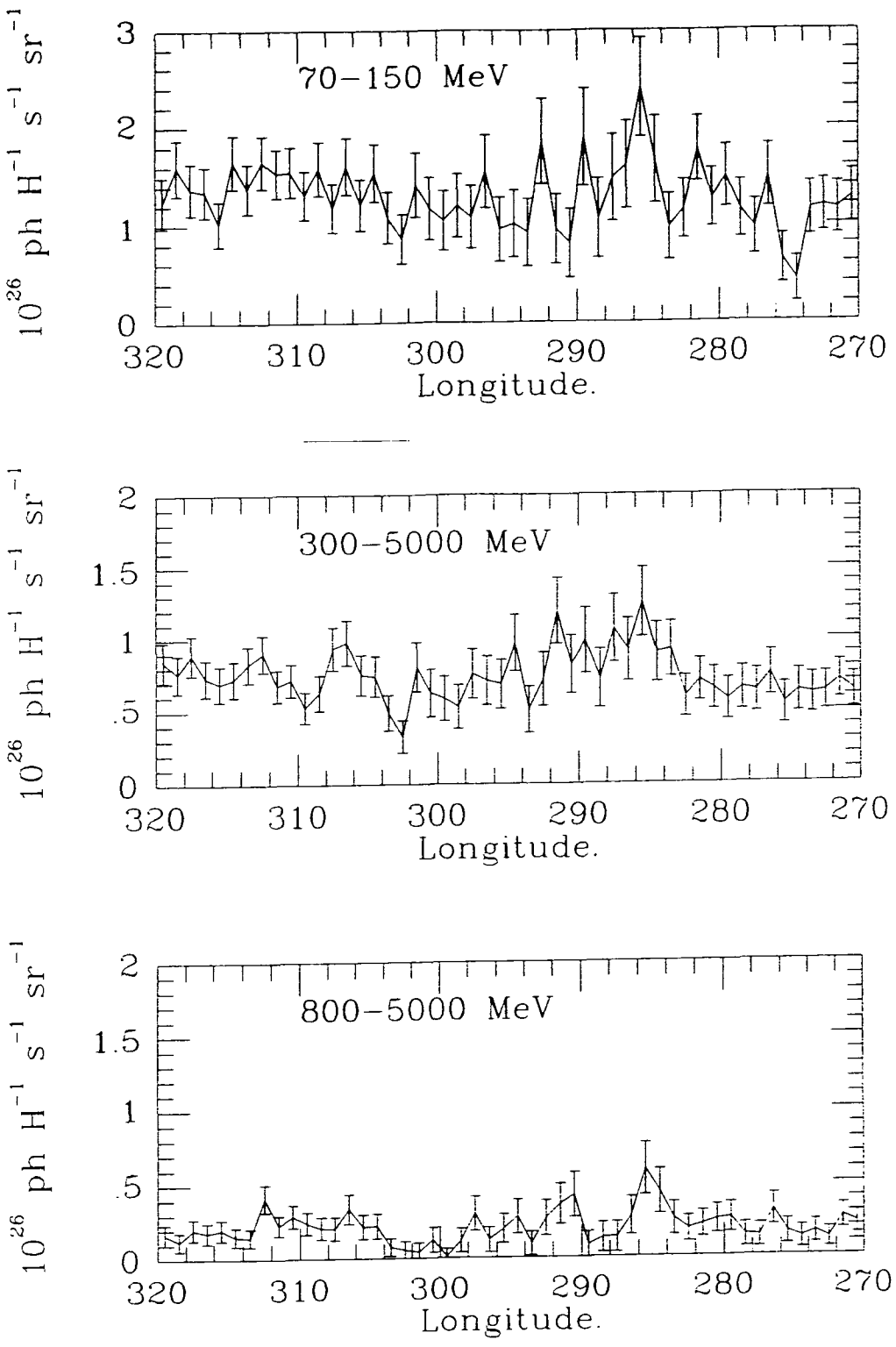

Figure 3.6
Emissivity profiles through the source for three energy bands. The longitude bin is 1°

index between arm and interarm was about 0.6, consistent with the value of about 0.4–0.5 found by Bloemen *et al* (1988) using different energies and galactic areas. The argument used by Rogers *et al* is that the parent protons

and low energy electrons gain considerable amounts of energy from processes within the spiral arm giving enhanced γ-ray emission at higher energies (> 300 MeV) and producing a flatter γ-ray spectrum.

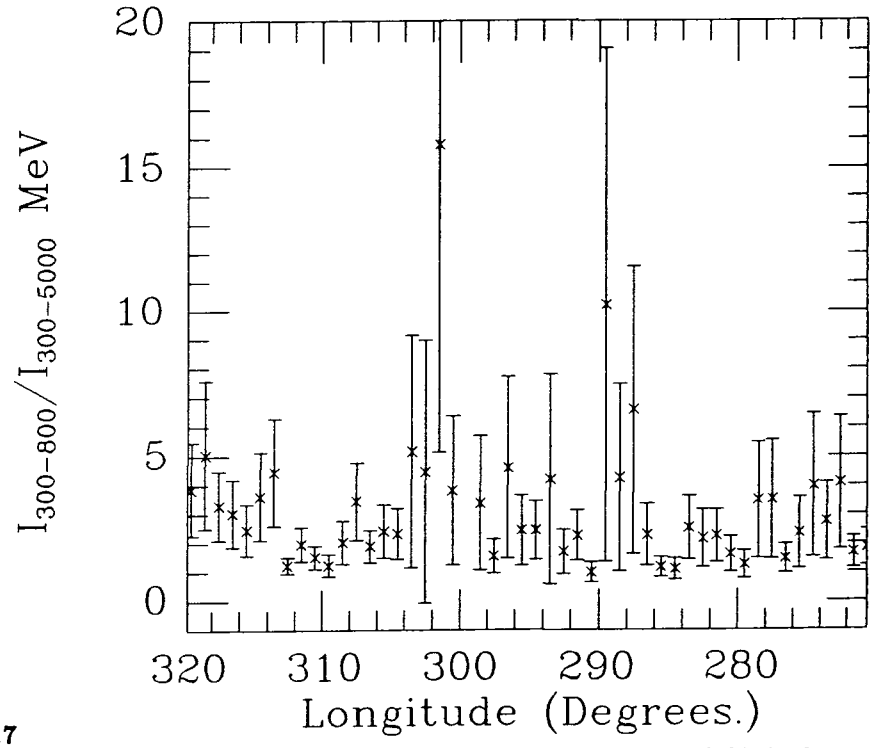

Figure 3.7
Spectral index $I_{300-800}/I_{800-5000}$ profile through the source. The longitude bin is 1°

The use of intensities > 300 MeV and > 800 MeV in Rogers *et al* is not strictly accurate as the energy ranges are not independent. Within the errors, however, the results will not be altered. Bloemen *et al* use intensities between 300–800 MeV and > 800 MeV, and for comparison, these same energy ranges are taken here. Figure 3.7 shows the variation of spectral index with 1° longitude bins with $|b| < 5°$. There are two features worthy of note: firstly, a general decline of the spectral index from $l = 270°$ to $l = 290°$ and around $l = 310°$, the latter being the narrower. Secondly a sharp increase in the index occurs between $l = 287°$—$289°$ and between $l = 298°$—$303°$.

If the spectrum is flatter in the arm then the spectral index should

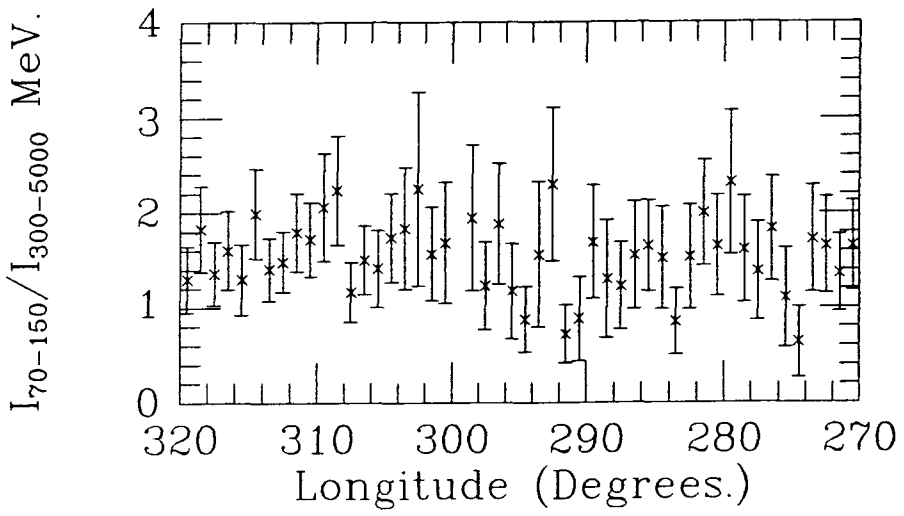

Figure 3.8
Spectral index $I_{70-150}/I_{300-5000}$ profile through the source. The longitude bin is 1°

decrease as the longitudinal position of the arm is approached and therefore the general decline in spectral index mentioned above can be attributed to the line of sight passing through an arm whilst the sharp increase must be associated with some other phenomenon that produces fewer high energy γ-rays. Figure 3.8 shows the spectral index derived from the ratio of intensities at 70–150 MeV and 300—5000 MeV. The situation is less obvious than the index derived from the higher energy bands, but the index is on average lower between $l = 283°.5$ and $l = 295°.5$ than at other longitudes which supports the result from higher energies. The size of the change between arm and interarm is not large however, suggesting that either the low energy particles are inefficiently accelerated in the arms, or that they diffuse away quickly. Also, of course, the resolution of the γ-ray data at 70–150 MeV is much poorer than at 300–5000 MeV which acts to obscures any true variation in the spectral index.

The high energy ratio of intensities show the regions $l = 286°.5$—$289°.5$ and $l = 298°.5$—$303°.5$ both have steep spectra caused by a deficiency in the higher energy (> 800 MeV) component, suggesting that genuinely fewer

photons are produced there. The CR generating these high energy γ-rays will not be excluded from these regions, although the low energy particles may be.

At the position of η Carinae, the γ-ray data suggests that there is no excess of low energy particles, but at high energy there is a distinct deficit. This would imply that any acceleration mechanism present in this region is unable to accelerate the higher energy CR required to produce the $>$ 800 MeV γ-rays.

3.4 A Model for the Carina Region.

The gas and γ-ray observations have been described in earlier sections, along with possible CR sources including the spiral shock. From all of these, a model is now developed that can explain the gross features of this region.

Firstly, it is obvious from the CO data that the Carina arm is tangential to the line of sight at around $l = 284°$, corresponding to a spiral arm with pitch angle $i = 9°.04$ and scale factor $R_l = 9.17$ kpc. The WR stars delineate an arm with $i = 5°$ and $R_l = 9.6$ kpc an therefore lie on average at greater galactocentric radii than the molecular clouds. The latter may be caused by the gas moving faster than the spiral pattern causing a shock to form compressing the gas and giving rise to the molecular clouds and subsequent star formation (e.g. Shu 1972). The location of the WR stars downstream of these clouds is in accord with this scenario. Given the position of the spiral arm as delineated by the gas, the shock is expected to lie inside it with smaller R_l and approximately the same i. The difference in gas velocity and pattern speed determines the shock velocity and how far from the shock on average the stars will form. This velocity is given by:

$$v_s = (\Omega_g(R) - \Omega_p(R))R \sin i \qquad 3.1$$

where the pattern speed is $\Omega_p = 13.5$ km s^{-1}kpc^{-1} and the gas velocity, Ω_g, is approximately flat around the solar position. Therefore as R increases, the shock velocity decreases and the peak star forming regions should occur nearer the shock. Eventually, the shock velocity will be lower than the local sound

speed and there will be no shock at all which may explain the lack of molecular clouds at large galactocentric radii (see, for example, Dame 1984, Bhat *et al* 1986c).

At $R = 9.5$ kpc with $\Omega_g = 250$ km s^{-1}, the shock velocity is ~ 19 km s^{-1}. If star formation lasted $\sim 3 \times 10^7$ years, such a drift velocity implies a distance of 590 pc and the peak in star formation should be $\sim 590 \sin i = 90$ pc further out from the Galactic centre. This agrees very well with the arm as defined by WR stars and provides excellent support for the model.

The results presented in §3.1 show that in all the three energy bands considered there is a narrow peak in emissivity at $l = 285°.5$. This peak is caused by an increase in γ-ray intensity rather than any sudden drop in gas column density at this longitude and cannot be attributed *directly* to a discrete source such as η Carinae (which lies at $l = 287°.6$) or WR stars (which peak around $l = 289°$) because of the lack of any such objects near the emission peaks.

The possibility that the enhanced emission is due to CR diffusing from η Carina must be examined. Montmerle (1981) has presented arguments based on estimates of the mass of the Carina complex that the γ-ray emissivity in Carina is probably much higher than locally. To account for the γ-ray flux of the source 2CG288-00, a mass of over $\sim 4 \times 10^6 M_\odot$ is required but there is no evidence from molecular gas studies that such a mass of gas exists at this position. Alternatively, the SNR hypothesis can be tested and excluded largely on the basis of both X-ray results and estimates of power required to support this X-ray emission (see §3.2.2). Montmerle (1981) put forward a stellar wind shock acceleration model for CR production, concluding that there is no energetics problem with this idea, but that reasonably efficient CR confinement is required unless the mechanical power from the stellar winds is many orders of magnitude greater than the γ-ray luminosity. In the HII region produced by the powerful O stars surrounding η Carinae, the CR confinement is purported to be caused by resonant interactions of CR with self-excited Alfvén waves as they move through the gas at a velocity greater than the local Alfvén speed (e.g. Wentzel 1974). In an HII region, these waves are only weakly damped providing strong confinement of the CR. The presence of O3

stars in the Carina nebula means that the number of ionizing photons is very high, producing a large HII region ($\sim$ 50 pc radius) which may confine the CR within this radius.

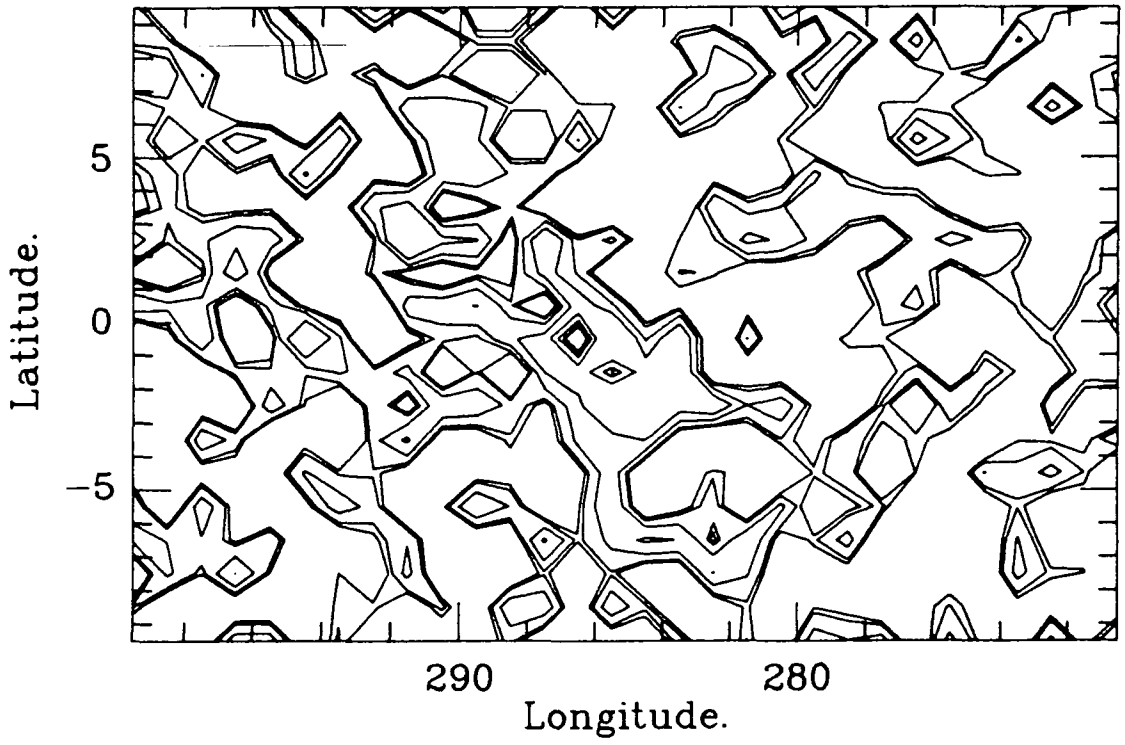

Figure 3.9
Contour map of excess γ-ray emission i.e. total γ-ray intensity minus that expected from the gas using $q/4\pi = 0.61 \times 10^{-26}$ph atom^{-1}s^{-1}sr^{-1} and $\alpha_{20} = 4.0$. Contour levels at: $(1, 2, 5, 10) \times 10^{-5}$ph cm^{-2}s^{-1}sr^{-1}

To investigate possible CR diffusion, the expected γ-ray intensity must be subtracted from the observed intensity to give ΔI_γ which will indicate where γ-ray emission and therefore CR intensity, is high. Figure 3.9 shows ΔI_γ for the 300–5000 MeV band with the data binned in 1° × 1° bins. A slight excess is observed in the direction of the source, but the bulk of the excess extends to lower longitudes and below the Galactic plane. Naturally, if any CR are diffusing from the source, they will manifest themselves only by interacting with the gas. Comparing figure 3.9 with figure 3.10 which shows

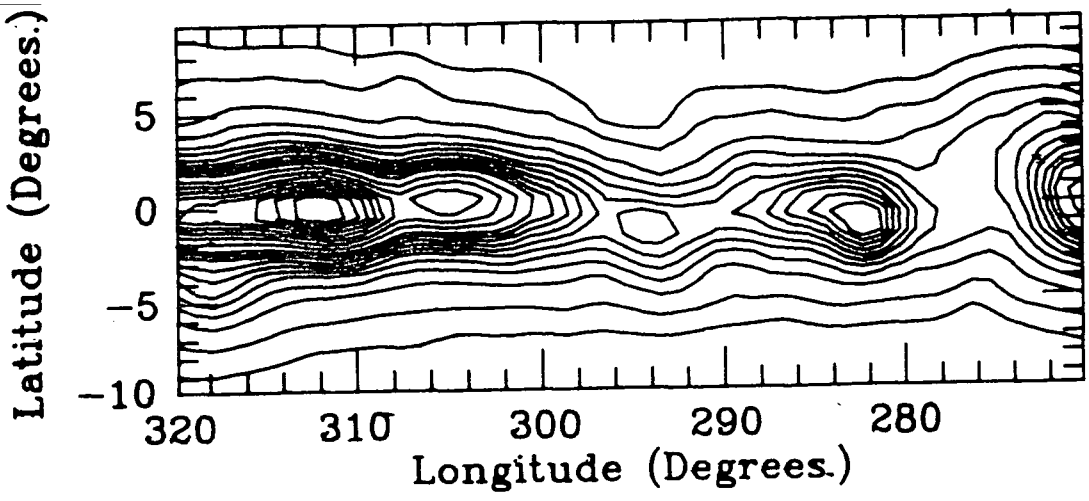

Figure 3.10
Contour map of CO gas from Columbia CO survey. Contour levels at: 0.5,1,2,3...10,12,14...26 K km s^{-1}

the CO gas distribution, reveals that the enhancement lies somewhat below the molecular gas over the whole of the excess γ-ray emission region. The ΔI_γ peak at $(l, b) = (292, +3)$ does not correspond to any CO peak and is responsible for the enhancement in $q/4\pi$ around $l = 292°$ seen in the higher energy bands. The geometry of the high gas density regions compared to the high ΔI_γ make it unlikely that these enhancements are due to CR diffusing from η Carinae. Comparing ΔI_γ with the distribution of WR stars and taking their distances into account, it would be possible to attribute some of the higher γ-ray emission to these objects, especially when the total power output by a WR over its lifetime is of the order of that produced by a SNR. Unfortunately, the combination of poor angular resolution and low counting statistics make such an association tentative at best and clarification must await future γ-

ray observations of the region. In any case, the fact that the excess emission extends over a number of degrees indicates that certainly not all the excess γ-ray emission can be attributed to active stars and it is likely that most emission comes from another source. *It is proposed here that the source of excess γ-radiation is due to CR accelerated by the spiral shock.* These CR interact with the gas along the length of the arm and produce γ-rays which are observed most prominently in the direction of the tangent. The poor angular resolution of the COSB satellite means that there is no chance of showing that the γ-ray peak does not coincide with the shock position; any difference between the two will again have to await improved telescope resolution. The fact that the γ-ray emission is displaced to lower latitudes below that of the CO on the near side of the arm is no longer a problem as the gas responsible for the emission is distributed over the whole arm. Additionally, the arm is warped, dropping below the plane for increasing R (Grabelsky *et al* 1987) in the same way as the HI layer (Henderson *et al* 1982). The maps of HI column density (Fig. 3.11) show that a large amount of gas over the whole line of sight is present in the enhanced emission region. The enhancement in $q/4\pi$ observed in all three energy bands at $l = 285°.5$ is attributed to the line of sight passing along the tangent to the shock. The inclination of the shock is taken to be $9°.04$ using the result obtained from the molecular clouds, and the scale factor is slightly less than that of the CO. The equations governing the geometry of the arm are Equation 3.1 and

$$\tan(360° - l) = \frac{R \sin \phi}{R_0 - R \cos \phi} \qquad 3.2$$

where ϕ is the azimuthal angle, increasing anti-clockwise such that $\phi = 0°$ when $l = 0°$. Combining Equation 3.1 with Equation 3.2, and finding the stationary point gives the longitude of the tangent to the arm, which can then be used to find R_l. For a tangent at $l = 285°.5$, the scale length is ~ 9.1 kpc which is slightly less than 9.17 kpc for the gas arm and gives a distance of 0.46 kpc between the shock and the gas peak. With a drift velocity of ~ 20 km s^{-1}, a distance of 0.46 kpc corresponds to a time $\sim 2 \times 10^7$ years which is a typical age for many of the OB associations in the region. It is also within the $\sim 3 \times 10^7$ years quoted by Roberts (1969) as the average length of time an association lasts.

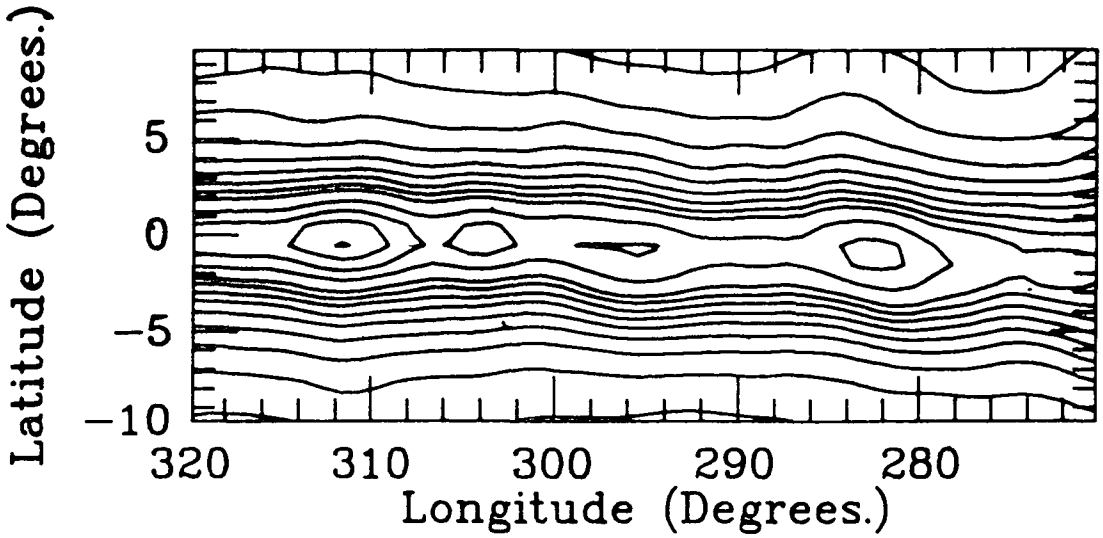

Figure 3.11
Contour map of HI gas. Contour levels at: (2,3,4...12,14,16,18) $\times 10^{21}$ atoms cm^{-2}

The excess γ-ray emission observed at 70–150 MeV is attributed to CR electrons and which is especially important in the light of work by Duric (1986a, b) and Duric *et al* (1986), as well as observations of external galaxies at 20cm and at visible wavelengths by Matthewson *et al* (1972). These papers present evidence for the existence of strong density waves by showing that the electron synchrotron radiation observed at 20 cm is displaced closer to the galactic centre relative to the optical arms. Duric calculates the CR energy density to be in the range 1 to 50 eV cm^{-3} which appears to be similar to the energy density of the gas turbulence and supports the concept of energy equipartition between gas, CR, and magnetic fields. This calculation allows the 20 cm enhancements to be attributed to increases in both magnetic field strength and number of CR particles. The importance of these observations also lies in the fact that the products of the spiral shock (SNR, OB stars etc.)

are not found at the peak in the synchrotron radiation and thus can be ruled out as the sources of the CR. Additionally, measurements of the synchrotron spectral index show that it flattens towards the centre of the spiral arm.

Such flattening is difficult to see in the ratio $I_{70-150}/I_{300-5000}$ but there are certainly no large positive excursions of this ratio between $l = 280°$ and $l = 292°$ whereas there are three bins with a low value of the ratio (Fig. 3.9). The behaviour of the ratio $I_{300-800}/I_{800-5000}$ shows a pronounced steepening of the CR spectrum between $l = 286°.5$ and $l = 289°.5$. This steepening can be attributed to η Carinae rather than the spiral arm, since if a latitude range is chosen to exclude it, then the spectral steepening disappears. The longitude range in which the steepening is observed is bracketed by three low bins with a spectrum in agreement with the models of Rogers *et al* (1988), Bloemen (1987) and Bloemen *et al* (1988). It could be that the presence of the spiral arm manifests itself either side of the active region whereas between $l = 286°$ and $l = 289°$, CR from η Carinae swamp the emission. These spectral ratios indicate that the η Carinae region is relatively weaker in high energy γ-rays than the spiral arm although the intensity is higher from the Carina Nebula region in all energy bands. This would seem to imply that the arm is capable of accelerating higher energy CR, a conclusion which is reinforced by the distinct deficit in $q/4\pi$ at 800–5000 MeV at the position of η Carinae in contrast to the clear peak at the tangent. At lower energies, there are more γ-rays from around both sites.

Some estimates put the maximum energy of CR produced by the spiral arm shock at 1 GeV (Völk 1987), and since the average proton energy for γ-rays of energy > 300 MeV is $\sim$ 7 GeV (Rogers *et al* 1988) η Carinae should be responsible for the particles producing these higher energy γ-rays rather than the spiral shock. Völk's calculation is based on an average shock speed of $\sim$ 30 km s^{-1}, and requires $v_{shock} > v_{alfven}$ for a shock to form. With $B = 3\mu$G and $n_e \sim 3 \times 10^{-2}$cm^{-3}, v_{alfven} is $\sim$ 38 km s^{-1} so the inequality is not satisfied and the diffusive shock acceleration process cannot work. The above calculations are based on the work of Duric (1986) who calculates that, providing a shock does form, particles can be accelerated by the diffusive shock mechanism to *at least* 1 GeV with high efficiency; greater energies can in fact be attained at the expense of this efficiency. He also notes that protons will

be easier to accelerate than electrons because of deflections by the shock, but that beyond a few GeV there is a problem in providing sufficient numbers of high energy particles. Also, dense neutral clouds provide heavy damping for Alfvén waves preventing the acceleration mechanism from working. The preferred site for the acceleration of CR is one which is mostly ionized with a temperature of $\sim 10^4$K in a fairly dense medium. Lower density regions require a smaller ionized fraction, typically $\sim$ 10% for the warm intercloud medium. Such conditions are often encountered in the interstellar medium.

The results obtained for the Carina region may be summarised thus: between $l = 286°$ and $l = 290°$ there is a deficit of high energy (> 800 MeV) γ-rays below that expected on the basis of local emissivity values, whilst the low energy (70–150 MeV) band is slightly enhanced but not prominent. Between $l = 283°$ and $l = 285°$, all three energy bands have a high emissivity, indicating a possible source(s) of CR.

The commonly proposed mechanisms for these two longitude regions are the spiral shock and stellar wind shock acceleration. The former is expected to produce CR to a few GeV whilst the latter can produce CR beyond 10^6 GeV (Cesarsky and Montmerle 1983, and see also Cassé and Paul 1980, Völk and Forman 1982). It would appear then that the η Carinae region should produce the high energy CR whilst the spiral arm should produce more at low energy. This is the reverse of the situation that is actually found here and means that either CR diffuse from η Carinae and interact with the gas associated with the spiral arm, or that they are efficiently confined to η Carinae and the spiral arm is much more efficient at CR acceleration than has previously been estimated, providing of course that no other factors are involved which could lower the emissivity (e.g. α_{20} is higher in the arm than the interarm). Cesarsky and Montemerle argue that HII regions provide good confinement for CR, implying that CR are not able to diffuse out of the Carina region to produce the extensive emission observed around $l = 285°$. The proposed geometry of the arm also precludes this possibility, as there should be some emission longward of η Carinae as well as towards the tangent, and this does not appear at any energy. Although the emissivity is high at the position of the tangent, it must be borne in mind that the line of sight through the gas is very long so that the acceleration efficiency need not be very high as there

is a great deal of target material. However, what is perhaps more relevant is that if the shock can only produce lower energy CR, there should be a steep spectral index towards the tangent point. This is not observed and indeed the spectrum flattens (Rogers *et al* 1988, Bloemen *et al* 1988). Interestingly, Blandford (1980) predicts a flatter spectrum from a weak shock even, as the CR have a lower effective specific heat ratio than the background medium. The shock velocity must be sufficiently high, however, and this may not be the case for a spiral shock.

WR stars in the arm could be the source of the high energy CR, but there are only five within 8 kpc of the Sun between $l = 283°$ and $l = 286°$ and not all are good source candidates since two lie well below the CO and another lies between the Sun and the majority of the gas. WR are not therefore expected to be the dominant source of CR over the arm. It is, of course, perfectly possible that these stars do contribute to the CR budget, but more than two are required to explain the observed γ-ray emission.

Clearly then, there may be a problem with the high energy component of the emission that appears to come from the spiral arm ($l = 285°$) rather than a particular active region. The whole of the emission at this longitude has been attributed to the spiral shock, but this is not likely to be an accurate model as Nature usually has more than one string to her bow. The line of sight along the spiral arm allows for a large number of potential CR sources to be produced by the shock. Observations of such objects are sparse. WR and OB associations are known to occur out to large distances (over 10 kpc) but they do not appear to be able to account for the excess at high energies otherwise η Carinae, which contains many of these objects, would then have a flatter spectrum than observed. SNR are the one class of objects that are capable of producing the high energy enhancement, but none have been reported in this region near the Galactic plane (Green 1984, 1987). Some are expected because of the large numbers of OB stars which are believed to end as SNe. A detailed radio survey of non-thermal sources of the kind performed recently in the first quadrant (Kassim 1988) is required in this longitude region. Such a survey should be capable of detecting the remnants associated with the spiral arm which would provide support for the shock–gas compression–OB star–SNR scenario (Elmegreen and Elmegreen 1979), as well as providing high energy

CR source candidates. In fact, an analysis of synchrotron emission performed by Broadbent *et al* (1988) has revealed a possible SNR at $l = 286°, b = 0°$. There is therefore a good chance that more remnants could be found.

3.5 The Sagittarius Arm.

If the spiral shock is capable of producing substantial fluxes of higher energy CR particles which are then translated into γ-rays above 300 MeV, then there should be evidence for enhanced γ-ray emission from other spiral tangents around the Galaxy. The ambient conditions elsewhere in the Galaxy are not likely to be the same as in Carina, if only because the tangents to other arms will not be observed at the same galactocentric radius and there are a number a relevant parameters that depend on R (e.g. the shock velocity, ambient CR electron density etc.). Attention is restricted here to the Sagittarius arm which is seen in the gas profile at a tangent at $l = 312°$. The various spiral tracers that provide a rather confused picture of the Carina arm also leave open to doubt the existence of this tangent. There is a large amount of gas at the tangent point, seen as a prominence in the longitude–velocity diagram at negative velocities (see for example, Grabelsky *et al* 1987) although it must be noted that the increase in gas at $l = 305°$ is a zero velocity feature which is probably local and not connected with the distant spiral arm of the Sagittarius tangent.

The greater distance to this tangent will mean that any γ-ray excess will be lower than that observed in Carina making the analysis more difficult.

As expected, the 70–150 MeV emissivity is only marginally enhanced around $l = 310°$ probably due to the poor angular resolution. There is a small increase in emissivity at 300–5000 MeV at $l = 312°$ which becomes more obvious at 800–5000 MeV, in line with the improvement in resolution. Little is revealed from an examination of the spectral index $I_{70-150}/I_{300-5000}$, because of the errors, whilst $I_{300-800}/I_{800-5000}$ suggests a distinct flattening around $l = 310°$ similar to that for the Carina tangent.

The region between $l = 298°.5$ and $l = 303°.5$ containing the large zero

velocity cloud has a particularly high spectral index indicating that no arm is seen at these longitudes. It is the absence of high energy γ-rays that produces this low index, rather than an enhancement at low energy so it is particularly interesting to note that a number of SNR and pulsars have been detected in the region by *EXOSAT* (Warwick *et al* 1988). Presumably these objects have been produced by the Sagittarius shock and they might be expected to contribute at higher energies and flatten the spectrum, but this is not observed. Such observations give considerable support to the idea that it is the spiral arm regions that are responsible for the high energy CR component and that it is the Galactic shock that provides the acceleration mechanism.

Thus there is now also evidence from γ-rays as well as gas and optical tracers for a tangent point to a spiral arm at $l = 312°$, i.e. as an increase in emissivity and as a flattening of the γ-ray spectrum towards the arm centre. For a pitch angle of 6°.2, which is the most commonly quoted value for the major arms from density wave theory, $R_l \sim 6.8$ kpc giving an arm spacing of 2.1 kpc at $l = 0°$. A value of $i = 9°$ (i.e. the same as for the Carina arm) would give an interarm spacing of ~ 2.5 kpc. The evidence for this arm in γ-rays is weaker than that from Carina because of the greater distance to the tangent and consequently more of the gas in the line of sight is not connected with the arm. It does give considerable support to the interpretation put forward here that most of the γ emission at $l = 285°$ is due to the spiral arm rather than any other source such as η Carinae.

3.6 Conclusion.

In this chapter the γ-ray evidence for CR sources in the longitude interval $l = 270°$–$320°$ and latitudes less than 5° has been examined at three energy intervals: 70–150, 300–5000, and 800–5000 MeV. The raw γ-ray intensities indicate a substantial increase longwards from around $l = 280°$ and declining with longitude. Consideration of both molecular gas and neutral HI, using the CO to H_2 conversion ratio $(\alpha_{20}) = 4$ gave an estimate of the total unionized gas. Dividing the intensity by the total gas column density gave the emissivity for each 1° longitude bin, from which the regions of enhanced CR activity could

be determined.

There are two good source candidates for the production of CR in the region: the Carina Nebula and the spiral arm shock.

The Carina Nebula lies at $l = 287°$, just below the Galactic plane, and contains large HII regions, active stars and the (possibly massive) peculiar object, η, at the centre. This whole complex is clearly seen in molecular gas and in HII emission and has a complicated morphology. The large lower density HII regions have not been included in the total gas column density estimates used when calculating the emissivities. It has been pointed out that in some cases the neglect of this ionised component could lead to significant errors in the emissivity. This is not the case in Carina as there are insignificant amounts of ionised gas and the error arising from its neglect is smaller than the errors in the γ-ray and neutral gas data. However, the presence of low density ionised gas has a more indirect effect on the measured flux as it can have a significant effect on the ability of the region to produce a shock. Although the Carina Nebula is classified as a 2CG source, the emissivity derived at higher energies is not significantly above that expected from ambient CR-gas interactions.

As the energy of the γ-rays decreases the emissivity rises indicating that the lower energy particles (which are probably electrons) are more responsible for the emission than nuclei.

At first sight, it is perhaps surprising that such an active region of the Galaxy does not appear as a genuine CR source at all energies. When the mechanism for CR acceleration is understood, it is in fact to be expected as the sound speed in the ionized gas in the Nebula is higher than in the denser molecular cloud. This in turn requires a higher velocity for any disturbance before a shock can form and may contribute to the lack of higher energy particles. Thus the ionised gas inhibits the formation of shocks and consequently reduces the overall CR production efficiency in the region. It is also worth noting that if the HII column density was significant, and there was therefore more target material than is estimated here, then the probability that the Nebula is a substantial source of CR would be even less likely. Higher energy particles are present in the Nebula since some emission is observed at 800–5000 MeV, but the existence of an enhancement above the expected ambient background at

low energies only is probably a result of efficient confinement by the ionized gas as mentioned in section §3.4. This means that the fairly large bins necessary in this present analysis to obtain adequate counting statistics would tend to smear out any signal from a genuine higher energy CR source. Improvements in γ-ray telescope resolution should be able to resolve this question.

It is at lower energies (70–150 MeV), where electrons are dominant, that η Carinae becomes more evident. Unfortunately, the spatial resolution is poor making the conclusions more tentative. There is evidence from the emissivity profiles and the spectral information for a low energy CR source at the position of η Carinae which shows a high ratio of low to high energy particles. Restricting the latitude range of the analysis to exclude the Nebula removes the emissivity enhancement suggesting that it is the Carina complex that produces these effects. The poor resolution of the γ-ray data is insufficient to make a distinction between the source candidates in the area, so whether active stars contribute or whether the whole of the emission is from η Carinae is not clear. The production of low energy particles clearly occurs and such active stars are the strong contenders for the production sites. Much better resolution must be achieved in order to distinguish between η Carinae and other active stars, but some support can be given to Montmerle's (1979) contention that active stars are able to accelerate CR.

The second source of CR is just shortward of the Carina Complex and lies between $l = 280°$ and $l = 285°$. The spiral arm contains a shock that is not as strong as, say, a SNR blast wave but should still be able to accelerate particles to CR energies. The main problems lie in the difference between the gas velocity and the speed of sound in the medium and how efficiently Alvén waves can propagate in the medium. These arguments have been used against the whole idea of spiral arm shock acceleration. The γ-ray results presented here show that there is an effect directly associated with the spiral arm and in the absence of any other more compelling sources such as SNR, the spiral shock seems to be the best candidate. SNR might be expected to be found near a spiral arm so it is surprising that none have to date been observed (Green 1988). SNR only persist in the interstellar medium for up to 10^6 years before the velocity of the remnant gas is of the order of a few kilometres per second, so it could be postulated that the emission is due to

CR produced by old remnants that are no longer seen as non-thermal radio sources. The problem then is similar to that of the spiral shock model: the shocks will be weak and unlikely to produce the higher energy particles and the advantage of the long line of sight through the gas in the spiral arm that could enable the spiral shock to contribute to the higher energies cannot be applied to the much smaller old SNR shocks. Also, the numbers of SNR in each 1° longitude bin over the line of sight will be small not only because the SN rate of one per 30–100 years permits only two every 10^5 years on average, but the spatial extent of the older remnants will make them more difficult to observe. The strength of the evidence that remnants can accelerate CR to high energies requires a detailed survey for these objects in this longitude interval. They would be better candidates for CR acceleration than the spiral shock in view of the problems of this latter model with the weakness of the shock and uncertainties about whether it can be formed at all.

Other source candidates should also be surveyed as the strongest evidence for the spiral shock producing the CR is that there is no other source candidate in the region. Pulsar surveys, for example, are still under-sampled, and these objects could certainly be responsible for some of the emission as the 'halo' around the Vela pulsar found in Chapter 2 showed. There may be some pulsars that are undetected as yet, or are undetectable because the angle of the radio pulse emission does not intersect with the line of sight. Until the survey is complete, the numbers expected in any line of sight are still highly uncertain. Also, distributed reacceleration has recently been suggested (e.g. Giler *et al* 1987a,b, Osborne and Ptuskin 1987, Letaw *et al* 1987, Wandel *et al* 1987) as a mechanism for the production of CR in spiral arms. There are problems with this model however, in that the resulting primary to secondary ratios do not appear to be correct. Modifications of the theory might resolve such difficulties and the numerous weak shocks expected in a spiral arm may then be a significant contributor to the CR flux.

Estimates of the Galactic γ-ray point source population undetected by COSB have been made by a number of authors. Since point sources are likely to be associated with spiral arms and their enhanced gas density, it is possible that it is such a population that contributes in this longitude region. The nature of these sources is open to speculation; pulsars, Geminga-type objects,

young SNRs such as the Crab, or obscured active stars in regions of high gas density have all been suggested.

The positions and distances of WR and O3 stars are such that they are unable to account for the emission. In addition, there is excess γ-ray emission at higher energies at the location of the Carina tangent that is not present in the Carina Nebula where such stars are relatively common. The evidence would thus seem to point away from active stars being responsible for all the emission, although those stars that are distant and obscured could still make a contribution at lower energy.

In the absence of any other source that is both consistent with γ-ray observations at other longitudes and is actually observed, the spiral shock model would appear to be the only remaining viable candidate. Alternative, hypothetical sources associated with the spiral arm can be put forward, such as SNR or pulsars, but these will remain speculative until the required observations for the alternatives are made.

There are problems with the spiral shock acceleration mechanism however, as it is not expected *a priori* to produce the higher energy CR necessary for the > 800 MeV γ-ray emission. Certain parts of the gas distribution can be selected by restricting the latitude range of the γ-ray data to exclude η Carinae, rather than just taking the whole latitude range of the molecular gas data, namely $|b| < 5°$. The velocity information of the CO data can be used to distinguish those molecular clouds that are in the arm and lie at various distances from the Sun. This is what Cohen *et al* (1987) have done. It is found that the excess emission follows the arm to greater heliocentric distances and is therefore associated with the arm generally and not just the tangent. This does not eliminate any of the sources mentioned above as they are expected to follow the shape of the arm. However, it does reduce the probability of the excess being associated with a more local source. Restricting the latitude range in such a manner decreases the number of bins over which the average is taken which consequently increases the uncertainty in the γ-ray intensity and makes the association of the excess γ-ray emission with the arm open to doubt. Hopefully, when much improved spatial resolution γ-ray measurements are made, the photon counting statistics will be sufficient to begin to attribute

γ-ray fluxes to gas at various distances.

In conclusion, the Carina region of the Galaxy remains one of the most fascinating parts of the Galaxy because it offers a view towards a spiral arm uninterrupted by large quantities of dust or other obscuring material. There are now strong candidates for CR sources both in the Carina Nebula and also towards the spiral arm tangent. Active stars and/or η Carinae seem to provide lower energy CR responsible for the low COSB energy γ-ray energy band emission observed from the Nebula, whilst in the absence of a more compelling source, the excess near the tangent has been ascribed to the spiral shock believed to be contained in the arm. More observations at radio and γ-ray wavelengths are needed to clarify the nature of this complex region. γ-ray measurements with improved spatial resolution and photon counting statistics are the most important for CR studies.

Chapter 4. Cosmic Ray Variations.

4.1 Introduction

The study of cosmic ray (CR) variations is one that brings together many disciplines. From a CR physicist's point of view, the temporal variations of CR are most important as part of their overall study, giving information about not only their past and present characteristics but also about their possible future behaviour. For example, such information can be used to tackle the problem of the formation of the solar system, or perhaps give some indication of the frequency of geomagnetic reversals. Cosmic rays continually bombard material in the solar system, some of which is accessible for analysis: Moon-rock and dust, meteorites, the atmosphere and lithosphere of the earth are all targets that bear scrutiny. Cosmic rays produce various cosmogenic nuclides in these targets that may or may not be radioactive, and the quantity of this material provides information about the CR exposure time of the target and any intensity variations. Excellent reviews of these matters may be found in the last two CR conferences (Povinec 1987, Raisbeck 1985) and of earlier work in the review by Lal (1974).

Some methods for investigation of CR variations (e.g. meteorites and lunar material) give an 'integral' response to a given CR fluctuation, and hence give the mean production rate of the nuclide over the exposure time of the target. Such an average is of little value when actual time histories are required and therefore, studies using 'differential' detectors are required (e.g. ^{10}Be in core samples or ^{14}C in organic reservoirs such as tree rings). Each sample contains a time sequence that records the different radionuclide concentration at each epoch. One difficulty is that samples must be independently dated to

obtain an absolute time history. The use of studies of CR variations can be typified by the studies of solar phenomena (Burchuladze *et al* 1980, Povinec 1977, Stuiver and Quay 1981). For example, ^{14}C in tree rings is anticorrelated with sunspot numbers in the 11 year solar cycle. ^{10}Be results from polar ice have revealed a 20 year periodicity in solar activity during the Maunder minimum (Galli *et al* 1985).

For the timescales covered by this chapter, ^{10}Be is one of the best candidates for studying the CR history of the Solar System. It has a half-life of 1.5×10^6 years and can be detected in cores from both Antarctic ice and the ocean bed. Ice cores and ocean sediments have been obtained with ages to 2×10^6 years. The isotope is produced by the spallation on atmospheric ^{14}N by protons and then diffuses down from the stratosphere, being deposited within a few weeks on to ice or the shallower ocean layers. Up to a further 3×10^3 years are required for the radionuclide to reach the ocean sediments. With such a complex time history, there are many factors which can alter the amount of ^{10}Be produced and/or the deposition rate before it reaches the (hopefully) stable reservoir. Fluctuations in this record can be attributed to solar phenomena such as the 11 year sunspot cycle and Maunder-type minima, to geomagnetic effects such as field reversals, and also to climatic conditions. Each of these variations has a different timescale ranging from the 11 year sunspot cycle to the 10^4 year period of geomagnetic effects. ^{14}C measurements can be used over the last 10^4 years and are thus excellent monitors of CR fluctuations during this period. Finally, the CR variation that is considered here is that due to phenomena external to the solar system, and in particular, that attributable to supernova (SN) explosions. For such work, ^{10}Be is the most suitable isotope having a long half-life and a means of deposition that allows a differential-type of detection.

In this chapter, a Monte-Carlo model which has been developed for studying the long-term variations in CR intensity is described. The results obtained thereby are compared with the observed fluctuations in the record of ^{10}Be and other cosmogenic radioisotopes with similar half-lives. Conclusions about the model are drawn from this comparison and suggestions about improvements to it are made in the light of continuing improvement in the data.

4.2 ^{10}Be measurements

Many groups of researchers around the world have taken core samples of polar ice or ocean sediment and using sensitive mass spectroscopic techniques have measured the quantities of ^{10}Be present at various depths. The independent dating of the core allows the age of the sample to be determined. The half-life of the isotope is quoted above (1.5×10^6 years), but is only accurate to 20% and various methods of measurements have given $(1.6 \pm 0.2) \times 10^6$, $(1.5 \pm 0.3) \times 10^6$, and $(1.7 \pm 0.4) \times 10^6$ years. Raisbeck *et al* (1985) adopt $(1.6 \pm 0.3) \times 10^6$ years in their earlier work but use $(1.5 \pm 0.3) \times 10^6$ years in more recent studies, as do Tanaka and Inoue (1979). The most recent measurements (Hofmann *et al* have determined the half-life to be $(1.51 \pm 0.06) \times 10^6$ years. Figure 4.1 contains the data from six ocean core samples of Tanaka and Inoue (1979) and Tanaka *et al* (1977) as well as that of Raisbeck (1985).

The ratio of ^{10}Be to ^{9}Be is used in the more modern measurements as an attempt to compensate for deposition fluctuations in the ocean sediment and acts therefore as a 'normalising' species.

Data Set	a	b
1	2.56 ± 0.31	-0.318 ± 0.076
2	2.76 ± 0.42	-0.374 ± 0.123
3	2.40 ± 0.25	-0.400 ± 0.068
5	1.53 ± 0.20	-0.365 ± 0.088
6	1.02 ± 0.16	-0.288 ± 0.096
R	6.54 ± 0.518	-0.486 ± 0.012

Table 4.1

If a least-squares fit is performed using an exponential of the form ae^{bt}, values for the decay constant ($\equiv b$) can be obtained for each of these data sets. Table 4.1 summarises these results. The units of parameter a for each data set are the same as in Fig. 4.1 and multiplied by an appropriate power of ten.

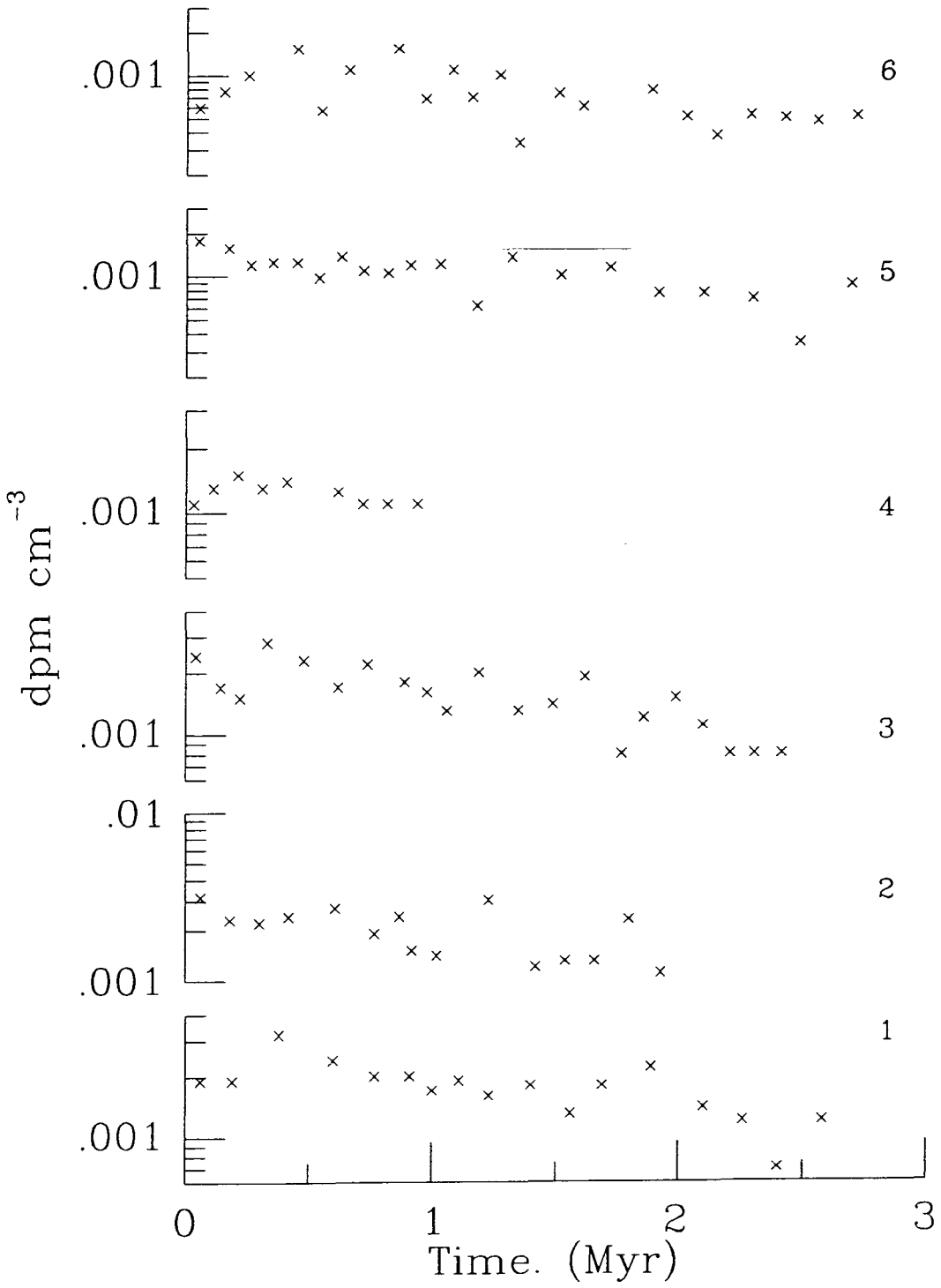

Figure 4.1a

The ^{10}Be concentrations in six ocean core samples. The ordinate units are disintegrations per minute per cm^{-3}. From Tanaka and Inoue 1977 and 1979.

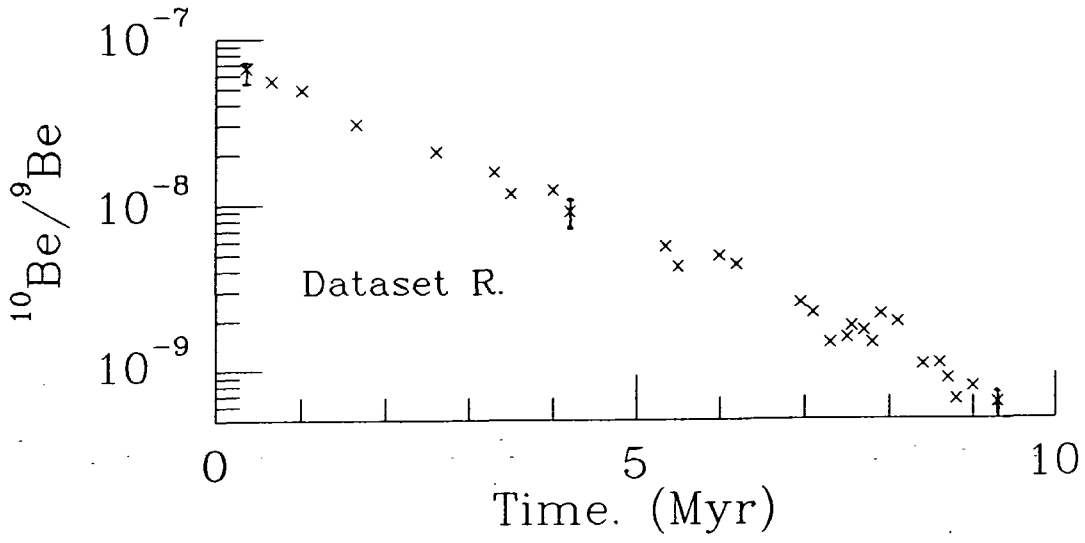

Figure 4.1b

^{10}Be data from Raisbeck (1985). A typical error is shown.

The half-life may be calculated from b according to: $T_{1/2} = ((\log_e 2)/b) \times 10^6$ years. Set 4 has been ignored as the time sequence is not co-extensive with the others.

The most obvious fact evident from this table is that the Tanaka and Inoue samples have half-lives greater than the expected value, 1.5×10^6 years. This figure is within the errors for most of the samples, but the values of the half-lives are not uniformly distributed about it. The Raisbeck data, however, imply a half-life of less than 1.5×10^6 years and have a much higher precision since they were taken from a core with an age of over $\sim$ 5 times longer than the cores of Tanaka and Inoue. Even over the shorter times of $\sim 2 \times 10^6$ years of these authors, no geomagnetic or solar effects are expected to manifest themselves and Nishiizumi *et al* (1980) find that the flux of solar CR has also been constant over the past $\sim 10^7$ years. That the half-life of ^{10}Be as estimated from the data does not equal the laboratory value indicates a trend in the data. Either a new very long-term geomagnetic effect is evident, or

there is some deposition effect, or it is due to CR variations. The sense of the trend for the Tanaka and Inoue data is different from the Raisbeck data. The Tanaka and Inoue data indicate that the ^{10}Be production rate has been dropping with time to the present, whilst Raisbeck finds that the production rate was lower in the past. Any model of CR variations must discriminate between these the Raisbeck results and those of Tanaka and Inoue, but *a priori*, the Raisbeck data are expected to be more accurate firstly because the measurements extend to nearly 10^7 years and therefore the estimate of the half-life is more precise, but also because the accuracy of the measurements themselves has improved with the use of new spectroscopic techniques. The Tanaka and Inoue data can be fitted with a function of the form given above, but also with a *linear* function. The least-squares error on the gradients obtained in both cases are similar. The problem with the analysis is that there are not enough measurements and the scatter in the points is too large to permit an accurate assessment of the long-term trend.

The latest analysis of an ocean core (Bourles *et al* 1988) has just been completed but unfortunately was completed too late for this analysis. Briefly, the long-term trend is apparent in the data by a linear regression fit. The apparent 'half-life' of the cores was found to be in all cases lower than the theoretical value indicating a slow increase in the amount of ^{10}Be relative to ^{9}Be with time to the present. The half-life determined from different sections of the core gave values either in rough agreement with or slightly lower than the 'R' value in Table 4.1.

The long-term trend in the data sets can be easily demonstrated by subtracting the expected ^{10}Be values from those observed using a half-life of 1.5×10^6 years and normalising to the present day ($t = 0$) using the intercept from the least-squares fit. Fig. 4.2 shows the result of this subtraction.

It is clear that nearly all the points lie below the expected (i.e. 1.5×10^6 years half-life) curve showing that the observed production rate of ^{10}Be is lower than expected over the whole time-span of the measurements. Another method of displaying this trend is to multiply each ^{10}Be/^{9}Be measurement by the exponential decay term, e^{t/T_l} (where T_l is the lifetime), to find the initial value predicted at that time. This has the advantage of not requiring

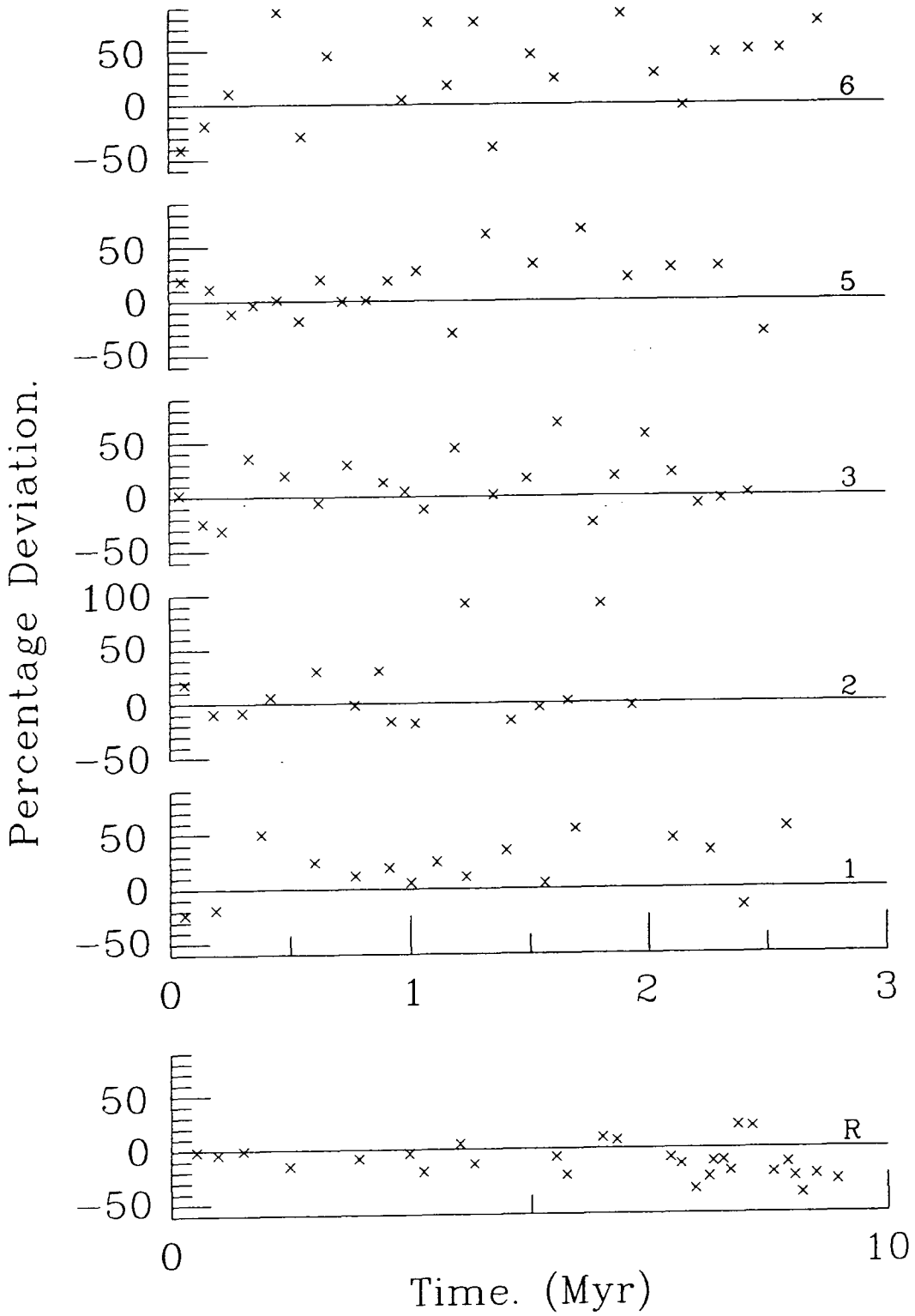

Figure 4.2

Percentage deviation of ^{10}Be data from expected curve using a half-life of 1.6×10^6 years. Dataset 4 has been excluded.

normalisation at the present, but also shows the trend quite clearly. (Fig. 4.3). In the Raisbeck data (denoted by 'R' in the figures), there are four positive points which were thought to be evidence for CR excursions at those times by indicating higher ^{10}Be production at those times. (See Chapter 5 for the latest results on the excursions.)

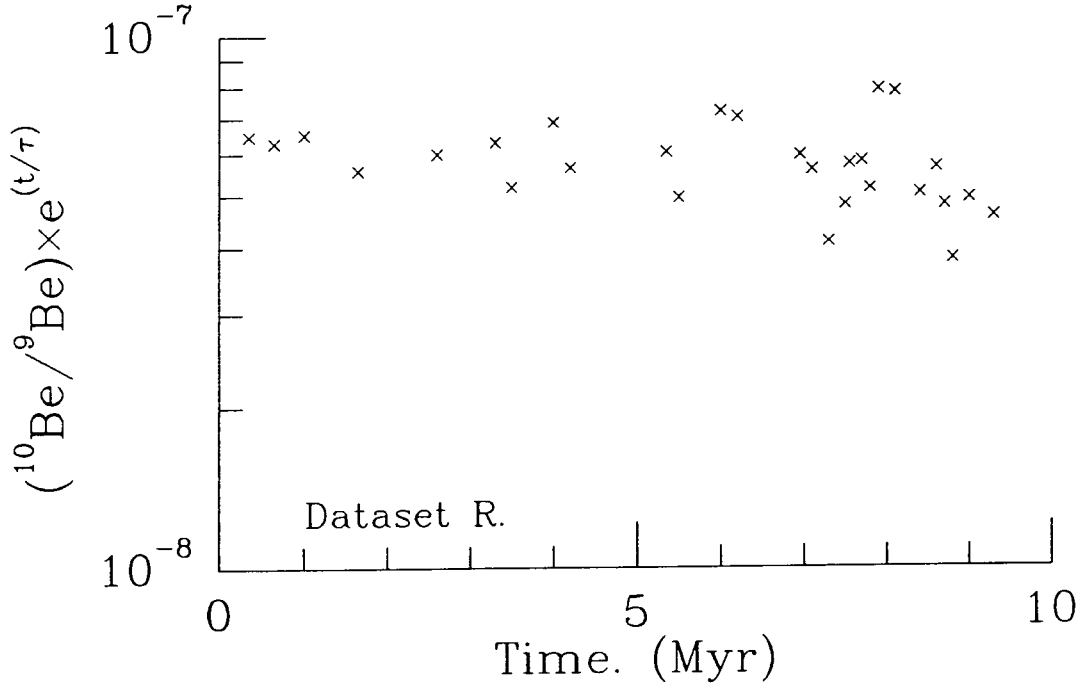

Figure 4.3b

^{10}Be data from Raisbeck (1985) multiplied by $e^{(t/\tau)}$

It is proposed by the present author that this long-term increase is a result of the motion of the solar system through the Galaxy and not is due to any geomagnetic effects. There is support for this idea from a number of authors using a variety of techniques and different radioisotopes. For example, Raisbeck argues that over timescales greater than 10^4 years geomagnetically induced variations of CR intensity should be attenuated. Kohl *et al* (1978) indicate that the solar CR flux is constant over the past $(1-10)\times 10^6$ years from

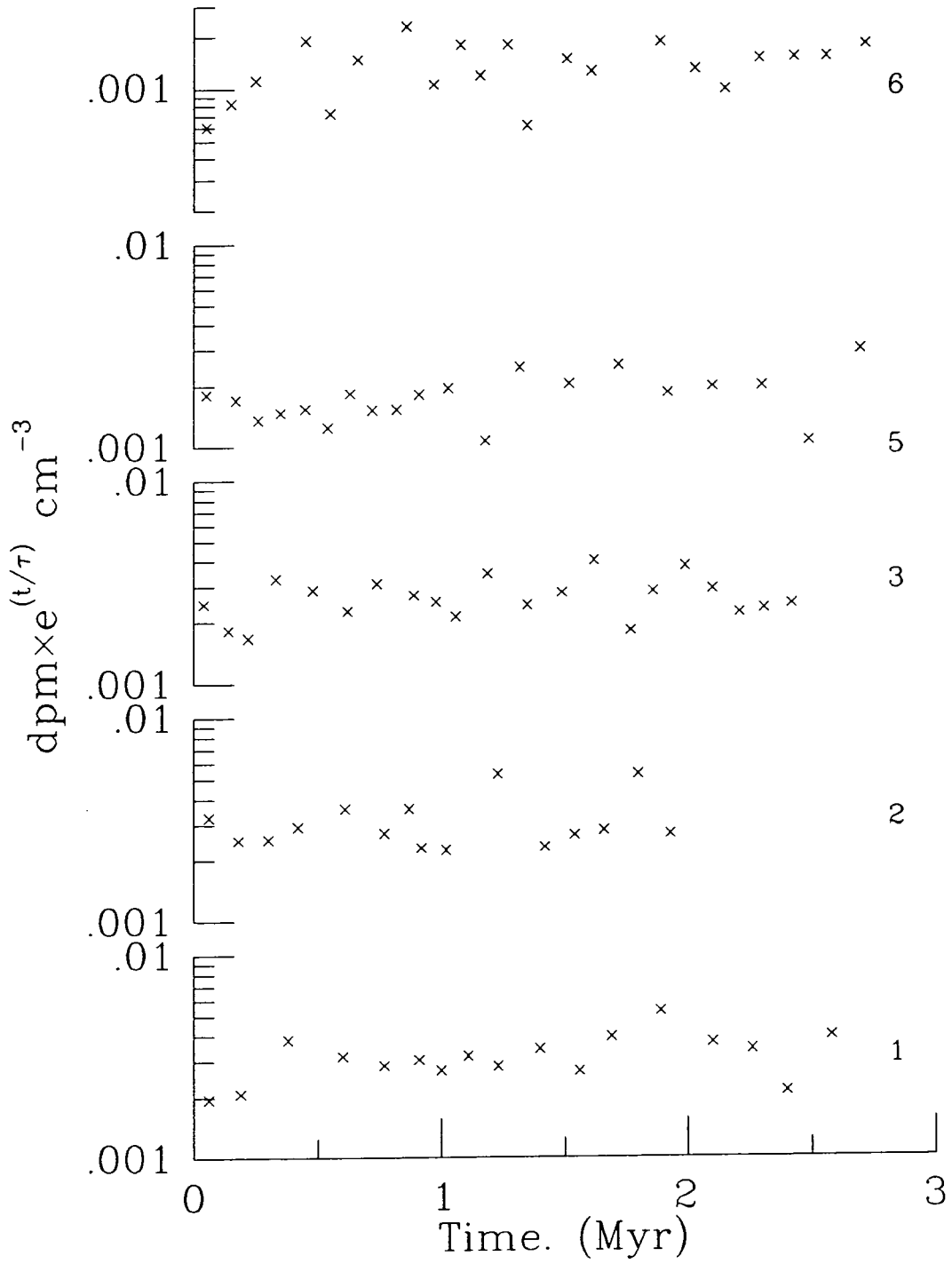

Figure 4.3a

^{10}Be concentrations from Tanaka and Inoue multiplied by $e^{(t/\tau)}$

measurements on lunar rocks. Voshage (1967) finds Galactic CR intensities 30% lower in the past 10^9 years than in the last 10^6 years contradicting the Tanaka and Inoue results. This is confirmed by Hampel and Schaeffer (1979) in their work on ^{26}Al in iron meteorites.

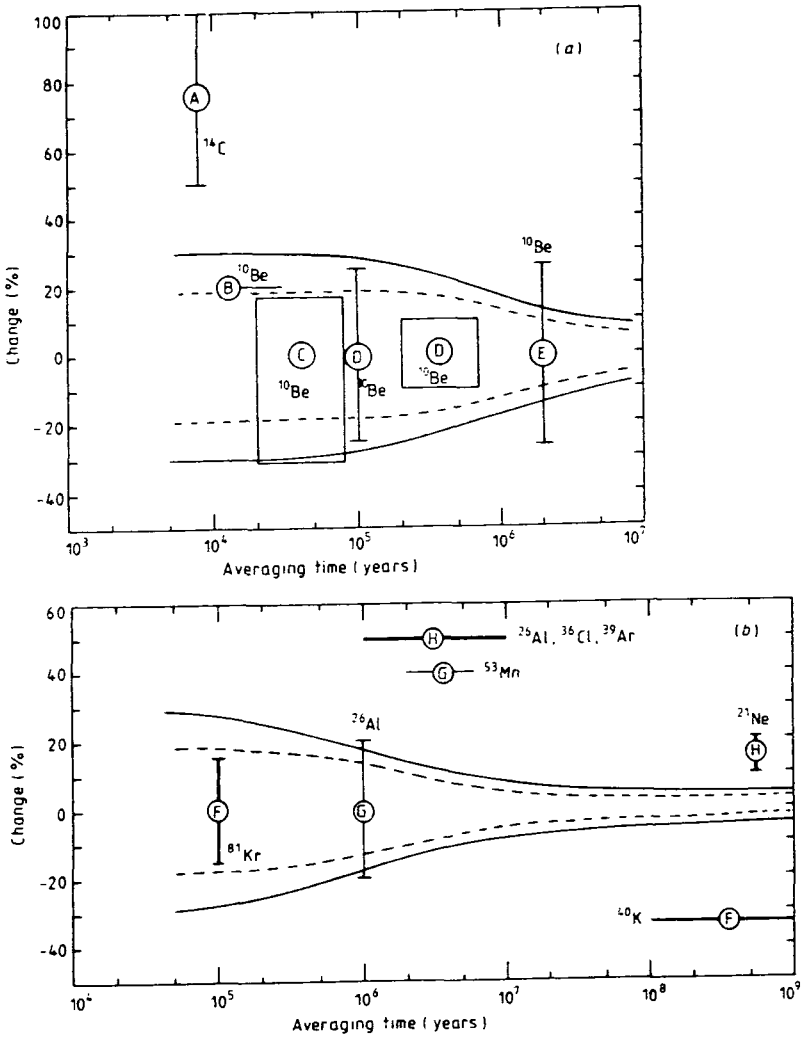

Figure 4.4

CR intensity variations about the contemporary value from an analysis of cosmogenic nuclides. *a*.Terrestrial samples. *b*. Non-terrestrial samples. Meteoritic data is shown with a thick line, lunar data with thin. The full and broken curves represent the model predictions of Bhat *et al* (1987) with $D = 5 \times 10^{28}$ and $D = 5 \times 10^{27} \mathrm{cm}^2\mathrm{s}^{-1}$ respectively. Refs.: A: Dergachev *et al* 1983, B: Kocharov and Konstantinov 1983, C: Raisbeck 1985, D: Tanaka and Inoue 1979, F: Nishiizumi *et al* 1985, G: Tokar and Povinec 1983, H: Voshage 1984. (This figure is taken from Bhat *et al* 1987.)

Bhat *et al* (1987) proposed a simple model for the energy density variations expected at the Earth due to CR produced by supernova remnants (SNR). A Monte-Carlo approach was used with a model of both the SNR shell and of the subsequent diffusion and loss from the Galaxy of the CR produced by the SNR. The model produced variations in CR intensity that did not contradict the results from ^{10}Be and numerous other radioisotopes. (Fig. 4.4). Using an autocorrelation technique, long-term variations were investigated and a distribution function of energy density values found. (Fig. 4.5). From this, the probability of a given increase in CR energy density (and therefore in ^{10}Be production) was calculated and hence the probability of a certain number of fluctuations away from the expected value in a given time period. The results suggested that the two possible excursions mentioned earlier i.e. the four points in the Raisbeck data available at the time the paper was written(Fig. 4.1b) were consistent with the model in that they had the amplitude and width similar to that expected from a 'local' supernova. However, subsequent improvement in the data (by taking more core samples) have prompted the statement by Raisbeck (1988) that these excursions are not present any longer, but the latest results allow the possibility of an excess around 8×10^6 years ago. (The long-term increase is, however, still evident.) The lack of excesses poses a problem for the Bhat *et al* model as the predicted probability of there being no 'local' supernova within the time period of the ^{10}Be observations is rather low. Therefore, refinements are required to this model to bring it into line with the new observations. Indeed, Povinec in his invited talk to the 20th International CR Conference in La Jolla urges further work along these lines (Povinec 1987). A further problem with the Bhat *et al* model is that it does not produce the canonical energy density value of 1eV cm^{-3} (Ginzburg and Syrovatskii 1964), but values of at least a factor of six times higher. Naïvely, one might expect that the average energy density predicted by the model would not be this canonical value, but further consideration reveals that if the model is to be at all credible, the value produced must bear some resemblance to that found in nature. The reason is that the construction of the model is based on actual functional relationships between the age, radius and energy expected for a SNR. These equations should produce sensible results when combined in the model. A further critisism of this model can also be made which leads naturally to improvements described in later sections. The critisism is this: the

probability per unit area of the Galactic disk of a SN occurring in a given time was taken in the Bhat *et al* model to be the same in all directions. Clearly, in the real Galaxy this is not the case. Observations of external galaxies show spiral patterns that are delineated by bright stars (usually OB associations), giant HII regions and areas of obscuration. HI and CO observations also show this spiral structure revealing that giant molecular clouds occur mainly in the arms (Fig. 4.6). (Stark 1979, Dame 1984). It is well documented that SN occur in or near OB associations and giant molecular clouds (Montmerle 1979a,b and references therein) and this observation is backed up theoretically with the prediction that the more massive and luminous the star the shorter its lifetime and the more likely it is to end its days as a SN.

The modelling of temporal variations needs improvement and some of the ways this may be achieved have been discussed above. The elements necessary for the new model will now be introduced.

4.3 Past History of the Solar System.

4.3.1 Introduction.

The past history of the Solar System is an integral part of the problem of CR variations. An extensive literature survey has been made for evidence of events in the past that may have had a bearing on the CR energy density at the Earth. Such events include local supernovae (SNe) (where 'local' is left undefined at present but certainly < 1 kpc), solar crossings of a spiral arm, encounters by the Sun with giant molecular clouds etc. Also needed is the spatial velocity of the Sun with respect to the Galaxy as a whole (both motion in the Galactic plane and perpendicular to it.) Such a survey covers a great many interesting topics from mass extinctions of flora and fauna and the possibility of a solar companion, to the local galactic mass density and galactic dynamics.

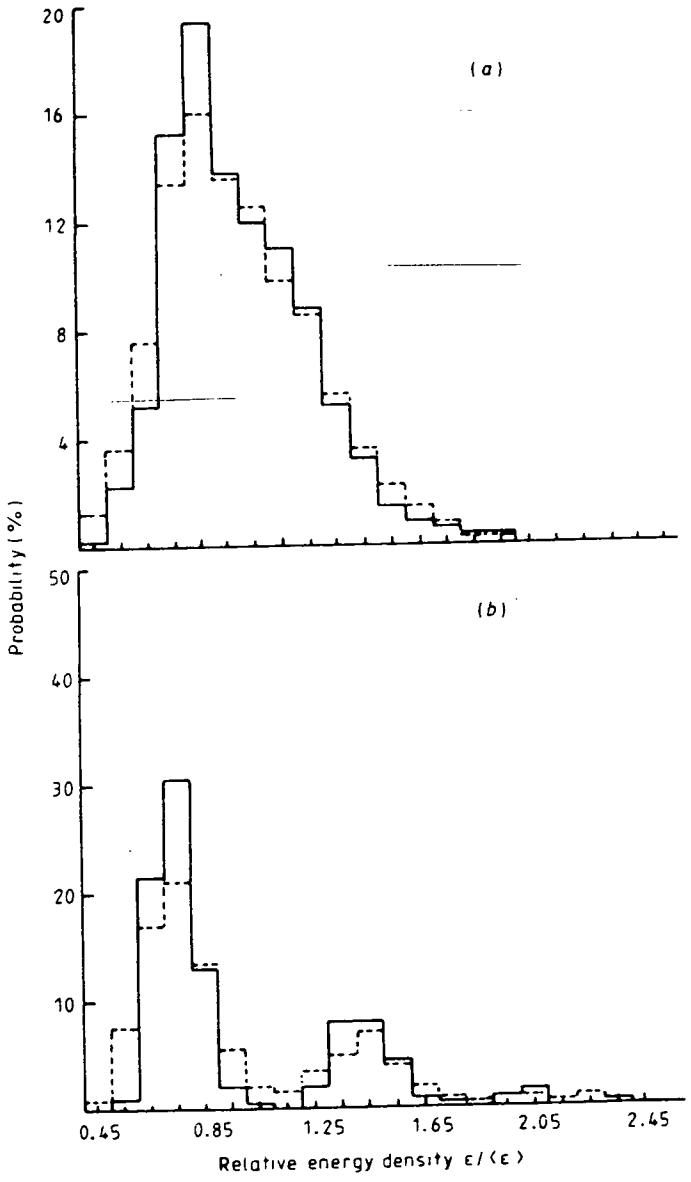

Figure 4.5

Model predictions of the frequency distribution of the relative energy density $\epsilon / <\epsilon>$ at the Earth for $\tau = 5 \times 10^6$ years and *a*. $D = 5 \times 10^{27} cm^2 s^{-1}$, *b*. $D = 5 \times 10^{28} cm^2 s^{-1}$ The broken line histograms are the model data (full line) modulated with a Gaussian noise approximately equal to that of Raisbeck (1985). The faster diffusion in *b*. gives rise to the multiple peak structure corresponding to local (< 130 pc) SNR being explicitly observed. This figure is taken from Bhat *et al* 1987.

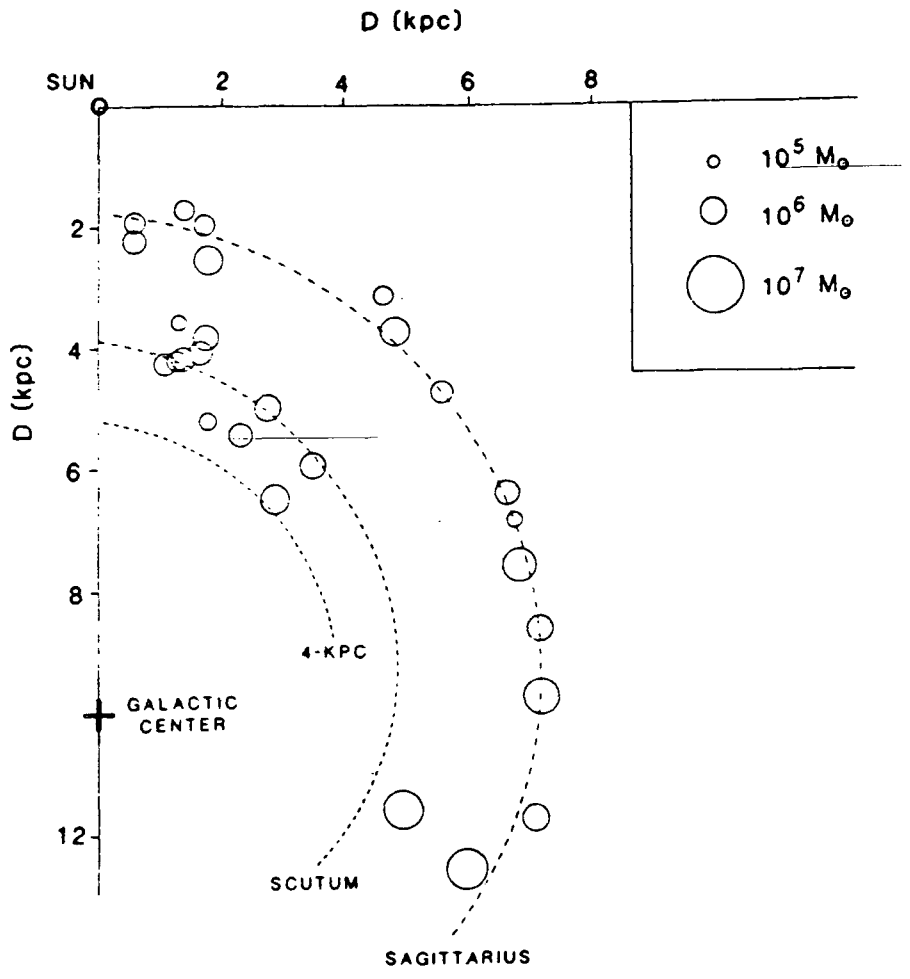

Figure 4.6

Diagram showing molecular gas (CO) clouds in spiral arms.

4.3.2 The Local Interstellar Medium.

The local interstellar medium (LISM) consists of matter in many different states of ionization and having a wide variation in temperature (Paresce 1984). The region near the Sun (3—6 pc) contains neutral gas surrounded by a hot plasma. This neutral gas is warm ($(12 \pm 3) \times 10^3$ K) with a density of $\sim$ 0.05 cm^{-3}. Soft ($<$ 0.3keV) X-ray background measurements indicate temperatures of $10^5 \rightarrow 10^6$ K with n$\sim$ 0.01 $\rightarrow$ 0.001 cm^{-3}, and suggest that beyond the 'near' region, the average plasma density falls with increasing dis-

tance from the Sun. One model for the LISM proposes that a shock front passed the Earth within the last 10^5 years since this would explain the X-ray observations and also provide a source of energy to maintain the temperature of the warm clouds. If the shock front was nearby (~15 pc from the Sun) it would cause the disruption of grains and dust that may have been present at one time, thereby explaining the lack of dust in the LISM. (Perry, Johnston and Crawford 1982, Crutcher 1982.)

The Sun moves in the LISM region with a relative velocity of 15-20 kms^{-1} towards $l = 55°$, $b = 23°$ (Bruhweiler and Kondo 1982, Frisch 1981).

The X-ray data mentioned above, along with other such observations have prompted Sanders *et al* (1977) and Davelaar *et al* (1980) to suggest that the Sun is immersed in the hot gas bubble produced by a local supernova. An age of 2×10^6 years is suggested for the SN, roughly consistent with estimates which show that the average CR intensity increased about 2.5×10^6 years ago (Nishiizumi *et al* 1980, Muller, Hampel and Kirsten 1981). A candidate for this SN is the large feature known as Loop I or the North Polar Spur. The centre of this structure, if spherical, lies ~130 pc away from the Sun, with a radius of ~115 pc. It appears as a shell in 21 cm radiation and in X-rays, but the temperature of the X-ray emission is not consistent with the age and energy of the SNR implied by the size of this shell. Thus, it has been proposed (Iwan 1980) that this SNR reheated a second SN explosion with a age of 2×10^6 years and initial energy of 6×10^{50} ergs. Loop IV is the prime candidate for this role. Ikeuchi (1978) on the other hand, proposes Loop I as the SNR that reheated the circumsolar bubble, but this does not seem likely in view of the neutral gas sheet lying in front of Loop I. Davelaar *et al* (1980) propose an old cooling-phase SNR to explain the local hot region, with Loop I located in a cavity created by winds from the Sco-Cen OB association, with which Loop I may be associated (Weaver 1978). Weller and Meier (1981) measure the interstellar helium component near the Sun and conclude that the photo-ionization rate of the gas is substantially higher than expected from either soft X-rays or CR, but can be explained by UV radiation from hot stars. Morfill and Hartquist (1985) review the evidence for SNe activity in the solar neighbourhood over the last few 10^6 years. They use estimates of the local ^{26}Al production rate and derive the γ-ray line flux from it, concluding that the Solar

System is immersed inside an old 'superbubble' (Innes and Hartquist 1984). This ^{26}Al emission is not inconsistent with a recent local SN, but when the galactic emission is taken into account, the evidence becomes 'less compelling'. Additionally, high measurements of the ^{26}Al/^{27}Al ratio in meteorites show that if there is a local origin for ^{26}Al then special conditions must have prevailed when the Solar system formed.

Forman and Schaeffer (1979) estimate that only SN explosions within 100 pc of the Sun could lead to an observable excursion from the background CR flux. This gives a first approximation for the term 'local'.

There are problems with finding a candidate SNR responsible for the conditions prevailing in the solar environment. The gas front forming part of the shell of Loop I, for example, does not appear to have reached the Sun, and some authors do not consider some of the other giant radio Loops to be real features. Apart from SNR, there are objects capable of producing these conditions. Stellar winds from OB stars and their ionizing UV flux seem to provide the most likely source of the hot gas. However, this does not explain the observed increase in the CR intensity around 2.5×10^6 years ago.

Studies of the young star distribution around the sun have revealed two belts or extended associations of stars. One is associated with the galactic plane, and the other is known as Gould's belt (Gould 1874). Frogel and Stothers (1982) have analyzed the motion of this belt and concluded that there was some disturbance that 'knocked out' a slab of gas from the Galactic plane. The stars that have condensed from this slab now form Gould's Belt. Unfortunately it seems that this occurred approximately 2×10^7 years ago and therefore it is unlikely to account for the observed increase in CR intensity. However, suggestions about disturbances of this sort must be borne in mind because whatever phenomenon created this belt might also have caused an increase in CR intensity lasting much longer than the initial disturbance.

Finally, the idea that the Sun may have interacted in the past with the Orion molecular cloud complex must be dealt with. Such an encounter was considered a possibility in view of the proximity of the complex and would have had consequences not only for the CR intensity near the Earth, but also on the Sun's motion around the Galaxy.

From the literature, the mean centennial motions in Right Ascension and declination are:

$< \mu_\alpha >= -0.45 \pm 0.45$ seconds of arc.

$< \mu_\delta >= -0.1 \pm 0.5$ seconds of arc. and the radial velocity is $+23.0 \pm 8.1$ km s^{-1}. Orion is currently at an approximate position of $(l, b) = (206°, -18.°75)$ at ~450 pc (Blaauw 1956, Strand 1958, Lesh 1968, Warren and Hesser 1977, 1978)

Converting these numbers into motions in and perpendicular to the Galactic plane, and using the Sun's velocity with respect to the local standard of rest (LSR) as motion in its epicycle about a point moving around the Galactic Centre with a constant velocity (Woolley 1969, Allen 1973, Delhaye 1965 and §4.3.4), then the closest approach of the Sun to Orion was around $\sim 1.5 \times 10^7$ years ago at a distance of ~200 pc.

This calculation relies on measurements of the velocities of the Sun and the Orion complex and neither quantity is well determined. The errors in the derived motions of the Orion complex are considerable, but if the presently accepted values are of the right order then it does not appear likely that such an encounter took place. The dynamical history of the two objects cannot be known with certainty over times $\sim 10^7$years or more, so an interaction cannot be ruled out altogether. Unfortunately, little more can be said until more refined observations are performed

4.3.3 z-motion and Cosmic-Ray variations.

The components of standard solar motion are (Allen 1973):
X = 10.4 kms^{-1} (towards $l = 0°$ $b = 0°$)
Y = 14.8 kms^{-1} (towards $l = 90°$ $b = 0°$)
Z = 7.3 kms^{-1} (towards $b = 90°$)

The values are somewhat dependent on the stellar class and sample used

The motion perpendicular to the Galactic plane has an amplitude of 80 pc, with the Sun currently about 10 pc above the plane and moving in the

positive z-direction. Usually this motion is assumed to be simple harmonic of the form:

$$z = A \sin \omega(t + T) \qquad 4.1$$

with $A = 80$ pc, $\dot{z} = 7.3$ kms^{-1} and $z = 10$ pc at $t = 0$ (the present) implying that the last two Galactic plane traversals by the Sun occurred at 1.3×10^6 years and 3.2×10^7 years ago. The oscillation has a half period of 33×10^6 years.

This z-motion has been used by a number of authors to provide a disturbing influence on the Solar System via, for example, the gravitational interaction of giant molecular clouds and the Oört comet cloud. (Rampino and Stothers 1984, Innanen *et al* 1978). It has been argued that these interactions may explain mass extinctions seen in the geological record which seem to have a frequency of 33×10^6 years.

Such arguments have been the subject of controversy (Thaddeus and Chanan 1985). It has also been proposed that the solar z-motion would have an effect on the CR intensity at the Earth, and consequently be visible in the radionuclide data. Schwartz and James (1984) argue that the intensity of CR (or soft X-rays) might increase with z, as there is less absorbing material higher above the plane. Schaeffer (1979) on the other hand, combines the radionuclide data with a CR intensity profile of the form $I_z = I_0 e^{(-|z|/z_r)}$, to derive a scale length z_r for the CR of 100 pc. If this were the case then there would be a factor of two increase in the CR intensity as the Sun moved from z =80 pc to the Galactic plane over the past 18×10^6 years. Clearly, this is rather too high to be consistent with the latest ^{10}Be data (§4.2). It seems likely therefore that the use of such a simplistic CR profile must be questioned. If the CR were to follow the Gaussian gas distribution with a FWHM of 220 pc (Burton 1974) then the variations over the same period would have been $\sim \times 1.4$ — which is more consistent with the data, although still rather high. For the present, a simple exponential will be used, and the half-height predicted by the radioisotope data calculated.

Using the data of Raisbeck (1985) and assuming that the ^{10}Be/^{9}Be ($= B$) concentration ratio is proportional to the CR intensity then: $B =$

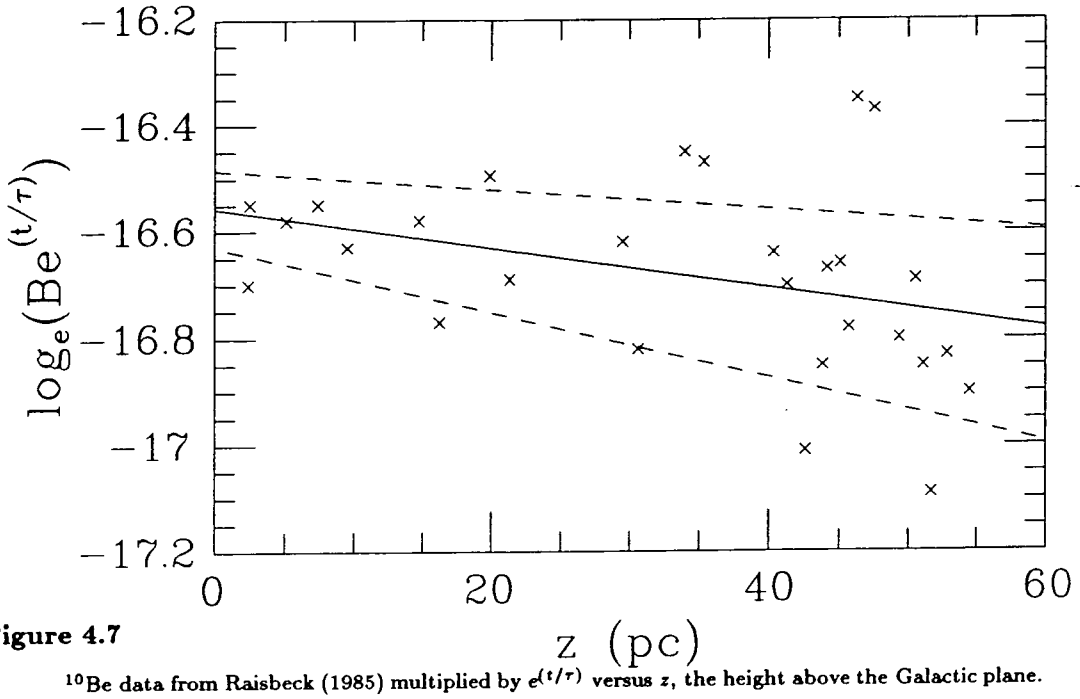

Figure 4.7

^{10}Be data from Raisbeck (1985) multiplied by $e^{(t/\tau)}$ versus z, the height above the Galactic plane. See text for details of the derivation of z.

$B_0 e^{-t/T_l} I_0 e^{-|z|/z_r}$ where z is given by Eqn. 4.1 and T_l is the ^{10}Be lifetime. Putting this into a suitable form and performing a least-squares fit, z_r was found to be $270 \pm {}^{280}_{90}$ pc. Fig. 4.7 shows the fit. Leaving out the four high points at around $z = 35$ pc and $z = 46$ pc from the fit, z_r drops to $190 \pm {}^{60}_{40}$ pc. This value compares favourably with the gas scale height, and hence within the errors the slow increase in ^{10}Be concentration relative to ^{9}Be over the past 10^7 years could be due to the Sun's motion within a gas disk of scale height 190 pc. If the scale height were less than this, it would mean that the z-motion 'over-compensates' for the slow increase in ^{10}Be concentration, implying the necessity for extra CR activity at earlier times. Alternatively, if the CR do extend beyond the gas (as seems likely) (Kniffen, Fichtel and Thompson 1977), then there is still a deficit in CR activity to be made up, i.e. not all the increase in ^{10}Be concentration can be attributed to the Sun's vertical motion.

The model of solar z-motion producing the observed increase in ^{10}Be

with time is just one extreme of a whole range of models. The other extreme is to consider that any effect on the CR intensity produced by the z-motion is negligible, and that all the CR intensity variations deduced from the radionuclide data are the result of solar motion in the galactic plane. At present, there seems to be no way of disentangling these two effects and one or other model must be chosen. As there seems to be much evidence that CR leak from the galactic disk and therefore have a scale height greater than of the gas, the effect on the CR intensity due to the z-motion will be set aside, and solar motion in the Galactic plane will be examined.

4.3.4 Solar motion in the Galactic Plane.

As a good first approximation, the Sun's orbit around the galactic centre is an epicyclic one. This is defined as follows. If a small perturbation is made to an object in a Keplerian orbit, a peculiar velocity is developed in both radial and angular directions causing it to move in an epicycle about the path of the original orbit. It is easily shown (Bowers and Deeming 1984) that the epicyclic frequency κ of this peculiar motion at a given galactocentric radius is:

$$\kappa^2 = \frac{2\Theta_0^2}{R_0^2}\left[1 + \frac{R_0}{\Theta_0}\frac{d\Theta_c}{dR}\Big|_{R_0}\right] = 2\Omega^2\left[1 + \frac{R_0}{2\Omega}\frac{d\Omega}{dR}\Big|_{R_0}\right] \qquad 4.2$$

where Θ_c is the circular velocity, Θ_0 is the local circular velocity, R is the galactocentric radius, R_0 is the Sun–Galactic centre distance, and $\Omega = \Theta_c(R)/R$

The displacements (ξ,η) in the radial and angular directions are given by:

$$\xi(t) = \frac{\Pi_0}{\kappa}\sin\kappa t \qquad 4.3$$

and

$$\eta(t) = \frac{2\Theta_0\Pi_0}{R_0\kappa^2}\cos\kappa t \qquad 4.4$$

where κ is evaluated at R_0 and $\Pi_0 = \dot{\xi}(0)$ in the solar neighbourhood κ = 31.62km s^{-1}kpc^{-1}, $\Pi = \dot{\xi} = -10.4$km s^{-1} and $\Theta = \dot{\eta} = 14.8$km s^{-1}

Putting in these figures the Sun is currently close to perigalacticon, nearly 300 pc inward (i.e. nearer the Galactic centre) of the epicyclic centre and trailing ~500 pc behind it. These values may be compared to earlier results by Woolley (1969). It is interesting to note that, using his figures with a spiral arm width of 0.8 kpc and with the arm parameters of Yuan (1977), the Solar System last crossed a spiral shock $\sim 2.5 \times 10^8$ years ago. As a consequence, for such a 'grand design' spiral pattern, there should be no evidence for such a shock in most radionuclide measurements.

4.3.5 Spiral Parameters.

The Galaxy, according to the density wave theorists and some observers, consists of a grand design spiral pattern that extends throughout most of disk. Several equations have been used to describe the spiral of which $R = A + B\theta$ and $R = Ae^{B\theta}$ (Weaver 1970) are two common examples. The most commonly used equation is of the form: $R = R_l e^{\phi \tan i}$ where ϕ is the azimuthal angle, R_l is a scale length and i is the inclination angle of the arm, defined as that angle between the tangent to the arm and the tangent to a circle at that point. Chapter 3 deals with the Carina region of the Galaxy and the various estimates of i are discussed there. Here, it is sufficient to state that the values of i and R_l used are those of Yuan (1970, 1977) for his global pattern.

This pattern rotates with an angular velocity Ω_p that is derived from density wave theory. A value of 15 km $s^{-1}kpc^{-1}$ was found initially, but when the thickness of the gas disk was taken into account, this dropped to 13.5 km s^{-1} kpc^{-1} (Lin 1977). It is this last mentioned value that is used here.

The gas density contrast between the arm and interarm regions is commonly taken as 3:1 (Kniffen, Fichtel and Thompson 1977) from observations at 21 cm and in the optical waveband. The width of the arms is another uncertain quantity. Commonly used values are $\sim 0.5 \rightarrow 1$ kpc, obtained both from observation and theoretical work. (Innanen, Patrick and Duley 1978, Roberts 1970, Pawsey 1965).

4.4 The Model.

4.4.1 Introduction.

In a series of papers produced by the Durham group on CR from SNR (Bhat *et al*1986a,b, 1987) Monte-Carlo simulations of the temporal and spatial intensity variations of the Galactic CR were made. The hypothesis in these papers, and the one employed here, is that CR are produced by the shock-acceleration mechanism widely discussed in the literature (for example, Bell 1978a,b, Blandford and Ostriker 1978, Blandford and Cowie 1982). A feature of this mechanism is that the energy input into CR is not made at once at the initial explosion, but over a period of time as the remnant expands. It is unlikely that the remnant will have a uniform CR density inside (Bogdan and Völk 1983) because the acceleration mechanism does not smooth the CR distribution over volumes the size of a SNR.

In common with most analyses, the SNR is assumed to spherically symmetrical and expanding into a uniform medium. This is an assumption, but any other more realistic geometry is considerably more difficult to handle both analytically and numerically. As the remnant expands the energy content of accelerated nuclei (protons) is given by:

$$E_p = 2.8 \times 10^{45} r^{2.5} \text{ergs} \qquad 4.5$$

where r is in parsecs. Equation 4.5 is within a factor of two of the estimate of E_p given by Blandford and Cowie (1982). Bhat *et al* (1986b) show that such a relation is consistent with the estimated CR energy in the Loop I SNR. During the CR acceleration phase, the expansion proceeds as:

$$r = 0.66 t^{0.4} \text{pc} \qquad 4.6$$

where t is in years, and the energy density is given by:

$$\epsilon(t) = 19.16 t^{-0.2} \text{eV cm}^{-3} \qquad 4.7$$

In Bhat *et al* (1986a), this acceleration phase is followed by an adiabatic loss phase and finally the CR are allowed to diffuse away into the Galaxy. Here, as in Bhat *et al* (1987), the second phase is neglected. The diffusive phase i.e. the one in which CR diffuse away from the remnant, is characterised by a diffusion constant D, and diffusion occurs from the end of the previous phase (when r =130 pc) until the escape time τ is reached. At this point, the CR are assumed to escape entirely from the Galaxy and no longer contribute to its energy density. The CR diffuse away from the SNR site in a sphere of radius

$$X = \sqrt{2Dt} \qquad 4.8$$

where t is the time since diffusion began. Strictly, for three dimensional diffusion the factor 2 in Eqn. 4.8 should be replaced by 6, and an anisotropic diffusion constant D should be used. Ginzburg and Ptuskin (1985) quote $D_{\|}/D_{\perp} \sim 6$ when the smooth magnetic field component equals the random component. Also, the diffusion constant D is not a well established quantity but is probably in the range: $5 \times 10^{27} \rightarrow 5 \times 10^{28}$ cm^{2}s^{-1}

As these CR diffuse away from the SNR, their contribution to the energy density is given by:

$$\epsilon(t) = 3.01 \times 10^6 \eta d^{-3} \text{eV cm}^{-3} \qquad 4.9$$

where η is an efficiency factor and d is the diameter of the diffusion volume given by:

$$d = X + 130 \text{ pc} \qquad 4.10$$

For η=1, 55% of the available energy from the SNR goes into CR. Völk *et al* (1984) have estimated η to be in the range $0.5 < \eta < 1$.

Such equations are obviously approximations and many of the simplifications are necessary to make the problem tractable, as well as for ease and speed of computation. As the simulation is performed over a great length of time compared to the lifetime of a typical SNR (a few 10^5 years), the results are not expected to be significantly different from those from a more accurate SNR model. This assumption can only be tested with such an accurate SNR

model, but improvements that may be made to the simulation described here are discussed in §4.6.

4.4.2 An Analytical and One-dimensional Model.

As part of the work involved for Bhat *et al* (1987), a one-dimensional Monte-Carlo model was developed using the above parameters for the SNR and CR. A Poisson distribution random number generator was used to assign SNR to radial bins a specified distance away from the Earth, up to a maximum given by $X_{\max} = \sqrt{2D\tau}$. The SNR were allowed to occur in the bins at random and the CR energy density resulting was followed at the Earth for 10^8 years. Three parameters were varied: the CR escape time, τ, the diffusion coefficient,D and T the step length of the integration. Values of the average energy density, $< \epsilon >$, over the whole simulation run were obtained for each set of these parameters, with the averages taken only after equilibrium had been reached. This usually required τ/T number of integration steps to achieve this. The results were compared to an analytical model using the same parameters. It was found that the two models agreed to within 4% in their predictions of the energy density. As the diffusion constant was increased from 1.8×10^{28} to 1.7×10^{29} cm^{2}s^{-1} the energy density dropped smoothly from 2.8 to 1.1 eV cm^{-3}. Increasing the escape time from 6.7×10^6 to 6×10^7 years produced a smooth increase in $< \epsilon >$ from 0.9 to 3.2 eV cm^{-3}. As a test of the stability of the program, the time step T was varied from 3×10^4 to 10^6 years which resulted in varying the average energy density by less than 7%.

This one dimensional model served as a useful check on the two dimensional version used in Bhat *et al* (1987) as it showed the feasibility of the method and that meaningful results could be obtained from it. The analytical solution confirmed that the program was behaving as expected and that the energy densities it produced were not artifacts of the simulation. The two-dimensional version developed by C. L. Bhat and and as well as radial distance from the Sun, also involved taking heights above the Galactic plane for the SNR of up to 100 pc, above which no SNR were said to occur. This feature was included because the authors were considering two sections of the Galaxy — one near the Sun as represented by high latitude data, and the other far

from the Sun represented by the data at low latitude.

4.4.3 Galactic Model.

It is evident that the Galaxy is not a smooth distribution of gas, dust and stars, particularly if attention is focussed on young objects where the distribution becomes very inhomogeneous. Molecular gas is also found predominantly in clumps of varying sizes even up to the largest and most massive objects in the Galaxy, the giant molecular clouds. It is probable that two phenomena are largely responsible for this state of affairs. The first is the supernova explosion and its associated remnant. These events, being the most energetic in the Galaxy, completely alter the interstellar medium whenever they occur as they produce copious quantities of material and ionizing radiation. They are thought to be responsible for the hot ionized component of the interstellar medium, as well as being triggers for the collapse of gas clouds and the initiation of star formation. The second phenomenon is that of the spiral pattern as delineated by bright young OB stars, HII regions and molecular clouds (Casoli and Combes 1982). Associated with these objects and probably responsible for them, is the spiral shock produced by the spiral fluctuation in the gravitational field of the Galaxy. The spiral shock is also thought to be an initiator of star formation because it compresses the gas and precipitates massive stars formation. OB associations are thought to have formed in this way as they delineate the spiral arm. Such massive stars have a short lifespan, ending as SNe before they leave the arm (Burbidge 1969, Clark *et al* 1977). It is also likely that these SNe will give rise to further star formation downstream of the shock, so that not all SNe will occur in the arms. This idea has been used by Gerola and Seiden in their papers on stochastic self-propagating star formation (Gerola and Seiden 1978, Seiden and Gerola 1979, Seiden *et al* 1979). Their models gave a spiral pattern, albeit a more fragmentary one than that of density wave theory.

The Solar System will not encounter SNR and their associated CR in a purely random fashion as it moves around the Galaxy since the frequency of an encounter will be modulated primarily by the spiral pattern. All previous models have assumed a uniform number density of SN in the Galaxy

i.e. they have neglected the Sun's motion altogether. The Bhat *et al* (1987) model seemed to mimic the data of Raisbeck (1985), but as has already been mentioned, the Raisbeck group at Orsay has improved its measurements and argue that the two possible excursions at 6×10^6 and 8×10^6 years are no longer present. This poses a problem for the model in that, as Bhat *et al* comment, the data seem to 'suffer somewhat from the relative paucity of large (+50%) positive excursions' common in the simulation. The solution proposed by Bhat *et al* of admitting a lower half-life for ^{10}Be does not seem to be suitable according to Raisbeck (1988) as laboratory measurements of the ^{10}Be half-life have confirmed the value of 1.5×10^6 years. Also, the slow increase in CR intensity described in §4.2 has not yet been explained and does not appear in any feature of the Bhat *et al* model.

Consequently a new Monte-Carlo simulation program has been written, tested and run on the Durham STARLINK Vax computers. The main feature of this model is that it attempts to trace the motion of the Solar System in the past whilst allowing SN to occur and produce CR which then diffuse away in the same manner as the previous models. In this way, it was hoped to test the hypothesis that CR are produced in SNR against the observed fluctuations in the ^{10}Be record, and also to model the long-term CR increase mentioned above. As §4.3 described, it is assumed here that the z-motion of the Solar System is negligible i.e. the model is two-dimensional with all motion occurring in the plane (see §4.3.4.). This assumption is valid if the scale height for ^{10}Be production from CR is greater than the amplitude of solar oscillation. It also permits the model to be executed on the computer without the unacceptably long execution times inherent in a three-dimensional motion.

The preceding sections have all introduced various parameters that are required for the model. The planar motion is described in §4.3.4. The parameters of the spiral arm model are given in §4.3.5, and §4.4.1 introduced those of the SNR model. However, there are still other parameters that are decisive in determining the outcome of the simulation, namely the variation of energy density with time.

Firstly, there is the rate of SN explosions in the galaxy, denoted μ. This is a much debated figure varying from between 1 in 25 years to 1 in 150 years.

For example, Clark and Caswell (1976) estimate μ to be of the order of 1 in 150 years from studies of historically observed SNe and Montemerle (1979) estimates 1 in 50 from observations of SN/OB associations. Other estimates can be made from the pulsar birthrate (if all pulsars are produced by SNe) and from extragalactic observations of spiral galaxies. (Tamman 1974, 1981 Lerche 1981, Tsvekov 1983).

Secondly, the scale of the galaxy is determined by the Sun–galactic centre distance. For a number of years now the accepted value for $R_\odot$ was 10 kpc, but recently a revision has taken it to 8.8 kpc. To a certain extent, the value of $R_\odot$ is unimportant as long as all the dependent quantities are scaled accordingly. The most important one of these is Θ_0, the circular velocity at R_0. The standard value is $\Theta_0 = 250\text{km s}^{-1}$ but with the revision of R_0, it has dropped to 220 km s^{-1}. It would be probably more consistent in future work to use the latest values, but as much of the work reported here needs to be compared with earlier results, the older values for $R_\odot$ and θ_0 have been adopted in the first instance. The conclusions are not sensitive to which pair of parameters is used.

Finally there are a number of program parameters that must be considered and which are generally constrained by computer resources. The escape time τ must be varied upwards by at least a factor of 5 i.e. to 10^8 years and the program must integrate over time for at least τ years before the value of the energy density, $< \epsilon >$, has settled to an equilibrium. (See, for example, the times sequence for the datum model in Fig. 4.8). Consequently the run must last this long before any $< \epsilon >$ values can be taken. In addition to this, the ^{10}Be data is reliable for the last 10^6years, so allowing for future improvements to the data, the length of time over which the simulation must occur must be at least 1.2×10^8 years, $(= I_{cylen})$. The time resolution of the ^{10}Be data is at present approximately 5×10^4 years, but is likely to improve. The incremental time step, T_{step}, is taken as 10^4 years. Combining I_{cylen} with T_{step}, gives 1.2×10^4 steps in the integration. Each SN is followed for up to $\tau/T_{step} = 2 \times 10^3$ steps so if the whole galaxy were considered, 1.2×10^6 SN would be followed (assuming an explosion rate, $\mu = 1/100$ per year) giving a total of 2.4×10^9steps. Fortunately, it is unnecessary to use such a large number of steps because the Earth does not 'see' any SN that is further away

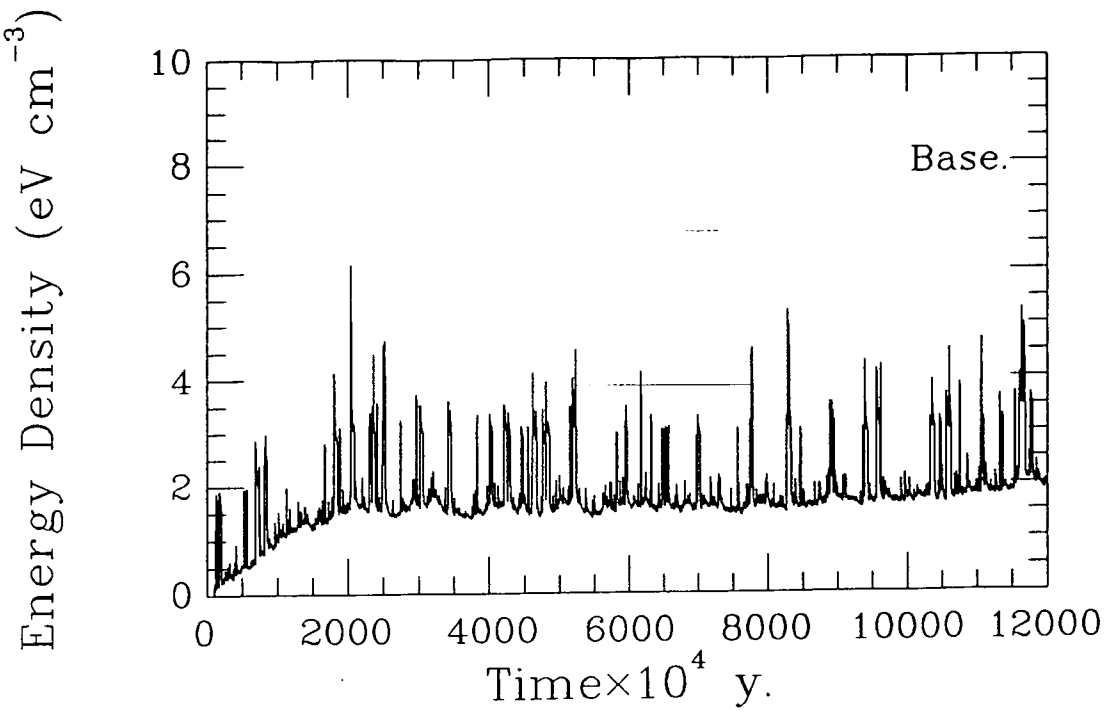

Figure 4.8

Time sequence of energy density values for the datum model (Model Base). Note the rise to 'equilibrium' in the first 2 x 10^7 years of the run.

than X_{max} (see §4.4.1). Therefore as the Sun moves around the Galaxy, sites of SN production that were once beyond X_{max} are brought into range. The program restricts the area of the Galaxy in which SN explosions are considered to a square of side $N_{bin} \times D_{bin}$ pc where D_{bin} is the length of the bin and N_{bin} is the number of bins on a side of the square. This quantity must satisfy

$$N_{bin} \times D_{bin} > 2X_{max} \qquad 4.11$$

If N_{bin} is small, the integration is more accurate but requires long integration times because there are more bins that must be considered. The square in which the SN explosions that are considered occur is moved as the Sun moves around the Galaxy, so that the only SN production sites that can affect $<\epsilon>$ are those that are within X_{max}. This technique reduces the number of SN that are considered during the simulation and makes the number of integration steps manageable. Even so, a typical run uses six hours of CPU time on an Vax

11/750. Table 4.2 gives a list of the parameters used in the program with their 'base' values.

Parameter	Value
i	6°.2
Ω_p	13.5kms^{-1}kpc^{-1}
R_l	3764 pc
R_0	10^4 pc
v_0	250kms^{-1}
R_{epi}	10282.5 kpc
κ	31.6228
Π_i	-14kms^{-1}
Π_{now}	-10.4kms^{-1}
Ratio	3
H_{width}	500 pc
SN rate	1/75
τ	2×10^7yr
D	5×10^{28}cm^{2}s^{-1}
R_{expn}	130 pc
T_{expn}	55×10^4yr
η	1.0
T_{step}	10^4yr
I_{cylen}	12000
D_{bin}	20
N_{bin}	299

Table 4.2

4.5 Results.

4.5.1 Parameter Space.

With such a large number of parameters, the size of parameter space available is enormous. However, some the model parameters can be treated as constants whilst some depend on the values of R_0 and Θ_0. For example, the Sun's velocity in the sense of Galactic rotation, Π is constant, and the

galactocentric distance of the epicentre of the Sun's epicyclic motion, R_{epi}, the epicyclic frequency, κ, and the initial value of Π all depend on R_0 and Θ_0. Some parameters need to be varied to test the stability of the program (T_{step}, N_{bin}, D_{bin}) and I_{cylen} should be increased if computer time was available. There are then nine parameters that could have a direct impact on $<\epsilon>$. Three of these are spiral pattern parameters of which the pattern speed, Ω_p seems to be reasonably well known. i and R_l are open to debate, but the result of holding these constant as the others are allowed to vary should be only that the model becomes only quantitatively less accurate. Given a global spiral structure, the values chosen above should be representative and not too far from the truth. This leaves six parameters which must be varied to find the model predictions for the long term CR variations. These are: the arm–interarm density contrast denoted Ratio, the SN rate, μ, the escape time, τ, the diffusion constant, D, the shock efficiency, η, and the width of the spiral arm, H_{width}. Table 4.3 gives the range of values over which these are varied.

Parameter	Range
Ratio	1–50
H_{width}	100–1500 pc
SN rate	1/200–1/50
τ	1×10^7–8×10^7yr
D	$(0.5–7)\times 5 \times 10^{28}$cm^{2}s^{-1}
η	0.1–1.0
T_{step}	10^4–5×10^4yr
D_{bin}	20–40
N_{bin}	249–399

Table 4.3

4.5.2. Initial Results.

Fig. 4.8 gives the results of one run (Base— the 'datum' values) and shows the initial increase to equilibrium which takes $\sim 2 \times 10^7$ years (i.e. roughly the escape time, τ). There are fluctuations in energy density about a

mean value, with an occasional 'spike' when a SN goes off close to the Earth. The form of this result is typical of all the runs. The only obvious change as parameter values are varied are the level of mean, the time taken to reach this mean, and the frequency of the spikes. An important feature of the time-sequences is the slow increase in mean energy density level observable in the last $\sim 2 \times 10^6$ years.

The simulation results can be processed in a number of ways. Firstly, an autocorrelation analysis may be performed similar to that in Bhat *et al* (1987). This will give the correlation timescale of the model results which indicates the likely duration of any effect. Secondly the energy density distribution for the whole run can be examined and integrated to estimate the probability of an excursion (i.e. an brief increase in energy density) of a given factor above the mean 'background'. Thirdly, any evidence for an increase in $<\epsilon>$ in the past $\sim 10^7$ years that appears in the model results must be treated with caution to avoid any numerical instabilities of the program. To this end, the program must be tested for any strong dependence say, on N_{bin} or T_{step}.

4.5.3 Autocorrelation Analysis.

The correlation scale of any regular time series can be estimated by evaluating the autocorrelation coefficient r_k:

$$r_k = \frac{\sum_{i=1}^{N-k}(\epsilon_i - <\epsilon>)(\epsilon_{i+k} - <\epsilon>)}{\sum_{i=1}^{N}(\epsilon_i - <\epsilon>)^2} \qquad 4.12$$

where ϵ_i is the ith energy density value, N is the total number of values in the time series (Chatfield 1975), k is the correlation length parameter and k_c denotes its value when r_k first approaches zero. It is k_c that when translated into a time, that gives the favoured timescale of the data. Fig. 4.9a shows the 'correlogram' for the base model along with that found when the model results are modulated with Gaussian noise comparable to that of the ^{10}Be data. This is done not only to show the effect of noise on the model, but also to enable a comparison of this model's performance with earlier work.

As may be seen in Fig. 4.9, k_c is approximately 60 which corresponds to 6×10^5years. Many of the models have values of k_c between 45 and 65 which

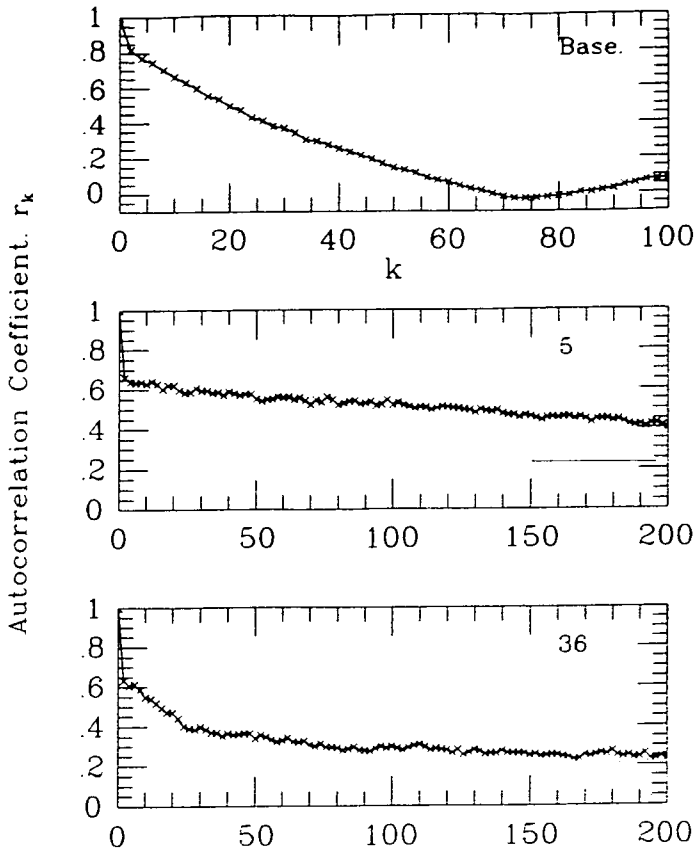

Figure 4.9

Correlogram for model *a*. Base. *b*. 5. *c*. 36.

is similar to the results of earlier work by Bhat *et al* (1987). This suggests a timescale of around 5.5×10^5 years which is the same as that at which the SNR acceleration mechanism switches off and diffusion of the CR begins. In most instances, the correlograms show no other interesting detail, (e.g. periodicity), which can be analysed, but it is worth considering in more detail those models that do not have k_c around 60.

Model 5 has a value k_c around 780 (Fig. 4.9b) corresponding to a time of 7.8×10^6 years with no evidence that r_k approaches zero around 5.5×10^5 years. This model has Ratio=30, with all other parameters equal to that of the datum model, so that the expected number of SNR close to the Sun is very small and distant SNe in the spiral arms will dominate. It is difficult to find a time of $\sim 8 \times 10^6$ years in the model as none of the input parameter times correspond to this value. The epicycle the Sun performs as it orbits the Galactic centre has a period of 1.9×10^8 years, so it performs only a half cycle over the length of the Model 5 run (Fig. 4.10), and thus cannot account

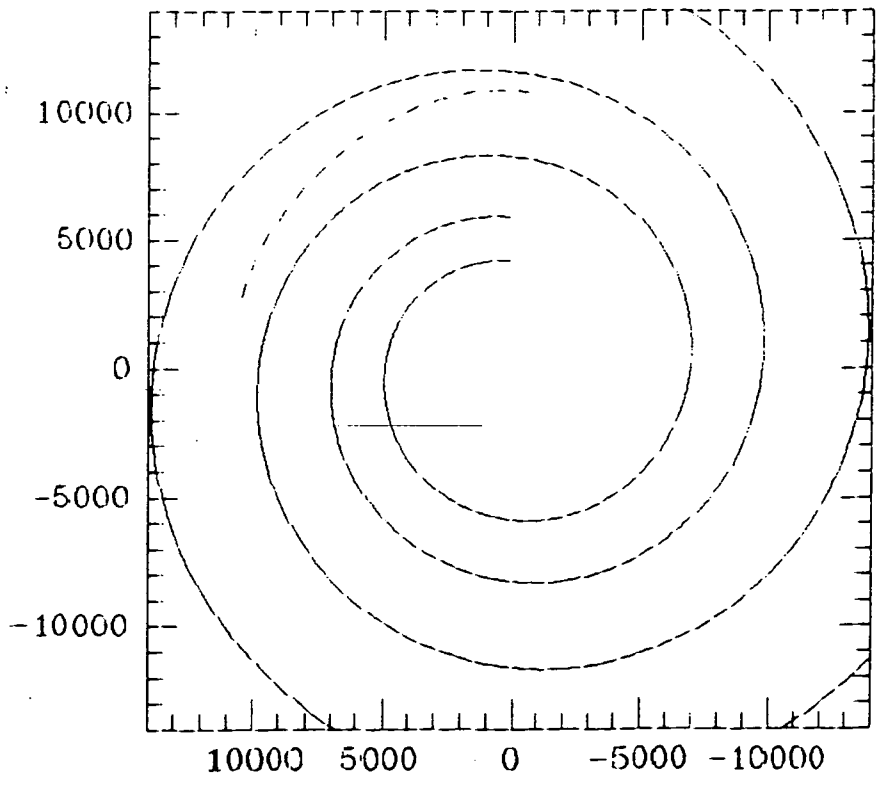

Figure 4.10

The orbit of the Sun with respect to the two-armed spiral pattern used in the model.

for the modulation at 7.8 × 10^6 years directly. Model 15 has Ratio=10, and exhibits similar modulation behaviour to Model 5, with k_c around 120 which is equivalent to 1.2 × 10^6 years. k_c for Model 36 similarly has a large value of k_c=690 for Ratio=50 (Fig. 4.9c), so it is clear that there is some form of connection between motions in the high CR density regions of the arm and in the solar orbit. For Ratio=3, the modulation is not detectable, and is not likely to feature in any radioisotope data. However, if the density contrast between arm and interarm is as high as in some density wave models, or follows the high density contrast of CO emission, for example, (13:1 Grabelsky *et al* 1987) then the nuclide data should be examined for modulation. For such modulation to be detectable, long periods of time (above a few 10^7 years) should be used, with as many measurements with high temporal resolution as possible.

As the width of the spiral arm is increased, the number of SN occurring in the arm increases and even though the number density contrast per bin of explosions (i.e. Ratio) remains constant, the CR density contrast between

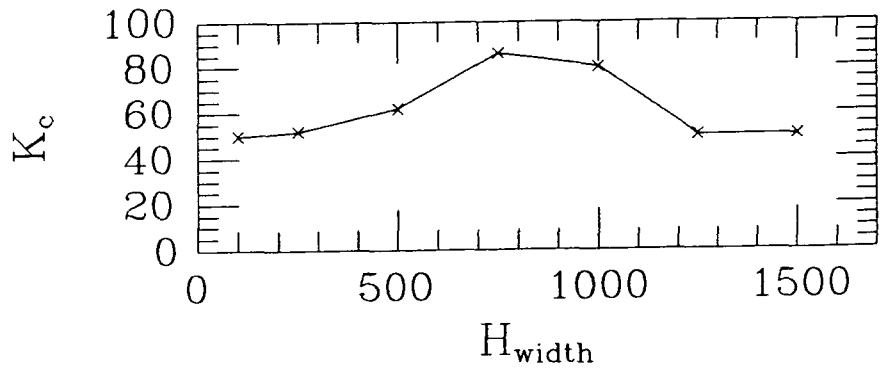

Figure 4.11

Variation of k_c with H_{width}.

arm and interarm experienced by the Sun becomes sharper. Thus, k_c should rise as the spiral arm width (H_{width}) increases, until the latter becomes large enough to ensure that most of the Galaxy is in an arm i.e. the interarm regions become very narrow. When this occurs, k_c should return to the lower values of around 55 corresponding to the time of the turn-off of the acceleration phase of the remnant. Figure 4.11 shows precisely this effect of the variation of H_{width} further strengthening the postulated connection between density contrast and the solar orbit. Unfortunately, it does not shed light on why such a connection should arise.

The correlogram for the ^{10}Be data can be examined to find any evidence for these timescales. Unfortunately, the data are not regularly spaced in time as is strictly required for the autocorrelation. Nevertheless, Figure 4.12 shows r_k for the data and it is evident that no preferred timescale exists. Figure 4.13 shows the Raisbeck (1985) ^{10}Be data sorted into regular time bins. The expected values obtained using the least-squares values for the data were in-

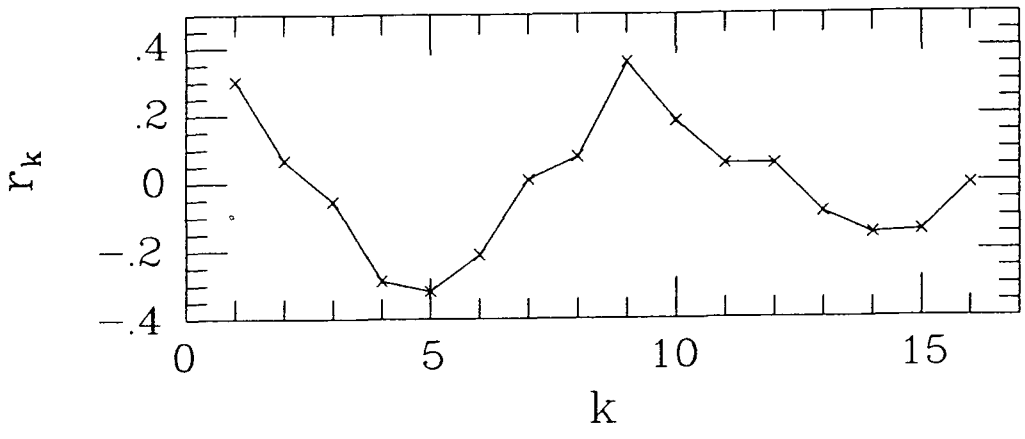

Figure 4.12

Pseudo-correlogram for the ^{10}Be data of Raisbeck (1985).

serted into those time bins that had no observations and the auto-correlation performed again. No preferred timescale is evident.

4.5.4 CR Excesses and the Probability of a Local Supernova.

The Raisbeck data consist of 28 observations spread over $\sim 9 \times 10^6$ years with a resolution of $\sim 5 \times 10^4$ years. In the simulation, a SN that goes off locally is followed for a maximum of 5.5×10^5 years before CR diffusion sets in and the energy density drops rapidly. The further away the SN, the shorter the time for which the acceleration phase is followed and the smaller the excursion from the background.

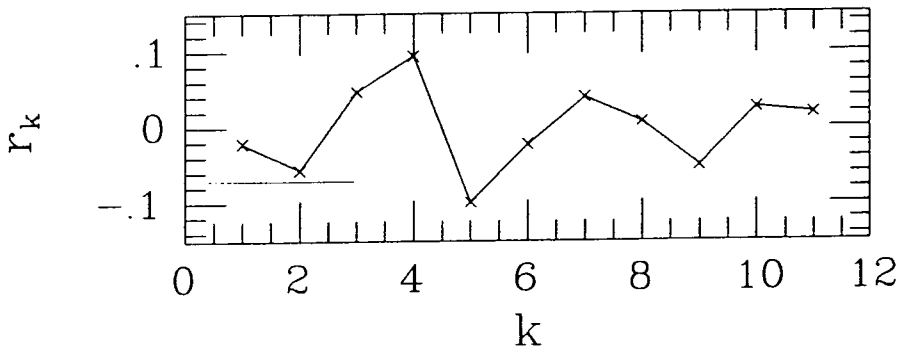

Figure 4.13

Correlogram for the ^{10}Be data of Raisbeck (1985) with regular binning.

The probability of a SN being observed in the ^{10}Be data can be estimated with a few simplifying assumptions as follows. The Raisbeck data covers approximately 9×10^6 years, a length of time which may be divided into 180 bins of 5×10^4 years each. The ^{10}Be data consists of 28 measurements taken roughly uniformly throughout the core. A SN occurring less than D_{bin} (20 pc) away from the Sun is seen for a maximum of 11 of these bins, ($11 \times 5 \times 10^4$ years), so the probability that such a maximal excursion above the background is actually unobserved by all of these 28 measurements is $(1 - \frac{11}{180})^{28} = 17\%$. The probability that at least one of the 28 samples of the core is within this 11-bin window is then 83%. This estimate presupposes that one excursion in CR intensity reflected in increased ^{10}Be production is actually present in the data and that one observation would be sufficient to identify it. Such a

requirement may be a little optimistic with the current data as preferably two or more observations of an excursion in adjacent bins would be desirable. The high probability of missing an excursion altogether shows the necessity of improvements in sampling of the ice or ocean-sediment cores. 73 measurements of a core would be sufficient to reduce the probability of missing a maximal excursion to 1%. In practise, of course, the number of measurements could be reduced by sampling the core regularly rather than randomly and excursions in radioisotope production of a given factor above the background could all be included with some confidence. This is not as easy as it first appears because separate dating of a core must first be performed which may lead to a non-linear time versus length relationship down a core.

Probabilities of observing a SN-produced increase in the radioisotope record must be combined with the probability of there actually being an excursion in the time over which the data are taken. For each of the simulations, the probability of an excursion in energy density greater than a factor f above the background was obtained from the simulated time sequence of energy densities. Generally, the probability of an excursion $> 10\%$ ($f = 1.1$) was below 30% falling to less than 15% for $f = 1.5$ and dropping to 1% in one simulation. Figure 4.14 contains the probabilities for various factors,f for the parameter space investigated with the simulations. The behaviour of each of these graphs can be understood by considering what is occurring as each parameter is varied.

Firstly, for each of the several values of f, and for $f > 2$, there is little change in the dispersion of probabilities as the escape time τ increases (Fig. 4.14a). Although for longer τ the CR from the SNR contribute to the energy density locally for longer (and hence give increasing $<\epsilon>$ with τ, Fig. 4.15), the percentage fluctuations in ϵ do not change even though the actual values of ϵ are very small at these long times.

Secondly, as the diffusion constant D is increased (Fig. 4.14b), two effects are seen. The spread in probabilities changes becoming smaller with D and then remaining constant. The probability of observing a fluctuation in the CR energy density less than a factor of 2 (denoted $p(f < 2)$) drops from 1 to 0.85. For small D, i.e. 'slow' diffusion, there is a relatively high contribution

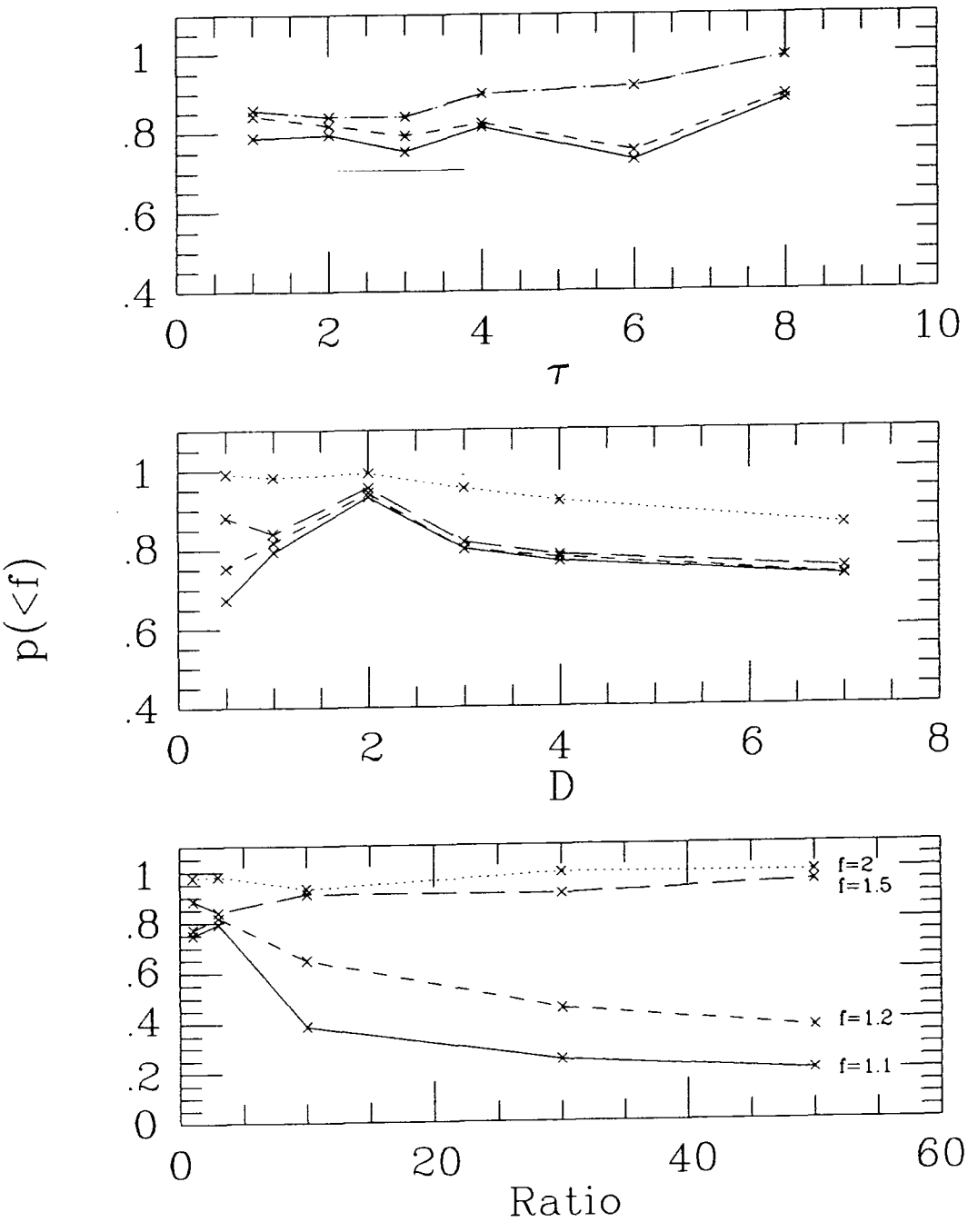

Figure 4.14

Dependency of the probability of energy densities less than a certain value f on the *a*. Escape time, τ. *b*. Diffusion coefficient, D. *c*. The arm-interarm density contrast, Ratio.

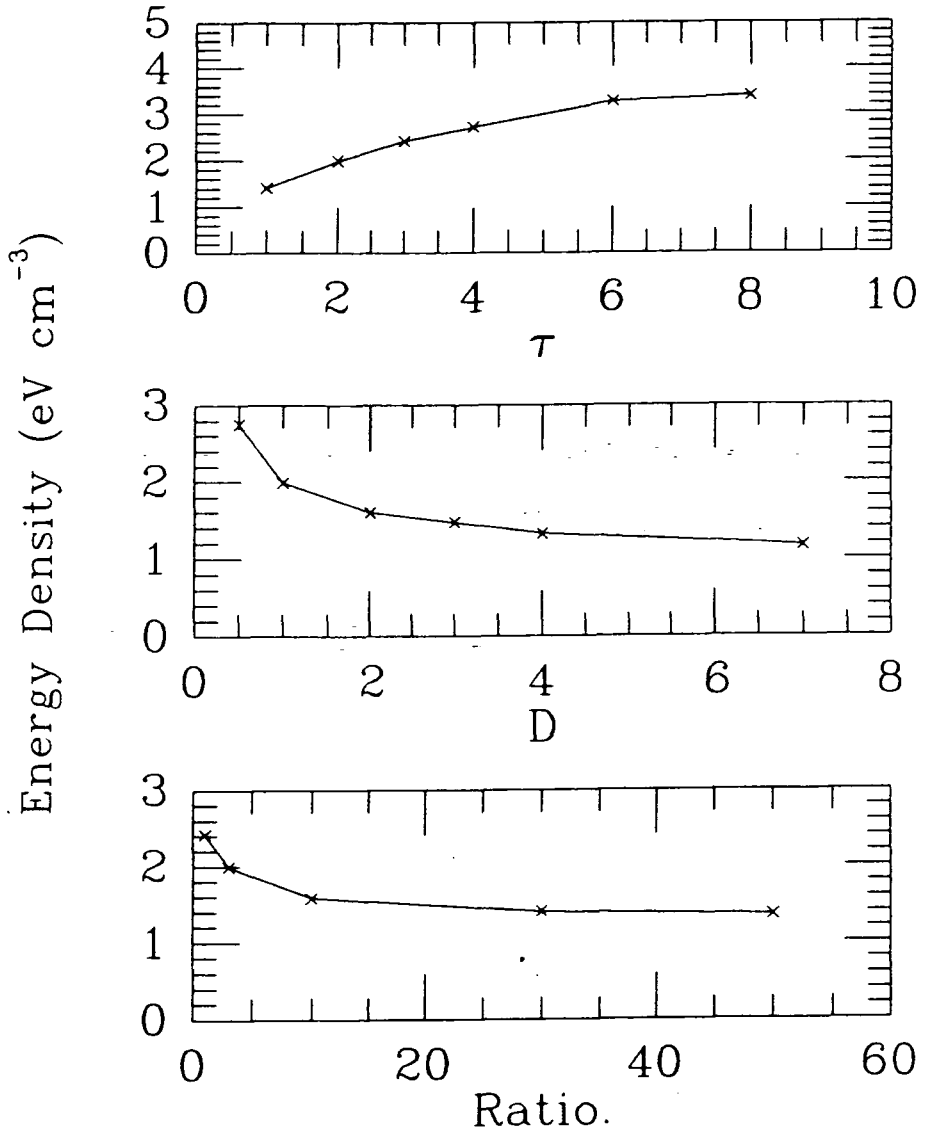

Figure 4.15

Dependency of the average energy density over the whole model run on the **a.** Escape time, τ, $\times 10^6$ years. **b.** Diffusion coefficient, D, $\times 5 \times 10^{28} cm^2 s^{-1}$ **c.** The arm-interarm density contrast, Ratio.

from the CR diffusion phase and so distant SNR have a greater effect on the fluctuations thereby broadening the spread of probabilities for each of the four f factors taken. On the other hand, 'fast' diffusion (high D) causes the CR from distant SNR to contribute very little to ϵ and thus have a smaller effect on the fluctuations. As a result, local SNR become more important, leading to the observed drop in $p(f < 2)$ as such SNR have a greater chance of affecting the probability distribution.

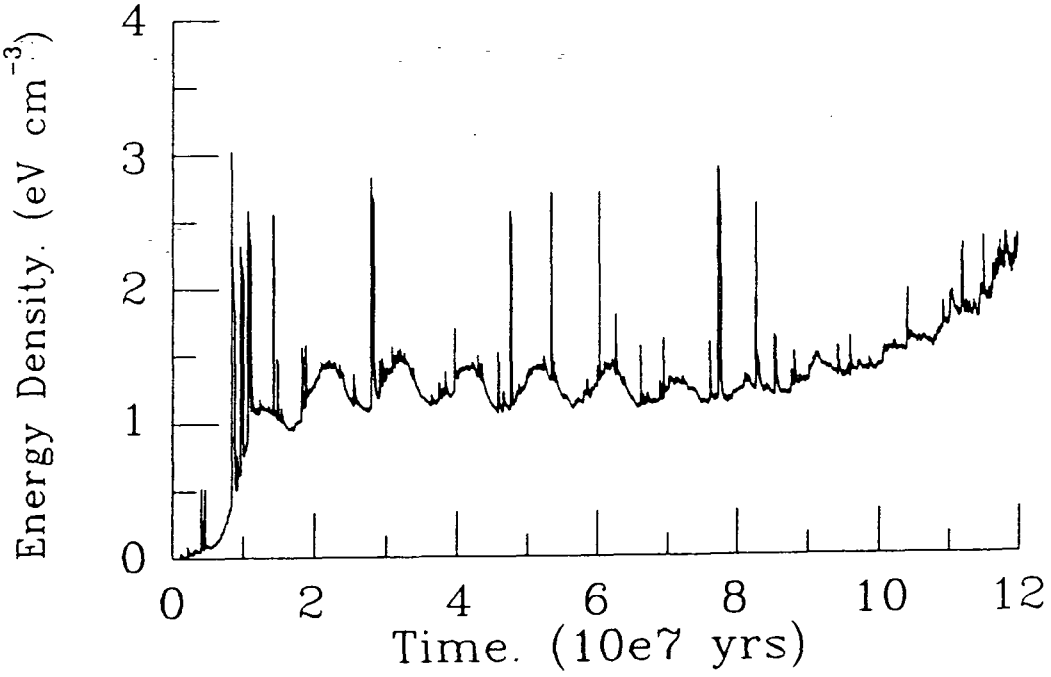

Figure 4.16

Time sequence of energy density values for model 5 (Ratio=30).

Thirdly, as the ratio between the number of SNR in arm and interarm is increased (Fig. 4.14c), the motion of the Sun in its epicyclic orbit becomes very important. Figure 4.16 shows the simulated time sequence for Ratio=30; the modulation in the energy density values is clearly visible (see §4.5.3). The effect of high Ratio on the probabilities is clear: not only does the local SNR

contribution become less important since most of the SNR are in the arms and hence $p(f < 2)$ is high, but the additional modulation produces a broader fluctuation in ϵ giving rise to the wide dispersion in the probability points seen in Fig. 4.14c.

The probabilities of fluctuations less than a certain factor are useful for deciding whether or not a SN has occurred close to the Sun in the time-span covered by any of the radionuclide results. Taking a SN rate of 1 per 75 years for the whole Galaxy (see §4.4.3) then the number of SN occurring within 108 pc in 9×10^6 years (the length of the Raisbeck data), is ~ 6. The Sun will experience a SN rate lower than the Galactic average because it is presently in an interarm region. Using Equations 4.6 and 4.7 to give the energy density in eV cm^{-3}, shows that SN occurring closer than 108 pc from the Sun will produce an excursion of $f > 1.5$ i.e. an increase of greater than 50% above the background or mean level. The apparent presence of two in the earlier ^{10}Be results would have given support to this theory, since the probability of these six excursions actually being present in the data but only four bins observed over 50% higher than the average is around 0.2. The probability of six SNR being present and unobserved is rather low at 2% (although this is not negligible) and places the theory under some strain.

The Monte-Carlo model suffers from the problem that if by chance a local SN were to go off very close to the Sun during the period of the run in which the cumulative frequency distribution is computed, then there will be an excess of high energy density values, and the frequency plot will be affected in such a way that the probability of SN producing large fluctuations will be enhanced. Though in reality SN presumably do explode nearby, for modelling purposes, the average probabilities are required i.e. the average of a number of runs of the simulation with the same parameters. To do this for all parameter sets would significantly and prohibitively increase the amount of computing time used, so only four runs with the datum model were performed from which the average cumulative frequency plot was derived. This point must be borne in mind when models other than the datum model are considered although the deviation of an individual run from the mean energy density is not large. Using the datum model probability values from the last 10^7 years, energy density variations having excursions of $f < 1.5$ should be observed for 88.6%

of the time. Taking 28 measurements at random from such an energy density distribution gives a probability that they all have $f < 1.5$ (as Raisbeck (1988) now claims) of 3.3%. For this probability to be high as, say, 15% would require an excursion with $f > 1.5$ to occur $\sim 7\%$ of the time.

The ^{10}Be data of Raisbeck (1985) appears to have no excursions of $f > 1.5$ which could be attributed to the measurements being made by chance in the 'wrong' places in the core. The probability of this occurring for 28 measurements assuming 6 SN within 108 pc in the time spanned by this data set is about 2%.

An alternative hypothesis is that there *are* no SN produced intensity enhancements in the radioisotope record. The probability of no SN within 108 pc when 6 are expected is very low at about 0.2%, so it is expected that somewhere in the core, one or more CR enhancements are present revealed by increased ^{10}Be production. The actual number of SN occurring near the Sun will be less than the Galactic average because of the Sun's position in the interarm. Using the parameters of the datum model, the interarm rate theoretically expected is 1/89 SN per year. The actual simulation is in excellent agreement with this , predicting 1/85 Sn per year. This lower value for μ increases the probability of seeing no SN within 108 pc from the Sun — to only 0.5%. The probability of 28 measurements all missing the approximately 5 SN expected with this rate within the same radius increases to 4%.

On the basis of this model, therefore, the probability of no SN occurring near the Sun is very low. Consequently, enough measurements of a sample of ice or of ocean sediment might reveal an increase with $f > 1.5$. That 28 measurements are now said to reveal no fluctuations above $f = 1.5$ creates a problem for the model which, simply put, is that the model predicts too many SN and ways must be found of reducing their numbers. Improvements have been made over earlier Monte-Carlo models however, in that the earlier work predicted many more SN than this simulation. Such a discrepancy between model and the experimental data should be an incentive to those working to measure the quantities of radioisotopes in various reservoirs. The low probability of accidentally missing CR enhancements with $f > 1.5$ in the radioisotope data places constraints on the probability of observing an $f > 1.5$ excursion at

any time in the sense that this probability must be also be low. It will remain to be seen whether future results reveal the expected fluctuations, or whether ideas about the production of CR in SNR must be revised.

4.5.5 The Long-term Trend.

It is immediately evident from the energy density versus time sequences produced by the model that there is a slow increase in $<\epsilon>$ over the past few 10^7 years. This was expected *a priori* from the construction of the model as at some point in the solar orbit, the Sun will be approaching a spiral arm and be closer to it than the one it has passed through. With the model parameters used in the present analysis, the Sun does not traverse an arm in the last 10^8 years, but remains wholly in the interarm region. This has a number of consequences of which only the long-term trend in CR intensity is considered here.

The energy density values from each simulation can be used to show the long-term trend easily though rather crudely by making a least-squares linear fit of the variation of energy density with time over the last 10^7 years (10^3 points). The gradient and intercept thus obtained cannot be interpreted in any sense other than by noting the sign of the gradient: If it is negative then the energy density has been falling with time. No further analysis may be made using the fit for each simulation because of its statistical nature. Some fluctuations are expected, of course, and some models do produce negative gradients. These are in the minority and tend to have smaller slopes.

In order to compare the model predictions with the ^{10}Be data, each model energy density value for the last 10^7 years can be multiplied by e^{-t/T_l} with the ^{10}Be lifetime, $T_l = 1.5 \times 10^6 / \log_e 2$ years, and then 28 measurements taken at random from the last 9×10^6 years of the time sequence. A least-squares fit of $<\epsilon> \times e^{-t/T_l}$ with these points gives the simulated ^{10}Be result of the long-term CR intensity increase and provides a valuable method of comparing the observations with the model. In particular, it can be used to examine whether the model adequately explains the increase seen in the Raisbeck data. Table 4.4 gives the values of $T_{1/2}$ expected from the data for some of the models and these may be compared to the Raisbeck result of

$(1.426 \pm 0.035) \times 10^6$. The errors on these values are of the order of 0.02 being the average of ten sets of simulated ^{10}Be results. It is obvious that most of the model half-lives are higher than that of the Raisbeck value, indicating that the model does not provide the complete picture of the increase of CR intensity over the past $\sim 10^7$years. However, that part of the increase can be explained is an important improvement on earlier work, and provides guidance for future studies.

Model Number	Half-life (Myr)	Parameter
Base	1.451	
3	1.316	$\tau = 1 \times 10^7$yr
5	1.417	Ratio=30
6	1.452	Ratio=1
8	1.438	D_{bin}=40
12	1.438	$D = 2.5 \times 10^{28}$cm^{2}s^{-1}
13	1.442	SN rate=1/50
14	1.426	SN rate=1/200
17	1.557	$H_{width} = 1000$
22	1.479	$H_{width} = 100$
25	1.629	$D = 35 \times 10^{28}$cm^{2}s^{-1}
26	1.452	$\tau = 8 \times 10^7$y

Table 4.4

4.5.6 Stability.

Checking of the stability of the computer program is a very important part of the analysis. Since the simulation is statistical in nature, fluctuations in the results from run to run are expected even without changing any parameters. However, if these fluctuations are attributable to program parameters (such as the size and number of bins considered for SN events (D_{bin} and N_{bin}) then any variation in the results when model parameters (such as the escape time,τ and the CR diffusion coefficient, D) are varied as well makes the results unreliable. Ideally, the results should be independent of any program param-

eters, thereby allowing all variations in the results to be easily interpreted in terms of model parameter variations. However, if a graph of the variation of a program parameter (known as the 'profile' of that parameter) against some result of the simulation, say, the average energy density, is not flat but varies slowly and predictably, the results from those simulations where model parameters have been varied can be adjusted for any variation in program parameter. An example illustrates this: the longer the escape time τ, the larger the size of Galaxy that must be sampled to include all the SNR that can affect the energy density at the Sun and the larger D_{bin} and N_{bin} must be and inequality 4.10 (§4.4.3) must hold. For $\tau = 8 \times 10^7$ years, $X_{max} = 5163$ pc, so for datum values of $N_{bin} = 299$ and $D_{bin} = 20$, there will be many 'missed' SNR, giving erroneous results as the energy density at the Sun will be lower than it ought to be when all SNR are included. To satisfy Eqn. 4.10, N_{bin} can be raised to 399 and D_{bin} to 26 to give the required inequality. The variation in energy density as these two program parameters are varied must be known before the effects of raising τ from the datum value can be assessed.

To find the program parameter profiles, all the model parameters involving CR diffusion and SNR were kept constant and N_{bin} and D_{bin} were varied in accordance with the inequality Eqn. 4.10. The results shown in Figure 4.17 confirm the stability and predictability of the model since the average energy density does not change by more than 20%. Furthermore, it does so in a linear fashion allowing the change to be easily incorporated into the results of other runs, e.g. in the example in the previous paragraph. Additionally, T_{step} was also varied producing variations in the average energy density of only 5

4.6 Comparison with ^{10}Be Results.

4.6.1 The Long-term Increase in CR Energy Density.

In §4.5.5 the results of the model showing a long-term increase in CR energy density values were examined. Most of the models showed such an increase, although some showed a decrease with time, but this was attributed to statistical fluctuations as the negative gradients were small. Simulated ^{10}Be

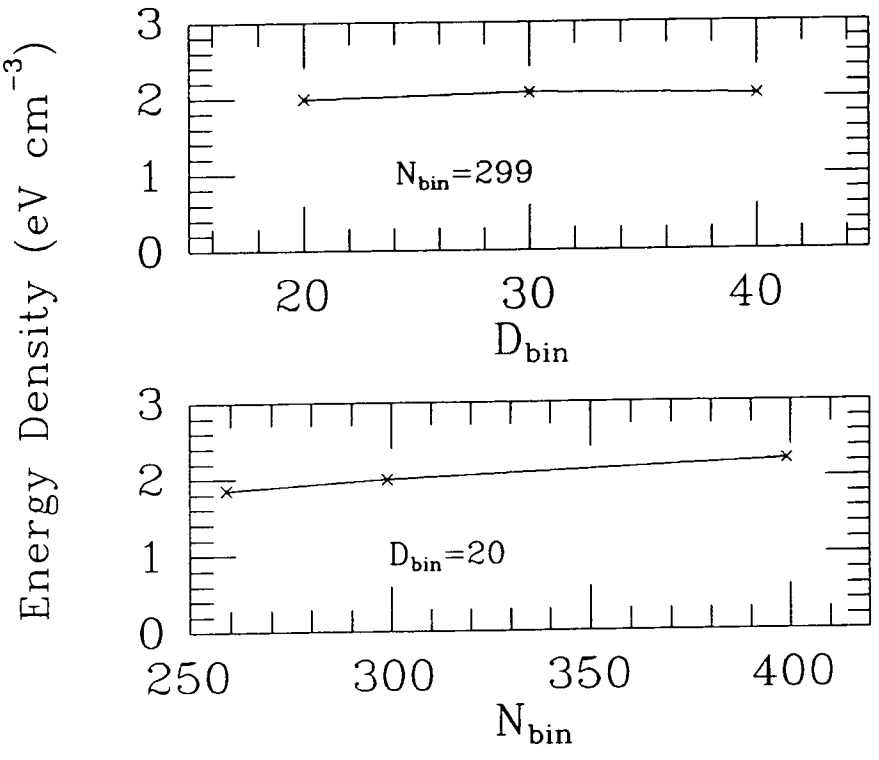

Figure 4.17

The profiles of two program parameters showing the dependency of the average energy density on *a.* N_{bin} and *b.* D_{bin}.

results were obtained using the laboratory value of the decay half-life, and in all cases of increasing energy density the half-life was greater than that of the Raisbeck data. The reasons for this are probably two-fold: Firstly although the Sun is approaching the Perseus arm in the model, in reality it is also approaching the much closer Local Spur or Orion arm. Observations show that the number density of young objects such as HII regions and OB stars within this Spur is the same as that of a major arm, (e.g. Lequeux, Dickel *et al* 1970, Fenkart 1979, Turner 1983, Humphreys 1983), so by implication, the SNR density may also be similar to that of the major arms. This means

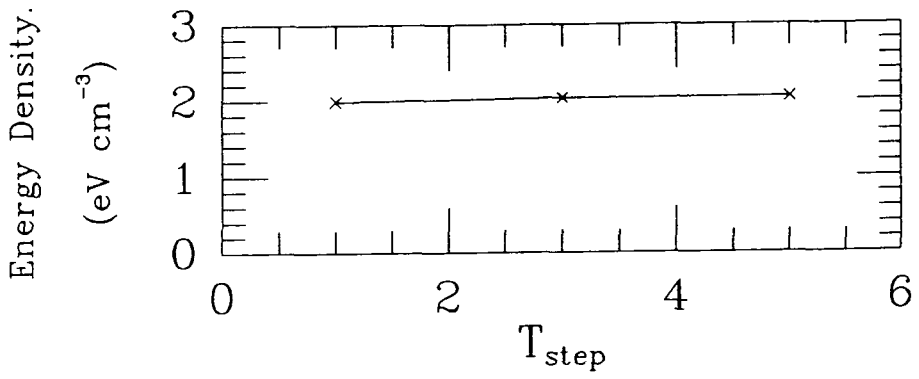

Figure 4.18

Profile of the program parameter T_{step} showing the variation of the average energy density.

that the Sun is actually much closer to a CR density enhancement than the model predicts. Because of the high pitch angle of the Orion Spur, the Sun is approaching in a direction near the normal to the Spur, thus giving a greater increase in CR activity than expected. The sense of this increase predicts a lower apparent half-life for the radioisotope data in qualitative agreement with the actual measurements.

Secondly, the z-motion of the Sun, which is ignored in the model, probably contributes to the increase of CR intensity with time. §4.3.3 reviewed its relationship to the ^{10}Be results and found that given some assumptions about how CR are connected to the gas distribution i.e. how they scale with z, the experimentally observed increase in CR activity could be due solely to this motion. Because of the leakage of CR from the Galaxy, this component of the solar motion is not thought to be the dominant influence on the CR intensity, but this z-motion should be incorporated into an improved simulation. It is worth speculating whether the neglect of the z-motion provides the explanation for the presence of too many SN in the model compared to the

^{10}Be data. The increase in ^{10}Be production has already been used to estimate the half-thickness of the CR layer in the Galaxy, so the motion towards the Orion arm and the z-motion until *about* 10^6 *years ago* are complementary in the sense that they both predict increasing CR intensities.

The Sun is now moving out of the Galactic plane, so when a simple exponential distribution of CR intensity with z is used, the intensity in the solar neighbourhood should be falling with time. This has been the situation for the last $\sim$ 10^6 years according to a simple-harmonic model of the Sun's motion, but this motion has not yet produced a change of the CR intensity significant enough to be visible in present radioisotope measurements. In 10^6 years the Sun moves $\sim$120 pc relative to the spiral arms, so depending on whether the z-motion or the motion towards the Orion Spur is dominant, the CR intensity in the future could go either way. If the CR intensity changes more rapidly with z than this model assumes, then future radionuclide measurements should be able to resolve these two effects: Over the past 10^7 years, the CR intensity measured at the Sun should increase followed by a flattening or decrease in the last $\sim$ 10^6 years as the z-motion reduces the intensity in competition with the planar motion. It is interesting to speculate whether the Tanaka and Inoue results described in §4.2 show this reversal since they cover 2×10^6 years with more points per unit time than the Raisbeck data. It is unfortunate that core samples could not be measured to earlier epochs with the same frequency of sampling as the Tanaka and Inoue results, otherwise much more detailed variations could have been seen. Given the other problems with the short timescale data mentioned in §4.2, the data are not of sufficient accuracy to be used in this detailed manner.

In conclusion, it is found that the model of the Sun's motion in the Galactic plane in which SN explosions occur can account for some of long-term increase in CR intensity found in the data. Shortcomings in this model have been discussed as well as predictions about how future results might be obtained.

4.6.2 Improvements to the Model.

The model of CR variations in the Galaxy arising from SNR acceleration

and subsequent CR diffusion is obviously a simple one. The reason is threefold: Firstly, with the present computing facilities, an accurate description of all the effects occurring would use too much CPU time even for one set of parameters and investigation of the full parameter space would be out of the question.

Secondly, the theories upon which the current model is based are not yet fully established. For example, the theory of CR diffusive shock acceleration has not been completely solved because it is a non-linear problem of great complexity. Current approximate solutions seem to produce meaningful results, but there are still problems outstanding that could affect η, the amount of energy from the explosion going into CR.

Thirdly, and probably most important, the analysis of radionuclides, including ^{10}Be are not yet of sufficient quality to permit more definite answers from the Monte-Carlo simulation used in this thesis. Improvements in the time resolution of the experimental data must be awaited, and a better understanding of the production and deposition processes of ^{10}Be is necessary before something definite may be said about the source(s) of the observed fluctuations. Until then, suggestions may be made about how future work might proceed in the light of the results already obtained using the simulation technique.

The approach that allows SN to go off at random in the Galaxy, (even preferentially in spiral arms), so that statistical effects may be examined has probably been taken as far as it can be, with the exception of some minor changes. For example, it might be possible to combine the Sun's motion with a 'fictional Galaxy' along the lines of Gerola and Seiden (1978) i.e. to do away with density wave theory and the grand design spiral and allow SN to trigger other explosions. This approach has the disadvantage that any real fluctuations in the radionuclide data cannot be attributed to actual events, but only to a statistical probability of a particular event occurring. In this sense it is a backward step, returning to a model similar to that of Bhat *et al* (1987).

Alternatively, the real Galaxy could be used in an attempt to pin down possible locations and times of expected excursions from the CR background.

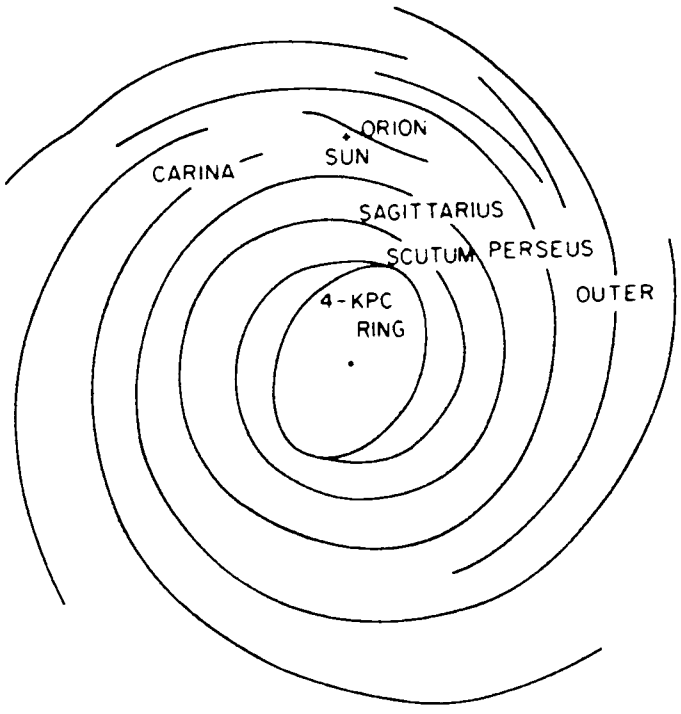

Figure 4.19

Simulated gas distribution in the Galaxy. (From Simonsen 1976).

This is a much more challenging problem as it involves a detailed knowledge of all pertinent objects — such as OB associations, SNR, gas clouds, pulsars etc. — along with with their ages and how they have evolved with time. The gas distribution of Simonsen (1976) could be used, for example (Fig.4.19). This approach would run into problems if integration times $> 10^7$years or so are required, as it becomes impossible to estimate the contribution that extinct objects made to the CR energy density at such early times (e.g. OB associations have ages of a few 10^6years.)

A fairly simple improvement would be to include more evolutionary phases in the SNR model, and to introduce variations in SN type. Inclusion of a period of adiabatic expansion following the CR acceleration phase would be an obvious example. Additionally, the 'onion-shell' model of Bogdan and Völk (1983) could be incorporated. However, such modifications to the model are probably minor as the timescales involved are of the order of a few 10^5 years, and the longest phase considered is that of CR diffusion. A probably more

significant change is that of varying the SN type. For example, those SN that produce pulsars could have a considerably longer effect on the energy density than those that do not. However, the connection between these two types of object must be more firmly established as there are only four 'definite' associations (Narayan and Schaudt 1988) and one of them (Vela) has recently been called into question (Bignami and Caraveo 1987). Obviously, once pulsars are included, an associated model for CR acceleration and/or reacceleration must be used which introduces more parameters and other dependency on another model.

The approximation of a unique escape time used here could be made more realistic by using an exponential dependence, so that not only would the energy density diminish with increasing CR confinement volume (X), but also decrease explicitly with time. Diffusion within the Galaxy is another part of the model that is treated very simply. The difference in the diffusion constant in and perpendicular to the Galactic plane should be incorporated. This implies that the Sun's z-motion should also be taken into account along with the scale height of the gas, giving a fully three-dimensional model.

4.6.3 Conclusion.

In this chapter, a Monte-Carlo simulation has been used to estimate the possible fluctuations in CR over the past few 10^7years as have been revealed by analysis of ^{10}Be data. The various parameters required for the model have been introduced and discussed and the modelling procedure described. The results obtained by investigating the parameter space have been compared to the ^{10}Be measurements. It can be said that, within the limitations of the model, the predicted amplitude and frequency of CR fluctuations are not such that SN cannot produce and/or accelerate CR. Therefore, SNR not excluded as CR source candidates. Restriction of the majority of SNR to spiral arms produces sensible results and seems to be improve the agreement between experimental data and the model. As a consequence of this, the CR energy density is found to be increasing over the past few 10^7 years as the Sun moves nearer a spiral arm (the Perseus arm in this model) and hence nearer the sources it contains. The increase in CR intensity observed in the model is

smaller than that observed in the data and this can be attributed to the Sun approaching not only the Perseus arm but also the Local Spur or Orion arm. The solar motion perpendicular to the Galactic plane may also be responsible. In this respect the model results and ^{10}Be measurements are in agreement.

The actual average energy density values obtained from the model are much closer to the canonical 1 eV cm^{-3} than earlier models. However, energy densities still tend to be too large. Reducing the efficiency of acceleration is one way of bringing these values down, but the required efficiency is 23%. Bringing down the Galactic SN rate is also a possibility, but the required rate would be 1 in 143 years. Although this is within the predicted range, preferred values are higher than the 1 in 75 years of the datum model. If the SN rate were 1 in 50 years, then the required efficiency to produce 1 eV cm^{-3} would be 14%. This may be acceptable for CR acceleration theories, but must place them under more stringent constraints. If higher efficiencies are still to be required then the estimates for SN rate and/or the escape time must be examined more closely.

Chapter 5. Summary and Prospects.

In this thesis, the problem of the origin of cosmic-rays (CR) has been addressed by examining the γ-ray evidence from two regions of the Galaxy.

Firstly, the Vela region has been studied. It contains a young pulsar and a supernova remnant (SNR) both clearly distinguished at many wavelengths and in γ-rays, there is a strong pulsed fraction, with a small non-pulsed component. This non-pulsed component is comprised of two parts: that due to ambient CR interacting with the gas in the line of sight, and that due to CR from the source itself interacting with the gas local to the source. The possibility of a third component — an unpulsed fraction direct from the pulsar — has also been studied, but this 'DC component' is found to be consistent with zero. This conclusion is reached because no significant signal is found in the unpulsed fraction with a point source distribution of γ-rays. Of the two components, it is the flux of γ-rays produced by CR from the source which is of interest. Assuming values for the ambient γ-ray emissivity, the expected intensity from the gas was estimated. Subtracting this from the unpulsed γ-ray flux left the source CR contribution to the γ-ray intensity. Fluxes were calculated in bins around the source and revealed a small but significant γ-ray component solely due to the presence of either the Vela pulsar or the SNR or possibly both. SNR models gave fluxes within a factor of 3 of those observed, but the main problem is with the extent of the emission. The SNR has a radius of around 20 pc whereas the extent of the γ-ray flux gives a radius of 45 pc. It is probable therefore that CR from the pulsar contribute to the γ-ray emission.

Studying the Vela region has enabled CR to be identified from an area of sky that was *a priori* believed to contain CR sources. This work together with that on Loop III and earlier studies of Loop I has shown that SNR definitely

contain high energy particles — both electrons and nuclei — that are capable of producing γ-rays.

Providing future γ-ray telescopes have sufficiently accurate timing resolution, better spatial resolution than COSB, and a well-determined point spread function, then there are excellent prospects for the improvement of the analysis performed here. The timing of each γ-ray enables the pulsed fraction to be identified, whilst better spatial resolution will reduce the angular size of the source γ-ray profile and enable a distinction to be made between pulsar and remnant. This distinction is crucial for determining whether the γ-rays due to CR from the source are pulsar-produced or remnant-produced. It would be helpful in this respect to be sure whether or not the pulsar and remnant are coeval. Improved radio measurements should help to refine age estimates of the remnant, as well as providing better data for models of SNR shock acceleration of CR.

This analysis has provided additional confirmation of what was already believed about SNR in their relationship to the origin of CR, and there are excellent opportunities for further understanding of the behaviour of CR in this region.

Chapter 3 dealt with Carina, both its Nebula, peculiar object and gas clouds marking the spiral arm. The γ-ray data has again been used at different energy bands to distinguish the active region of the Carina Nebula from the spiral arm tangent. A combination of calculations of emissivities and spectral indices has shown that both regions contain enhancements in emissivity suggesting the presence of CR sources, but also that there is a deficit of high energy particles in the region of the Nebula. Near the spiral tangent at $l = 284°$, high energy particles producing γ-rays with energies > 800 MeV are present. Massive, active stars such as WR or O3 stars are thought to be capable of producing such particles in stellar wind termination shocks. Unfortunately, most of these appear to be in the vicinity of the Nebula and in the same direction as the lack of high energy γ-rays. With no observations of SNR or pulsars, the only remaining candidate is the spiral arm shock. This hypothesis is not without its problems as some authors believe that the spiral arm shock is not capable of producing the high energy γ-rays observed here.

However, if confirmed, this analysis reveals explicitly for the first time γ-rays from the global spiral shock, and not just as a result of the increased column density of gas associated with the tangent. Clearly, there is a need for more observations at both γ-ray and radio wavelengths to search for other potential sources. SNR and pulsars particularly should be searched for, as these are the most likely candidates for high energy CR production. Some progress has already been made in this search with the possible identification of a SNR at $l = 286°$.

The Carina region has been the focus of interest for a number of decades and should remain so for years to come as these γ-ray results have indicated a new problem and so provide a stimulus for further observations. The prospects for study of the Carina region have always been good with the wealth of unusual, active and massive objects it contains and they will remain good with the new requirement to distinguish between sources of CR in the Carina Nebula and those in the spiral tangent.

Direct γ-ray and gas observations provide one of the best ways of determining the behaviour and distribution of CR sources. Theoretical models provide impetus and explanation for these observations and such models often have consequences in what might be initially thought to be unrelated astrophysical fields. This is the case with SNR production of CR.

Over Galactic timescales, SN occur very often and such extremely powerful events have effects which can extend over many parsecs and many hundreds of thousands of years. The CR they produce affect the production of radioisotopes on or around the Earth and SN nearby have a particularly noticeable effect.

The SN production of CR must be consistent with all the observations made directly at γ-ray or radio wavelengths for example, and also with the observations of the consequences of that CR acceleration process.

Chapter 4 examines the radioisotope data and specifically the ^{10}Be data. It uses the model of CR acceleration in SNR and makes assumptions about their temporal behaviour. It is found that the SNR model is consistent with the ^{10}Be data, although there may still be too many CR increases due to local

SN predicted by the model that are not seen in the data. New ^{10}Be result received just as this thesis was being completed (Raisbeck *et al* 1988) indicate that there appear to be no variations in CR intensity greater than $\pm 10\%$ over the past 7.5×10^6 years for data averaged over 10^5 years. It must be pointed out immediately that the model fluctuations of Chapter 4 are averages over 5×10^4 years so there will be more large excursions in the simulated energy density values as 10^5 year bins will smooth out the excesses. It is of considerable importance that Raisbeck *et al* (1988) suggest that there may be an excess at around 8×10^6 years ago as this would bring the data and the model into better agreement. Such claims will need to be carefully examined.

The Monte-Carlo technique has proved invaluable in determining the CR flux variations expected from given SNR models and the Sun's motion. Prospects for future work in this vein are more difficult to see than for the actual γ-ray observations, but perhaps when the mechanism for CR acceleration is more fully understood then such a simulation may again be attempted. Longer term variations in other radioisotopes could be the subject of Monte-Carlo simulations, but models of the cause of such variations will first be required.

In conclusion, the prospects for γ-ray astronomy and astrophysics are excellent, especially with the Gamma-Ray Observatory hopefully to be launched in the near future. All γ-ray studies will benefit from telescopes of improved resolution and much better photon counting statistics. These two factors are the main limitations of the γ-ray analyses to date, and although much important work has been done, it is but the tip of the iceberg of the whole of γ-ray astronomy. When the Observatory is launched, the next generation of telescope will be available and will hopefully clarify many of the outstanding γ-ray problems as well as aiding the hunt for the origin of the cosmic radiation.

Appendix A.

The Cross-Correlation Method.

The following method is based on Hermsen (1980) in his analysis of COSB sources in galactic γ-ray data.

When a source signal is superimposed on a background, it can be sometimes difficult to derive the actual source flux or number of counts. The correct method for this separation is known as the cross-correlation method and requires a *predictable* source distribution. The result of the correlation is either to prove the existence of the source or to place upper limits on the signal.

With specific application to COSB, the data is presented as either a number of γ-rays in a bin (N_{ij}) or as a flux (F_{ij}) expressed in units of ph $cm^{-2}s^{-1}$. For a given source position (r), the contribution of the source to a bin i, j is given by the response function $f(r, i, j)$. This will be the point spread function (PSF) in the case of a point source.

The correlation function is defined as:

$$C(r) = \frac{1}{n}\sum_{ij}(N_{ij} - \bar{N})(f(r,i,j) - \bar{f}) \qquad A.1$$

where n is the number of bins over which the summation is performed and $\bar{f}$ and $\bar{N}$ are the averages over the i, j bins. If fluxes are used instead of numbers of photons, the N_{ij} and $\bar{N}$ are replaced by F_{ij} and $\bar{F}$. There will be a positive correlation if in general the deviations of the numbers of γ-rays (or fluxes) from the mean have the same sign as the deviation from the mean of the response function.

For binned data, the restriction has to be made that the response function is evaluated at the centre of the bin as of course f is continuous. Also, the size of the array i, j must be limited to prevent contamination from other sources or structure in the Galactic plane. Additionally, when counts are used,

the array must be small enough to limit the variation of the exposure over the array.

The value of C obtained from Equation A.1 is not normalised. This can be achieved by equating the number of counts in a bin i, j to the total number of counts from the source (i. e. 'the correlated counts') thus:

$$N_{ij} = \frac{C_N}{\sum f} f(r, i, j) + B \qquad A.2$$

where B is the background and the summation is taken over i, j as before.

If B is not a smoothly varying function of position, then it is unlikely to produce a zero correlation signal. This obviously reduces the significance of any genuine signal because structure in the background can mimic source structure. Houston (1985) has examined this point in detail by using this technique to study the SASII data (Fichtel *et al* 1978) and to re-analyse the COSB results for spurious sources.

Provided then B is uncorrelated with F, then:

$$C_N = \left[\frac{\sum fN}{n} - \frac{\sum f . \sum N}{n^2}\right] \frac{n^2 \sum f}{n \sum f^2 - (\sum f)^2} \qquad A.3$$

In terms of fluxes, the expression for C_F is obtained by replacing N by F.

The variance of C is denoted s_c^2 and is given by:

$$s_c^2 = \frac{1}{n}(C - \bar{C})^2 \qquad A.4$$

and from the standard theory of errors it follows that:

$$s_c^2 = \sum \left(\frac{\partial C}{\partial N_{ij}}\right)^2 - s^2(N_{ij}) \qquad A.5$$

The variance in the number of counts in each bin ($s^2(N_{ij})$) is Poissonian.

Hence:

$$s_c^2 = \frac{1}{n^4}\left[n^2 \sum f^2 N + (\sum f)^2 \sum N - 2n(\sum f)(\sum fN)\right] \qquad A.6$$

The error in C is simply $\sqrt{s_c^2} = \sigma(C)$ so the error in C_N is:

$$\sigma_{C_N} = \sqrt{s_c^2} \cdot \frac{n^2 \sum f}{n \sum f^2 - (\sum f)^2} \qquad A.7$$

Providing their are no sources and therefore no correlation, then for a large number of bins the following can be used: $n \sum fN = \sum f \sum N$ and $n \sum f^2 = \sum f^2 \sum N$. When these are substituted into Equation A.5 and combined with Equation A.1, the significance of the correlation for a random count distribution results:

$$\frac{C}{\sigma} = \frac{n \sum fN - \sum f \sum N}{\sqrt{[n \sum f^2 - (\sum f)^2] \sum N}} \qquad A.8$$

For the earlier COSB PSF the response function is given by:

$$f(r, i, j) = exp(-(x^2/a^2 + y^2/b^2)^c) \qquad A.9$$

where x and y are the distances to the bin i, j from then point r where the evidence for the source is to be tested. The more recent form (Mayer-Hasselwander 1985) may also be used and is probably more representative of the genuine PSF for the three standard energy bands.

Bibliography.

W. I. Axford. 1965 Planet Spc. Sci. **13** 115

W. I. Axford. 1981a In: 'The Origin of Cosmic-rays.' eds. G. Setti, G. Spada and A. W. Wolfendale. IAU Symp. **94** 339. (Dordrecht:Reidel.)

W. I. Axford. 1981b Proc. N. Y. Acad. Sci. **375** 297

W. I. Axford. 1981c In: 'Plasma Astrophysics.' eds. Guyenne and Long (ESA Paris.) p425 ($\equiv$ 17th International Cosmic-ray Conference **12** 155)

W. I. Axford, E. Leer and G. Skadron. 1977 15th International Cosmic-ray Conference (Plovdiv.) **11** 132

F. Bash. 1986 In: 'The Galaxy and the Solar System.' eds. R. Smoluchouski, J. N. Bahcall, and M. S. Matthews. University of Arizona Press. p35.

W. Becker and R. P. Fenkart. 1970 In: 'The Spiral Structure of Our Galaxy.' eds. W. Becker and G. Contopoulous. IAU Symp. **38** p205. (Dordrecht:Reidel.)

A. R. Bell. 1978a MNRAS **182** 147, 1978b MNRAS **182** 443

C. L. Bhat, M. R. Issa, B. P. Houston, C. J. Mayer and A. W. Wolfendale. 1985a Nature **314** 511

C. L. Bhat, M. R. Issa, C. J. Mayer and A. W. Wolfendale. 1985b Nature **314** 515

C. L. Bhat, M. R. Issa, C. J. Mayer, A. W. Wolfendale and M. Zan. 1986a J. Phys. G: Nucl. Phys. **12** 1067

C. L. Bhat, C. J. Mayer, M. J. Rogers, A. W. Wolfendale and M. Zan. 1986b J. Phys. G: Nucl. Phys. **12** 1087

C. L. Bhat, C. J. Mayer, and A. W. Wolfendale. 1986c Phil. Trans. Roy. Soc. Lond. **319** 249

C. L. Bhat, C. J. Mayer, M. J. Rogers and A. W. Wolfendale. 1987 J. Phys. G: Nucl. Phys. **13** 257

G. F. Bignami and C. A. Caraveo. 1988 Ap. J. **325** L5

A. Blaauw. 1956 Ap. J. **123** 408

A. Blaauw. 1985 In: 'The Milky Way Galaxy.' IAU Symp. **106** eds. H. van Woerden, R. J. Allen and W. B. Burton. p335 (Dordrecht:Reidel.)

R. D. Blandford and J. Ostriker. 1978 Ap. J. **221** L29

R. D. Blandford and L. Cowie. 1982 Ap. J. **260** 625

R. D. Blandford and D. Eichler. 1987 Phys. Rep. **154** 1

J. B. G. M. Bloemen. 1985 PhD. Thesis. University of Leiden.

J. B. G. M. Bloemen, A. W. Strong, L. Blitz, R. S. Cohen, T. M. Cohen, D. A. Grabelsky, W. Hermsen, F. Lebrun, H. A. Mayer-Hasselwander and P. Thaddeus. 1986 A. & A. **154** 25

J. B. G. M. Bloemen. 1987 Ap. J. **317** L15

J. B. G. M. Bloemen, P. Reich, W. Reich and R. Schlickeiser. 1988 A. & A. Submitted.

T. J. Bogdan and H. J. Völk. 1983 A. & A. **122** 129

B. J. Bok. 1937 In: 'The Distribution of Stars in Space.' Univ. of Chicago Press. Chicago.

B. J. Bok. 1959 Observatory **79** 78

B. J. Bok, A. A. Hine, E. W. Miller. 1970 In: 'The Spiral Structure of Our Galaxy.' eds. W. Becker and G. Contopoulous. IAU Symp. **38** p245 (Dordrecht:Reidel.)

B. J. Bok. 1971 In: 'Highlights of Astronomy.' **2** p63

D. Bourles, G. M. Raisbeck and F. Yiou. 1988 Submitted to Geochim. Cosmochim.

R. L. Bowers and T. Deeming. 1984 'Astrophysics II.' p551

A. Broadbent, C. G. T. Haslam, J. L. Osborne. 1988 MNRAS. (In press.)

L. Bronfman, R. S. Cohen, H. Alvarez, J. May, and P. Thaddeus. 1987 Ap. J. **324** 248
E. M. Burbidge. 1969 In: 'Structure and Evolution of the Galaxy.' ed. L. N. Mavridis Ap. Spc. Sci. Lib. **22** p262
A. A. Burchuladze, S. V. Pagava, P. Povinec, G.I. Togonidze and S. Usacev. 1980 Nature **287** 320
F. C. Bruhweiler and Y. Kondo. 1982 Ap. J. **259** 232
W. B. Burton. In: 'Galactic and Extra-Galactic Radio Astronomy.' eds. G. L. Verschuur and K. I. Kellerman. Springer–Verlag. p82
F. Casoli and F. Combes. 1982 A. & A. **110** 287
M. Cassé and J. Paul. 1980 Ap. J. **237** 236
J. L. Caswell and D. H. Clark. 1975 Aust. J. Phys. Ap. Suppl. **37** 57
C. J. Cesarsky and T. Montmerle. 1983 Spc. Sci. Rev. **36** 173
D. H. Clark and J. L. Caswell. 1976a MNRAS **174** 274
D. H. Clark and J. L. Caswell. 1976b MNRAS **179** 87P
D. H. Clark and F. R. Stephenson. 1977 'The Historical Supernovae.' Pergamon: Oxford.
D. H. Clark, W. H. McCrea, F. R. Stephenson. 1977 Nature **265** 318
D. D. Clayton 1984 Ap. J. **280** 144
D. D. Clayton, D. P. Cox, and F. C. Michel. 1986 In: 'The Galaxy and the Solar System.' eds. R. Smoluchowski, J. N. Bahcall, M. S. Matthews. University of Arizona Press. p129
Courtès, V. P. Georgelin, Y. M. Georgelin, G. Monnet. 1970 In: 'The Spiral Structure of Our Galaxy.' eds. W. Becker and G. Contopoulous. IAU Symp. **38** p207 (Dordrecht:Reidel.)
R. M. Crutcher. 1982 Ap. J. **254** 84
T. M. Dame. 1984 PhD. Thesis. University of Columbia.
T. M. Dame, H. Ungerechts, R. S. Cohen, E. J. de Gues, A. Grenier, J. May, D. C. Murphy, L.-A. Nyman and P. Thaddeus. 1987 Ap. J. **322** 706
J. Davelaar, J. A. M. Bleeker, and A. J. M. Deerenberg. 1980 A. % A. **92** 231
J. Delhaye. 1965 In: 'Stars and Stellar Systems.' vol. 5. eds. A. Blaauw and M. Schmidt. University of Chicago Press, Chicago. p51
V. A. Derchachev, G. E. Kocharov and V. M. Ostryakov. 1983 18th International Cosmic-ray Conference (Bangalore.) **2** 342
C. D. Dermer. 1986 A. & A. **157** 223
H. R. Dickel, H. J. Wendker and J. H. Bieritz. 1970 In: 'The Spiral Structure of Our Galaxy.' eds. W. Becker and G. Contopoulous. IAU Symp. **38** p213 (Dordrecht:Reidel.)
L. O'C. Drury. 1983 Rep. Prog. Phys. **46** 973
L. O'C. Drury and H. J. Völk. 1981 Ap. J. **248** 344
N. Duric. 1984 Adv. Spc. Res. **3** 91
B. G. Elmegreen. 1979 Ap. J. **231** 372
B. G. Elmegreen and D. M. Elmegreen. 1979 In: 'Interstellar Molecules.' ed. B. H. Andrew. IAU Symp. **87** p191
R. P. Fenkart. 1979 In: 'The Large Scale Characteristics of the Galaxy.' ed. W. B. Burton. IAU Symp. **84** p101 (Dordrecht:Reidel.)
E. Fermi. 1949 Phys. Rev. **75** 1169
C. E. Fichtel, R. C. Hartman, D. A. Kniffen, D. J. Thompson, G. F. Bignami, H. Ögelman, M. E. Özel and T. Tuïner. 1975 Ap. J. **198** 163
C. E. Fichtel and D. A. Kniffen. 1984 A. % A. **134** 13
L. A. Fisk. 1971 J. Geophys. Res. **76** 1662
L. A. Fisk. 1979 Space Plasma Physics vol. 2. National Academy of Science, Washington. p127
M. A. Forman and O. A. Schaeffer. 1979 Rev. Geophys. Spc. Phys. **17** 552
P. C. Frisch. 1981 Nature **293** 377

M. Galli, G. Cini Castagnoli, M. R. Attolini, S. Cecchini, T. Nanni, G. E. Kocharov, V. A. Vasiliev and A. N. Konstantinov. 20th International Cosmic-Ray Conference (Moscow). **4** 284

S. L. Garzoli. 1970 In: 'The Spiral Structure of Our Galaxy.' eds. W. Becker and G. Contopoulous. IAU Symp. **38** p213 (Dordrecht:Reidel.)

Y. M. Georgelin and Y. P. Georgelin. A. & A. **49** 57

Y. M. Georgelin, Y. P. Georgelin and J.-P. Sivan. 1979 In: 'The Large Scale Characteristics of the Galaxy.' ed. W. B. Burton. IAU Symp. **84** p65 (Dordrecht:Reidel.)

H. Gerola and D. E. Seiden. 1978 Ap. J. **223** 129

M. Giler, B. Szabelska, J. Wdowczyk and A. W. Wolfendale. 1987a,b 20th International Cosmic-Ray Conference (Moscow). **2** 211,214

V. L. Ginzburg and S. I. Syrovatskii. 1964 'The Origin of Cosmic-Rays.' Pergamon: New York.

V. L. Ginzburg and V. S. Ptuskin. 1985 Sov. Sci. Rev. E. Ap. Spc. Phys. **4** 461

S. J. Gould. 1874 Proc. Amer. Assoc. Adv. Sci. p115

T. Goulet 1984 MSc. Thesis. University of British Columbia, Vancouver.

D. A. Grabelsky, R. S. Cohen, L. Bronfman, P. Thaddeus and J. May. 1987 Ap. J. **315** 122

D. A. Green. 1988 Ap. Spc. Sci. In press.

I. A. Grenier, W. Hermsen, and J. Clear. 1987 20th International Cosmic-Ray Conference (Moscow). **1** 77

J. E. Gunn and J. P. Ostriker. 1969 Phys. Rev. Lett. **22** 728

W. Hampel and O. A. Schaeffer. 1979 Earth Planet. Sci. Lett. **42** 348

F. R. Harden and P. Gorenstein. 1973 Nature **241** 107

F. R. Harnden, P. D. Grant, F. D. Seward and S. M. Kahn. 1985 Ap. J. **299** 828

C. Heiles and H. J. Habing. A. & A. Suppl. Ser. **14** 1

C. Heiles and M. N. Cleary. 1979 Aust. J. Phys. Ap. Suppl. **47** 1

W. Hermsen. 1980 Ph. D Thesis. Univ. of Leiden, The Netherlands.

V. H. Hess. 1912 Physik Zeitschr. **13** 1804

A. M. Hillas. 1972 'Cosmic Rays.' Pergamon Press.

J. L. Hilton and F. Bash. 1981 Ap. J. **255** 217

H. J. Hofmann, J. Beer, G. Bonani, H. R. Von Guten, S. Raman, M. Suter, R. L. Walker, W. Wölfli and D. Zimmermann. 1987 Nucl. Inst. Meth. Phys. Res. **B29** 32

B. P. Houston and A. W. Wolfendale. 1983 A. & A. **126** 22

B. P. Houston and A. W. Wolfendale. 1984 J. Phys. G. Nucl. Phys. **10** 1587

F. Hoyle. 1960 MNRAS **120** 338

P. D. Hudson. 1965 MNRAS **131** 123

P. D. Hudson. 1967 MNRAS **137** 205

R. M. Humphreys. 1972 A. & A. **20** 29

R. M. Humphreys. 1979 In: 'The Large Scale Characteristics of the Galaxy.' ed. W. B. Burton. IAU Symp. **84** p93 (Dordrecht:Reidel.)

K. A. Innanen, A. T. Patrick and W. W. Duley. 1978 Ap. Spc. Sci. **57** 511

D. E. Innes and T. W. Hartquist. 1984 MNRAS **209** 7

DeA. Iwan. 1980 Ap. J. **239** 316

Ikeuchi. 1978 preprint. (Referenced in Iwan 1980.)

E. B. Jenkins, J. Silk and G. Wallerstein. 1976 Ap. J. **209** L87

J. R. Jokipii. 1966 Ap. J. **143** 961

J. R. Jokipii. 1968 **152** 799

J. R. Jokipii. 1971 Rev. Geophys. Spc. Phys. **9** 27

S. M. Kahn, J. Brodie, S. Bowyer and P. A. Charles. 1983 Ap. J. **269** 212

S. M. Kahn, P. Gorenstein, F. R. Harnden, and F. D. Seward. 1985 Ap. J. **299** 821

G. Kanbach, K. Bennett, G. F. Bignami, R. Buccheri, P. Caraveo, N. D. Amico, W. Hermsen, G. G. Lichti, J. L. Masnou, H. A. Mayer-Hasselwander, J. A. Paul, B. Sacco, B. N. Swannenberg and R. D. Wills. 1985 A. & A. **90** 163
N. E. Kassim. 1988 Ap. J. **328** L55
D. A. Kniffen, C. E. Fichtel and D. J. Thompson. 1977 Ap. J. **215** 765
G. E. Kocharov, and A. N. Konstantinov 1983 18th International Cosmic-Ray Conference (Bangalore). **2** 233
J. Kota and J. R. Jokipii. 1983 Ap. J. **265** 573
J. Kristian. 1970 Ap. J. **162** L103
G. F. Krymsky. 1977 Sov. Phys. Dokl. **23** 327 (English Translation.)
C. G. Lacey. 1984 MNRAS **2-8** 687
D. Lal. 1974 Phil. Trans. Roy. Soc. **277** 395
B. M. Lasker. 1976 Ap. J. **203** 193
B. M. Lasker, S. D. Braker and O. Saá. 1972 Ap. J. **176** L65
H. Laumer, S. M. Austin, L. M. Panggabean and C. N. Davids. 1973 Phys. Rev. C **8** 483
G. Lemaître and M. S. Vallarta. 1933 Phys. Rev. **43** 87
J. Lequeux. 1974 In: 'The Interstellar Medium.' ed. K. Pinkau. NATO Advanced Study Inst. p191
I. Lerche. 1981 Ap. Spc. Sci. **74** 273
J. R. Lesh. 1968 Ap. J. **152** 905
J. R. Letaw, R. Silberberg, C. H. Tsao, D. Eichler, M. M. Shapiro and A. Wandel. 1987 20th International Cosmic-Ray Conference (Moscow). **2** 222
C. C. Lin, C. Yuan and F. H. Shu. 1969 Ap. J. **155** 721
C. C. Lin. 1970 In: 'The Spiral Structure of Our Galaxy.' eds. W. Becker and G. Contopoulous. IAU Symp. **38** p377 (Dordrecht:Reidel.)
C. C. Lin, C. Yuan, W. W. Roberts. 1973 In: 'Highlights in Astronomy.' **3** 441
B. Lindblad. 1941 Stockholm Obs. Ann. **13** No. 10
B. Lindblad. 1963 Stockholm obs. Ann. **22** No. 3
P. O. Lindblad. 1960 Stockholm Obs. Ann. **21** No. 4
R. N. Manchester. 1987 A. & A. **167** 117
K. Marti. 1985 Proc. of Workshop on Cosmogenic Nulides. Lunar Planet. Sci. Inst. In press.
H. A. Mayer-Hasselwander. 1985 'Explanatory Supplement to the COSB final database.' Issue 1.
M. Mayor 1972 A. & A. **18** 97
C. F. McKee. and J. Ostriker. 1977 Ap. J. **218** 148
D. K. Milne. 1971 In: 'The Crab Nebula.' eds. R. D. Davies, F. G. Smith IAU Symp. **46** p248 (Dordrecht:Reidel.)
D. K. Milne. 1980 A. & A. **81** 293
D. K. Milne and R. N. Manchester. 1986 A. & A. **171** 205
T. Montmerle. 1979a Ap. J. **231** 95
T. Montmerle. 1979b 16th International Cosmic-Ray Conference (Kyoto). **1** 185
T. Montmerle. 1981 Phil. Trans. Roy. Soc. Lond. **301** 505
G. E. Morfill and M. Scholer. 1979 Ap. J. **232** 473
G. E. Morfill and T. W. Hartquist. 1985 Ap. J. **297** 194
O. Muller, W. Hampel, T. Kirsten and G. F. Herzog. 1981 Geochim. et Cosmochim. Acta. **45** 447
R. Narayan and K. J. Schaudt. Arizona Theoretical Ap. Preprint # 87-40
A. Neftel, H. Oeschger and H. E. Suess. 1981 Earth Planet. Sci. Lett. **56** 127
K. Nishiizumi, D. Elmore, M. Honda, J. R. Arnold and H. E. Gove. 1983 Nature **305** 611
K. Nishiizumi, S. V. S. Murty, K. Marti and J. R. Arnold. 1985 19th International Cosmic-Ray Conference (La Jolla). **5** 379

K. Nishiizumi, S. Regnier and K. Marti. 1980 Earth Planet. Sci. Lett. **50** 156
H. Ögelman, C. E. Fichtel, D. A. Kniffen and D. J. Thompson. 1976 Ap. J. **209** 584
C. A. Olano. 1982 A. & A. **112** 195
J. L. Osborne, M. L. Parkinson, K. M. Richardson and A. W. Wolfendale. 1987 In: 'Physical Processes in Interstellar Clouds.' eds. G. E. Morfill and M. Scholer p81 Reidel: Dordrecht.
J. L. Osborne and V. S. Ptuskin. 1987 20th International Cosmic-Ray Conference (Moscow). **2** 218
J. Ostriker and C. F. McKee. 1988 Rev. Mod. Phys. **60** 1
J. Palous. 1983 Bull. Astron. Inst. Czech. **34** 286
F. Paresce. 1984 A. J. **89** 1022
E. N. Parker. 1958 Phys. Rev. **109** 1328
E. N. Parker. 1965 Planet. Spc. Sci. **13** 9
J. L. Pawsey. 1965 In: 'Galactic Structure.' Stars and Stellar Systems V. eds. A. Blaauw and M. Schmidt p219. University of Chicago Press, Chicago.
C. L. Perry, L. Johnston, and D. L. Crawford. 1982 A. J. **81** 1751
A. M. T. Pollock, J. B. G. M. Bloemen, I. A. Grenier, W. Hermsen, F. Lebrun and A. W. Strong. 1987 20th International Cosmic-Ray Conference (Moscow). **1** 88
C. B. Poon. 1983 PhD. Thesis University of Hong Kong.
P. Povinec. 1977 Acta Physica **18** 139
P. Povinec. 1987 20th International Cosmic-Ray Conference (Moscow). Invited Paper.
R. J. Protheroe, A. W. Strong, A. W. Wolfendale and P. Kiraly. 1979 Nature **277** 542
V. Radhadkrishnan, D. J. Cooke, M. M. Komesaroff and D. Morris. Nature **221** 443
G. M. Raisbeck. 1985 19th International Cosmic-Ray Conference (La Jolla). Rapporteur Paper.
G. M. Raisbeck. 1988 Private Communication.
G. M. Raisbeck, F. Yiou, D. Bourles and Z. S. Zhou. 1988 Chem. Geol. **70** 120
M. R. Rampino and R. B. Stothers. 1984 Nature **308** 709
S. Rappaport, H. Bradt, R. Doxsey, A. Levine and G. Spada. 1974 Nature. **251** 471
S. M. Read and V. E. Viola. 1984 Atomic Data Nucl. Data Tables. **31** 359
P. E. Reichley, G. S. Down and G. A. Morris. 1970 Ap. J. **159** L35
K. M. Richardson. 1988 PhD. Thesis. University of Durham.
W. W. Roberts. 1969 Ap. J. **159** 123
W. W. Roberts. 1970 In: 'The Spiral Structure of Our Galaxy.' eds. W. Becker and G. Contopoulous. IAU Symp. **38** p415 (Dordrecht:Reidel.)
M. J. Rogers and A. W. Wolfendale. 1987 20th International Cosmic-Ray Conference (Moscow) **1** 81
M. J. Rogers, M. Sadzinska, J. Szabelski, D. J. van der Walt and A. W. Wolfendale. 1988 J. Phys. G. Nucl. Phys. **14** 1147
M. T. Ruiz and J. May. 1986 Ap. J. **309** 667
W. Sacher and V. Schonfelder. 1984 Ap. J. **279** 817
D. B. Sanders. 1981 PhD. Thesis. State University of Stony Brook.
W. T. Sanders, W. L. Kraushaar, J. A. Nousek, and P. M. Fried. Ap. J. **217** L87
O. A. Schaeffer. 1979 14th International Cosmic-Ray Conference (Munich) **11** 3508
R. D. Schwartz and P. B. James. 1984 Nature **308** 712
L. Sedov. 1959 'Similarity and Dimensional Methods in Mechanics.' New York Academic Press. p210
P. E. Seiden and H. Gerola. 1979 Ap. J. **233** 56
P. E. Seiden, L. S. Schulman and H. Gerola. 1979 Ap. J. **232** 702
E. M. Shoemakeer. 1984 Bull. Amer. Astron. Soc. **16** 678 Abs.
E. M. Shoemaker and R. F. Wolfe. 1982 In: 'Satellites of Jupiter.' ed. D. Morrison. University of Arizona Press, Tuscon. p277

F. H. Shu, V. Milione, W. Gebel, C. Yuan, D. W. Goldsmith, and W. W. Roberts. 1972 Ap. J. **173** 557
S. C. Simonsen. 1976 A. & A. **46** 261
L. F. Smith. 1968a MNRAS **138** 109
L. F. Smith. 1968b MNRAS **140** 409
L. F. Smith. 1968c MNRAS **141** 317
L. F. Smith. 1982 In: 'Wolf-Rayet Stars.' eds C. W. H. de Loore and A. J. Wills. IAU Symp. **99** p597 (Dordrecht:Reidel.)
P. M. Solomon, D. B. Sanders and N. Z. Scoville. 1979a In: ' The Large-Scale Characteristics of the Galaxy.' ed. W. B. Burton p59 Dordrecht:Reidel.
P. M. Solomon, D. B. Sanders and N. Z. Scoville. 1979b Ap. J. **232** L89
P. M. Solomon and W. T. Sanders. 1980 In: 'Giant Molecular Clouds in the Galaxy.' eds. Solomon and Edmunds p41. Pergamon: New York.
P. M. Solomon, D. B. Sanders, and A. R. Rivolo. 1985 Ap. J. **292** L19
C. P. Sonnett. 1985 Meteoritics. **20** 383
T. A. Th. Spoelstra. 1972 A. & A. **21** 61
A. A. Stark. 1979 PhD. Thesis. University of Princeton.
F. W. Stecker. 1981. In: 'Cosmic Gamma Rays.' Mono Book Corporation. Baltimore, M. D.
S. A. Stephens and G. D. Bahdwar. 1981 Ap. Spc. Sci. **76** 213
B. Stenholm. 1975 A. & A. **39** 307
R. Stothers. Publ. Astron. Soc. Pac. **92** 145
K. Aa. Strand. 1958 Ap. J. **128** 14
A. W. Strong. 1985 Private Communication.
A. W. Strong, P. A. Riley, J. L. Osborne, and J. D. Murray. 1982 MNRAS **201** 495
A. W. Strong, J. B. G. M. Bloemen, T. M. Dame, I. A. Grey, W. Hermsen, F. Lebrun, L-A. Nyman, A. M. T. Pollock and P. Thaddeus. 1987 20th International Cosmic-Ray Conference. (Moscow). **1** 125
M. Stuiver and P.P. Quay. 1981 Earth Planet. Sci. Lett. **53** 349
H. E. Suess. 1980 Radiocarbon. **20** 200
B. N. Swannenberg, K. Bennett, G. F. Bignami, R. Buccheri, P. Caraveo, W. Hermsen, G. Kanbach, G. G. Lichti, J. L. Masnou, H. A. Mayer-Hasselwander, J. P. Paul, B. Sacco, L. Scarsi and R. D. Wills. 1981 A. & A. **243** L69
G. A. Tammann. 1970 In: 'The Spiral Structure of Our Galaxy.' eds. W. Becker and G. Contopoulous. IAU Symp. **38** p236 (Dordrecht:Reidel.)
G. A. Tammann. 1974 In: 'Supernovae and Supernova Remnants.' ed. C. B. Cosmovici. Ap. Spc. Sci. Lib. **45** p155
G. A. Tammann. 1981 In: 'Supernovae: A Survey of Current Research.' ed. M. R. Rees and R. J. Stoneham. NATO Advanced Study Inst. p371
S. Tanaka, T. Inoue and M. Imamura. 1977 Earth Planet. Sci. Lett. **37** 55
S. Tanaka and T. Inoue. 1979 16th International Cosmic-Ray Conference. (Kyoto). **2** 277
P. Thaddeus and G. A. Chanan. 1985 Nature **314** 73
K. O. Thielheim. 1987 20th International Cosmic-Ray Conference. (Moscow). **2** 248
D. J. Thompson, C. E. Fichtel, D. A. Kniffen and H. B. Ögelman. Goddard Space Flight Centre, Greenbelt, Maryland. Preprint April 1975.
D. J. Thompson, G. F. Bignami, C. E. Fichtel and D. A. Kniffen. Ap. J. **190** L51
S. Tokar and P. Povinec. 1983 18th International Cosmic-Ray Conference (Bangalore). **2** 381
D. Yu. Tsvekov. 1983 Sov. Astron. **27** 22
B. E. Turner. 1983 In: 'Kinematic, Dynamics and Structure of the Milky Way.' ed. W. L. H. Shuter. Ap. Spc. Sci. Lib. **100** p171
P. O. Vandervoort. 1971 Ap. J. **166** 37

F. H. Shu, V. Milione, W. Gebel, C. Yuan, D. W. Goldsmith, and W. W. Roberts. 1972 Ap. J. **173** 557
S. C. Simonsen. 1976 A. & A. **46** 261
L. F. Smith. 1968a MNRAS **138** 109
L. F. Smith. 1968b MNRAS **140** 409
L. F. Smith. 1968c MNRAS **141** 317
L. F. Smith. 1982 In: 'Wolf-Rayet Stars.' eds C. W. H. de Loore and A. J. Wills. IAU Symp. **99** p597 (Dordrecht:Reidel.)
P. M. Solomon, D. B. Sanders and N. Z. Scoville. 1979a In: ' The Large-Scale Characteristics of the Galaxy.' ed. W. B. Burton p59 Dordrecht:Reidel.
P. M. Solomon, D. B. Sanders and N. Z. Scoville. 1979b Ap. J. **232** L89
P. M. Solomon and W. T. Sanders. 1980 In: 'Giant Molecular Clouds in the Galaxy.' eds. Solomon and Edmunds p41. Pergamon: New York.
P. M. Solomon, D. B. Sanders, and A. R. Rivolo. 1985 Ap. J. **292** L19
C. P. Sonnett. 1985 Meteoritics. **20** 383
T. A. Th. Spoelstra. 1972 A. & A. **21** 61
A. A. Stark. 1979 PhD. Thesis. University of Princeton.
F. W. Stecker. 1981. In: 'Cosmic Gamma Rays.' Mono Book Corporation. Baltimore, M. D.
S. A. Stephens and G. D. Bahdwar. 1981 Ap. Spc. Sci. **76** 213
B. Stenholm. 1975 A. & A. **39** 307
R. Stothers. Publ. Astron. Soc. Pac. **92** 145
K. Aa. Strand. 1958 Ap. J. **128** 14
A. W. Strong. 1985 Private Communication.
A. W. Strong, P. A. Riley, J. L. Osborne, and J. D. Murray. 1982 MNRAS **201** 495
A. W. Strong, J. B. G. M. Bloemen, T. M. Dame, I. A. Grey, W. Hermsen, F. Lebrun, L-A. Nyman, A. M. T. Pollock and P. Thaddeus. 1987 20th International Cosmic-Ray Conference. (Moscow). **1** 125
M. Stuiver and P.P. Quay. 1981 Earth Planet. Sci. Lett. **53** 349
H. E. Suess. 1980 Radiocarbon. **20** 200
B. N. Swannenberg, K. Bennett, G. F. Bignami, R. Buccheri, P. Caraveo, W. Hermsen, G. Kanbach, G. G. Lichti, J. L. Masnou, H. A. Mayer-Hasselwander, J. P. Paul, B. Sacco, L. Scarsi and R. D. Wills. 1981 A. & A. **243** L69
G. A. Tammann. 1970 In: 'The Spiral Structure of Our Galaxy.' eds. W. Becker and G. Contopoulous. IAU Symp. **38** p236 (Dordrecht:Reidel.)
G. A. Tammann. 1974 In: 'Supernovae and Supernova Remnants.' ed. C. B. Cosmovici. Ap. Spc. Sci. Lib. **45** p155
G. A. Tammann. 1981 In: 'Supernovae: A Survey of Current Research.' ed. M. R. Rees and R. J. Stoneham. NATO Advanced Study Inst. p371
S. Tanaka, T. Inoue and M. Imamura. 1977 Earth Planet. Sci. Lett. **37** 55
S. Tanaka and T. Inoue. 1979 16th International Cosmic-Ray Conference. (Kyoto). **2** 277
P. Thaddeus and G. A. Chanan. 1985 Nature **314** 73
K. O. Thielheim. 1987 20th International Cosmic-Ray Conference. (Moscow). **2** 248
D. J. Thompson, C. E. Fichtel, D. A. Kniffen and H. B. Ögelman. Goddard Space Flight Centre, Greenbelt, Maryland. Preprint April 1975.
D. J. Thompson, G. F. Bignami, C. E. Fichtel and D. A. Kniffen. Ap. J. **190** L51
S. Tokar and P. Povinec. 1983 18th International Cosmic-Ray Conference (Bangalore). **2** 381
D. Yu. Tsvekov. 1983 Sov. Astron. **27** 22
B. E. Turner. 1983 In: 'Kinematic, Dynamics and Structure of the Milky Way.' ed. W. L. H. Shuter. Ap. Spc. Sci. Lib. **100** p171
P. O. Vandervoort. 1971 Ap. J. **166** 37

J. H. Völk. 1975 Rev. Geophys. Spc. Phys. **13** 547
J. H. Völk and M. Forman. 1982 Ap. J. **253** 188
J. H. Völk, L. O'C. Drury and J. F. McKensie. 1984 A. & A. **130** 19
H. Voshage. 1967 Z. Natureforsch **22a** 477 (Ref. in Earth Planet. Sci. Lett. **50** 156.)
H. Voshage. 1984 Earth Planet. Sci. Lett. **71** 181
H. Voshage. 1962 Z. Natureforsch **17a** 422
A. Wandel, D. Eichler, J. R. Letaw, R. Silberberg and C. H. Tsao. 1987 Ap. J. **316** 676
W. H. Warren and J. E. Hesser. 1977a,b Ap. J. Suppl. Ser. **34** 115, 207
W. H. Warren and J. E. Hesser. 1978 Ap. J. Suppl. Ser. **36**497
R. S. Warwick, A. J. Norton, M. J. L. Turner, M. G. Watson and A. Willingdale. MNRAS **232** 551
H. Weaver and D. R. Williams. 1973 A. & A. Suppl. Ser. **8** 1
H. Weaver. 1970 In: 'The Spiral Structure of Our Galaxy.' eds. W. Becker and G. Contopoulous. IAU Symp. **38** p126 (Dordrecht:Reidel.)
H. Weaver. 1978 In: 'The Large Scale Characteristics of the Galaxy.' ed. W. B. Burton. IAU Symp. **84** p295 (Dordrecht:Reidel.)
K. W. Weiler and N. Panagia. 1980 A. & A. **90** 269
K. W. Weiler R. A. Stramek. 1988 An. Rev. Astron. and Ap. **26** In preparation.
C. S. Weller and R. R. Meier. 1981 Ap. J. **246** 386
R. Wielen. 1974 In: 'Highights of Astronomy.' **3** ed. G. Contopoulos. Dordrecht: Reidel. p395
R. Wielen. 1977 A. & A. **60** 263
D. A. Wilkinson. 1987 PhD. Thesis. University of Durham.
L. Woltjer. 1965 In: 'Galactic Structure.' Stars and Stellar Systems V. eds. A. Blaauw and M. Schmidt p531. University of Chicago Press, Chicago.
R. Woolley. 1969 In: 'Structure and Evolution of the Galaxy.' ed. L. N. Mavridis Ap. Spc. Sci. Lib. **22** p183
C. Yuan. 1970 In: 'Galactic Astronomy.' eds. Hong-Lee Chiu and A. Muriel.**2** p233
C. Yuan. 1970 In: 'The Spiral Structure of Our Galaxy.' eds. W. Becker and G. Contopoulous. IAU Symp. **38** p391 (Dordrecht:Reidel.)
C. Yuan. 1973 A. & A. **58** 53
C. Yuan. 1983 In: 'Kinematic, Dynamics and Structure of the Milky Way.' ed. W. L. H. Shuter. Ap. Spc. Sci. Lib. **100** p47

Acknowledgements.

Firstly, I must thank Prof. Arnold Wolfendale for introducing me to cosmic-ray astrophysics 'many years ago' whilst I was at school, then during my three years as an undergraduate at Durham and finally as supervisor for this PhD.

I wish to express my thanks to members of the astrophysics group past and present at Durham University Physics Department for their help, encouragement and useful discussions: Drs. Chaman Bhat, Brian Houston, Chris Mayer, Iain McClaren, John Osborne, Ken Richarson, Jacek Szabelski, Johan Van der Walt, David Wilkinson, and to Prof. Mohammed Issa, Alison Broadbent and to Margaret Chipchase.

I also wish to thank Mr. Alan Lotts for his patient endurance and support during three years of computing on the STARLINK Vax cluster at Durham, especially during the development and running of MODEL.

Finally, special thanks to my family who supported me through all my education and support me through my life, especially to the person to whom this thesis is dedicated.